

NASA CR 73160

AVAILABLE TO THE PUBLIC

STABILITY OF THERMAL CONTROL COATINGS
EXPOSED TO COMBINED SPACE ENVIRONMENTS

By William R. Holland

December 1967

Distribution of this report is provided in the interest of information exchange. Responsibility for the contents resides in the author or organization that prepared it.

Prepared under Contract No. NAS 2-3646 by
AVCO ELECTRONICS DIVISION
TULSA OPERATION
Tulsa, Oklahoma

for

AMES RESEARCH CENTER
NATIONAL AERONAUTICS AND SPACE ADMINISTRATION

FACILITY FORM 602.	N 68 - 169 04	_____
	(ACCESSION NUMBER)	(THRU)
	11	1
	(PAGES)	(CODE)
CI - 73160	33	_____
(NASA CR OR TMX OR AD NUMBER)	(CATEGORY)	

ABSTRACT

An in situ reflectometer system was designed, fabricated and installed in an existing Avco space simulation facility. After installation of the in situ system, qualification tests were conducted on the system. Tests were conducted on twelve materials including combined environment of vacuum, protons and ultraviolet, protons and vacuum only, ultraviolet and vacuum only and vacuum only. The ZnO/K_2SiO_3 was found to be more susceptible to protons and less to ultraviolet radiation and the La_2O_3/K_2SiO_3 more susceptible to ultraviolet radiation with very little damage by protons. Of the powdered samples tested only the TiO_2 showed measurable damage with protons only irradiation.

FOREWORD

This draft report was prepared by the Avco Electronics Division, Tulsa Operation, as the final documentation of work performed under Contract NAS2-3646, issued by National Aeronautics and Space Administration, Ames Research Center, Moffett Field, California. Mr. Elmer Streed was Technical Monitor.

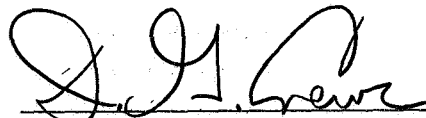
This report covers work performed from June 1966 to August 1967.

Prepared By:



W. R. Holland, Chief
Environmental Physics Section

Approved By:



D. G. Crews
Manager of Engineering

TABLE OF CONTENTS

	<u>Page</u>
I. INTRODUCTION	1
II. PROGRAM SCOPE	2
A. Phase I - Design, Fabrication and Qualification	2
B. Phase II - Test Program	3
III. TEST EQUIPMENT	7
A. <u>In Situ</u> Reflectometer System	7
B. Vacuum Chamber	11
C. Van de Graaff Accelerator	11
D. Transition Section and Beam Scanner	13
E. Solar Simulator	14
F. Lyman-Alpha Source	14
G. Reflectance Measuring Apparatus	14
H. <u>Non-In Situ</u> System	14
IV. EQUIPMENT CALIBRATION AND EVALUATION	15
A. <u>In Situ</u> Reflectometer System	15
B. Particle Energy and Flux	15
C. Solar Simulator Calibration	21
D. Vacuum Ultraviolet Calibration	21
E. <u>Non-In Situ</u> System	21
V. TEST PARAMETERS AND RESULTS	23
VI. DISCUSSION OF RESULTS	27
A. <u>In Situ</u> Tests	27
B. <u>Non-In Situ</u> Tests	70
VII. CONCLUSIONS AND RECOMMENDATIONS	84
A. Conclusions	84
B. Recommendations	85
VIII. REFERENCES	86
IX. APPENDIX	88

LIST OF ILLUSTRATIONS

<u>Figure No.</u>		<u>Page No.</u>
1	Schematic of Space Simulation Facility	8
2	Transfer Arm	9
3	Sample Rack Mounted in Chamber	9
4	Integrating Sphere - Vacuum View	9
5	Integrating Sphere - Atmosphere View	9
6	Schematic of Vacuum Chamber	12
7	Comparison (in air) of <u>In Situ</u> Integrating Sphere with Gier-Dunkle Sphere	18
8	Comparison (in air) of <u>In Situ</u> Integrating Sphere with Gier-Dunkle Sphere	19
9	Spectral Plot of Hg Xe Lamp	22
10	Effect of 10 Kev Protons on ZnO/K ₂ SiO ₃ - 5.3 x 10 ¹⁵ p/cm ² at 1.1 x 10 ¹² p/cm ² /sec	29
11	Effect of combined exposure of ZnO/K ₂ SiO ₃ , 10 Kev protons - 5.3 x 10 ¹⁵ p/cm ² at 1.1 x 10 ¹² p/cm ² /sec, 15 sun hours of near ultraviolet (Xenon) at 3 solar equivalents	30
12.	Transient proton damage in the infrared	31
13	Effect of Solar Radiation on ZnO/K ₂ SiO ₃	33
14	Effect of 10 Kev protons on ZnO/K ₂ SiO ₃ at 298°K. Average proton flux 3.8 x 10 ⁹ p/cm ² /sec	35
15	Effect of combined environment on ZnO/K ₂ SiO ₃ at 298°K. Average proton flux 3.8 x 10 ⁹ p/cm ² /sec - Ultraviolet unknown.	36

LIST OF ILLUSTRATIONS
(Continued)

<u>Figure No.</u>		<u>Page No.</u>
16	Rate and vacuum effect of proton radiation only - ZnO/K ₂ SiO ₃ (F-1-47-D)	37
17	Effect of total proton radiation to 5 x 10 ¹⁵ p/cm ² - ZnO/K ₂ SiO ₃ (F-1-47-D)	38
18	Effect of protons on 1-11-9-13 ZnO/K ₂ SiO ₃ , Remaining in vacuum after irradiation.	40
19	Effect of UV radiation only. ZnO/K ₂ SiO ₃ (F-1-47-D)	41
20	Combined effects versus sum of individual effects. Continuous low current - ZnO/K ₂ SiO ₃ (F-1-47-D)	42
21	Combined effects versus sum of individual effects. Accelerated current - ZnO/K ₂ SiO ₃ (F-1-47-D)	43
22	Combined effects with continuous current versus combined effects with accelerated current. ZnO/K ₂ SiO ₃ (F-1-47-D)	44
23	Effect of combined environment immediately after accelerated proton exposure and at the end of the test - ZnO/K ₂ SiO ₃ (F-1-47-D)	45
24	Rate and vacuum effect of proton radiation only - ZnO/Silicone (F-1-55)	47
25	Effect of increasing total proton flux from 2 x 10 ¹⁵ p/cm ² to 1 x 10 ¹⁶ p/cm ² - ZnO/Silicone (F-1-55)	48
26	Effect of UV radiation only. ZnO/Silicone (F-1-55)	49
27	Combined effects versus sum of individual effects. Continuous low current - ZnO/Silicone (F-1-55)	51
28	Combined effects versus sum of individual effects. Accelerated current - ZnO/Silicone (F-1-55)	52

LIST OF ILLUSTRATIONS
(Continued)

<u>Figure No.</u>		<u>Page No.</u>
29	Combined effects with continuous current versus combined effects with accelerated current. ZnO/Silicone (F-1-55)	53
30	Effect of combined environment immediately after accelerated proton exposure and at end of test. ZnO/Silicone (F-1-55)	54
31	Effect of proton radiation only. Accelerated current- immediately after radiation and at end of test. La ₂ O ₃ /K ₂ SiO ₃ (F-1-53A)	55
32	Effect of UV radiation only. La ₂ O ₃ /K ₂ SiO ₃ (F-1-53A)	56
33	Combined effects versus sum of individual effects La ₂ O ₃ /K ₂ SiO ₃ (F-1-53A)	57
34	Effect of combined environment immediately after accelerated proton exposure and at end of test La ₂ O ₃ /K ₂ SiO ₃ (F-1-53A)	58
35	Effect of proton radiation only - Accelerated current - immediately after radiation and at end of test. La ₂ O ₃ /K ₂ SiO ₃ (F-1-38)	60
36	Effect of total proton flux of 1×10^{16} p/cm ² - La ₂ O ₃ /K ₂ SiO ₃ (F-1-38)	61
37	Effect of UV radiation only - La ₂ O ₃ /K ₂ SiO ₃ (F-1-38)	62
38	Combined effects versus sum of individual effects - La ₂ O ₃ /K ₂ SiO ₃ (F-1-38)	63
39	Effect of combined environment immediately after accelerated proton exposure and at end of test - La ₂ O ₃ /K ₂ SiO ₃ (F-1-38)	64
40	Effect of proton radiation only (S-13G)	66
41	Effect of UV radiation only (S-13G)	67

LIST OF ILLUSTRATIONS
(Continued)

<u>Figure No.</u>		<u>Page No.</u>
42	Combined effect versus sum of individual effects (S-13G)	68
43	Effect of proton radiation only (TiO ₂ Silicone)	69
44	Effect of UV radiation only (TiO ₂ Silicone)	71
45	Combined effects versus sum of individual effects (TiO ₂ Silicone)	72
46	Effect of proton radiation only (SiO ₂ powdered)	73
47	Effect of proton radiation only (La ₂ O ₃ powdered)	74
48	Effect of proton radiation only (TiO ₂ powdered)	75
49	Effect of proton radiation only (AL ₂ O ₃ powdered)	76
50	Effect of proton radiation only (MgO powdered)	77
51	Effect of proton exposure on SP 500 zinc oxide at 298°K. 10 Kev protons - 2 x 10 ¹⁵ p/cm ² at 5.5 x 10 ¹¹ p/cm ² /sec.	79
52	Effect of combined environment exposure on SP 500 zinc oxide at 299°K. 10 Kev protons - 2 x 10 ¹⁵ p/cm ² at 7.4 x 10 ⁹ p/cm ² /sec. 750 sun hours of near and vacuum UV at 10 solar equivalents.	80
53	Effect of ultraviolet exposure of SP 500 zinc oxide at 299°K. 750 sun hours of near and vacuum UV at 10 solar equivalents	81
54	Effect of combined environment exposure on vacuum deposited Ag on fused silica at 304°K. 10 Kev protons - 1.5 x 10 ¹⁷ p/cm ² at 5.5 x 10 ¹¹ p/cm ² /sec. 750 sun hours of near and vacuum UV at 10 solar equivalents	82
55	Effect of ultraviolet exposure on vacuum deposited Ag on fused silica at 304°K. 750 sun hours of near and vacuum UV at 10 solar equivalents	83

LIST OF TABLES

<u>Table No.</u>		<u>Page</u>
I	Test Specimens	4 - 5
II	Comparison of Measurements in <u>In Situ</u> Sphere With Those in Gier-Dunkle Sphere at Atmosphere for ZnO/K_2SiO_3	16
III	Comparison of Measurements in <u>In Situ</u> Sphere With Those in Gier-Dunkle Sphere at Atmosphere for SiO_x on Vapor Deposited Aluminum	17
IV	Test Parameters and Results	24 - 26

I. INTRODUCTION

Reliable spacecraft thermal design requires a knowledge of solar absorptance of all spacecraft surfaces exposed to outer space and the stability of the thermal properties of these surfaces in the total space environment. Furthermore, this information must be obtained under conditions as near to outer space as possible, i. e., simulation and measurement without return to the atmospheric conditions.

This is borne out by the fact that during the course of work of many investigators⁽¹⁻⁷⁾ effects were noticed which were modifying data upon exposure of the samples to atmospheric environments.

A rapid bleaching of damage was taking place in some materials when exposed to atmosphere. This bleaching was masking the true results of the test and was leading to erroneous conclusions. In order to properly investigate the effects of space environment, certain improvements had to be made in the equipment. It became apparent that an in situ capability for making reflectance measurements was necessary.

The primary aim of NASA Contract NAS2-3646 was to fabricate equipment and perform the investigation of space degradation on selected thermal control coatings in situ. The parameters which could be simultaneously simulated were solar electromagnetic radiation, charged particles, ultrahigh vacuum and equilibrium temperature. Of these, the parameters chosen as variables were the electromagnetic radiation, proton energy and proton flux.

The first half of the contract was spent in the design and fabrication of in situ equipment and the last half in the performance of the tests to qualify the equipment and test coating materials as prescribed by NASA.

The system as fabricated under this contract was adapted to an existing chamber at Avco/Tulsa and is described under Section III, Test Equipment. It provides for multi-sample irradiation and selective transfer to the integrating sphere for reflectance measurements. In addition, during the time of fabrication of the in situ equipment, tests were conducted of non-in situ type on materials which were considered more stable. The results of these tests are reported in the pages following the results of the in situ tests.

II. PROGRAM SCOPE

The program consisted of two phases: (1) Design, fabrication and qualification of test equipment, and (2) in situ testing of designated materials. These phases are described in the following paragraphs.

A. Phase I - Design, Fabrication and Qualification

The scope of this portion of the program was the design of a mechanism which would adapt to an existing vacuum chamber and transfer four 15/16-inch diameter selective samples from the irradiation position to the reflective measurement position. The sample was to operate over a temperature range of -100°F to 300°F position and the samples easily removable for transfer. In addition, various accessory items were required in order to adapt the existing beam line and monochromator to the in situ chamber system.

The integrating sphere was to be mounted on the end of the vacuum chamber coated inside with magnesium oxide and having vacuum sealed windows for light input and detectors. This position was selected for the sphere because it was felt that (1) it would be more difficult to feed the light from the monochromator and optical switch into the sphere, (2) the detectors require special consideration to prevent outgassing problems, and (3) no vacuum tight electrical feedthroughs through the chamber were necessary if the sphere is on the outside.

The qualification was to consist of comparison measurements against a Gier-Dunkle integrating sphere over a wavelength range of 0.30 to 2.5 microns for both diffuse and specular samples. The diffuse samples were specified as $\text{ZnO}/\text{K}_2\text{SiO}_3$ and the specular samples as SiO_x on vapor deposited aluminum. Five sets of measurements were required on each sample and the mean spectral deviation determined to demonstrate the reproducibility of the equipment.

B. Phase II - Test Program

1. Sample Materials

The materials which were selected for in situ test were ZnO/K₂SiO₃, (two batches F-1-47-D and 1-11-9-13), La₂O₃/K₂SiO₃ (two batches F-1-53A and F-1-38), S-13G, ZnO/Silicone, TiO₂/Silicone and powdered samples of MgO, TiO₂, SiO₂, Al₂O₃ and La₂O₃. Non-in situ radiations were conducted on SP500 ZnO powder and vacuum deposited silver on fused silica. Test specimens are described in Table I.

2. Description of Irradiation Tests

In the majority of the in situ irradiation tests, one sample was to be subjected to an environment including vacuum and near ultraviolet. A second sample was to be subjected to a combined environment including proton irradiation, ultraviolet and vacuum ultraviolet. A third sample was to be subjected to protons radiation only and the fourth sample was to be used as a control sample and incurred only vacuum. The following parameters were to be used in the tests:

a. Near Ultraviolet Radiation

Ultraviolet radiation on the 2000-4000 angstrom range provided by a 5 KW xenon lamp installed in the solar simulator for the first three tests and a 5 KW mercury xenon lamp for all non-in situ tests and the remainder of the in situ tests. It was determined during the program that the xenon lamp would provide various irradiance values from 5.5 solar constants to 7.5 solar constants. The Hg Xe lamp was to operate at a rate of 10 solar constants. Total ultraviolet exposure was to be 750 sun hours with both lamps.

b. Vacuum Ultraviolet Radiation

Radiation in the 1050 to 2000 angstroms range was to be supplied by a hydrogen discharge lamp at 10 solar equivalents of Lyman-alpha for 75 hours per test.

SPECIMEN	SOURCE	PURITY %	PARTICLE SIZE	COMMENTS
AL ₂ O ₃	Linde Division Union Carbide Company	99.98	0.05μ	Metallurgical Grade Pressed into recessed AL holder 1/16" deep, with black coating, at 2000 psi, covered with quartz disk until exposed
La ₂ O ₃	Rare Earth Division American Potash and Chemical Corporation	99.99	3.5μ	Code 529, hygroscopic, could be partially La(OH) ₃ at surface
MgO	Vitro Labs	99.41	0.025μ	Sub micron size, Plasma arc product
SiO ₂	Thermal American Fused Quartz Co.	99.7	~ 40.μ	"Spectrosil" Grade or Better
TiO ₂	E. I. DuPont DeNemours and Company (Inc.)	88 TiO ₂ 3% Max. AL ₂ O ₃ 8% Max. SiO ₂	0.22μ	Ti Pure R-960 slightly hygroscopic This TiO ₂ has a SiO ₂ coating which increases particle size < 0.1μ
ZnO	New Jersey Zinc Co.	99.9	0.25-0.35μ	SP-500, Super purity
S-13G	This was a typical S-13G sample composition supplied by Jet Propulsion Laboratory.			

TABLE I - TEST SPECIMENS
DESCRIPTION

SPECIMEN	SOURCE	COMMENTS
1-11-9-13	S. P. - 500 ZNO New Jersey Zinc Co. P. S. - 7 (K_2SiO_3) Sylvania Electronics (35% Solids)	P. B. R. = 2.15 Ball Milled 2 Hours Sprayed ~ 6 coats oven cured $150^\circ C$ for 1 hour. Thickness ~ 6 mil. Paasche type AUTF Air Brush used to apply all coatings.
F-1-47D Binder P.S. -7	S. P. - 500 ZNO P. S. - 7 (K_2SiO_3) Same as above	P. B. R. = 5.2 Ball Milled 4 hours Sprayed 6 coats ~ 4 mil - Oven cured $150^\circ C$ ZNO calcined $1200^\circ F$ 16 hours cured vac. oven 29" HG & $150^\circ C$ 1 hour
F-1-55	S. P. 500 ZNO R. T. V. - 602 General Electric Silicone N-Butanol (Reagent Gr) Mallinckrodt Chemical	P. B. R. = 2.4 Ball Milled 2 hours Sprayed 6 coats - Oven cured $150^\circ C$ 1 hour ~ 6.5 Mil thickness - P. V. C. = 30% Undercoat SS4044 (General Electric) Silicone Primer - Sprayed ~ 5 mil
F-1-38 Binder P.S. -7	LA_2O_3 Code 529 Rare Earth Division American Potash & Chemical Corporation	P. B. R. = 5 LA_2O_3 Calcined $2000^\circ F$ - 16 hours Ball Milled 4 hours - Sprayed 6 coats Cured at Ambient ~ 6 mil LA_2O_3 converted to $LA(OH)_3$ during ball milling
F-1-53A Binder P.S. - 7	LA_2O_3 Code 529	P. B. R. = 1.75 LA_2O_3 Silicate treated (Encapsulated in K_2SiO_3) - Oven dry $150^\circ C$ 1 hour Ball Milled 2 hours - Sprayed 8 coats ~ 4 mil thickness
F-1-56	TiO_2 R-960 Ti Pure E. I. DuPont DeNemours and Company (Inc.) R. T. V. - 602 G. E. N-Butanol (R. G.)	P. B. R. = 2.5 Ball Milled 3 hours Oven cured $300^\circ F$ - 1 hour P. V. C. = 34.7% Sprayed 9 coats ~ 8 mil thickness Undercoat SS4044 (General Electric) Silicone Primer - Sprayed ~ 5 mil

TABLE I - TEST SPECIMENS
DESCRIPTION

c. Protons

All of the tests were to be conducted with 10 Kev protons. Total proton fluxes were to vary from 2×10^{15} p/cm² to 1×10^{16} p/cm².

In some tests proton irradiations were to be carried out at a continuous low flux rate for 75 hours, and in other tests, "accelerated", a higher flux rate was to be used at the beginning of the test.

d. Sample Temperature

Sample temperatures were to be maintained near 298°K for the various tests.

e. Chamber Pressure

No test was to be initiated until pressure in the test chamber was 10^{-7} torr or less.

3. Determination of α_s and $\Delta\alpha_s$

Spectral reflectance measurements were to be made on the samples before and after each irradiation in the non-in situ tests and before, during, and after irradiation in the in situ testing. Spectral reflectance curves were to be plotted from these data.

Solar absorptance values were to be obtained by averaging representative values of spectral reflectance obtained from the curves for each two percent extra-terrestrial solar energy increment in the measured wavelength range and subtracting these average values from unity. The solar absorptance values presented will not be total values relating to the entire spectrum, since this would require measured spectral reflectance values to 3.9 microns which is beyond the measured range of the detectors used. The values given will be related to the measured wavelength range.

III. TEST EQUIPMENT

Avco's space simulation facility is shown schematically in Figure 1. It consists of an ultra-high vacuum chamber with the newly designed in situ reflectometer system, solar simulator, transition section and Van de Graaff accelerator. The various components of the system, beginning with the new items designed under this contract, are described in the following paragraphs.

A. In Situ Reflectometer System

The system was designed to selectively transfer any one of four samples in the sample holder (irradiation position) to the integrating sphere or vice versa. This may be accomplished at pressures of 1×10^{-7} torr or less. It was designed to fit an existing Avco ultra-high vacuum chamber. Dimensional information for the various components is given in the appendix.

1. Transfer Arm Assembly

The transfer arm, shown in Figure 2, (Item 19, Figure 1), is mounted on a large flange at the side of the chamber and a bellows provides the necessary vacuum seal. The transfer arm is pivoted for movement in two directions and stops are provided to prevent over travel. The arm is coupled to a slider bar to which is attached "U" shaped fingers. These fingers will fit around a protrusion on the conical plugs on which the sample is fastened. The slider bar slides in a pivoted retainer mounted on arms also pivoted at the gimball mount on the flange. When the slider bar is caused to slide back against a spring stop, further movement of the transfer arm causes the arm to swing in an arc and thus turn the sample 180° . This movement of the transfer arm in an arc of approximately 60° will cause the sample to be removed from the sample holder and plugged in to the integrating sphere or vice versa.

2. Sample Holder Assembly

The sample holder assembly which was designed and fabricated for this study is shown in Figure 3 (Item 18, Figure 1). It is a large copper block which has four

8

7

6

5

4

3

2

1

LEGEND	
1	ION SOURCE
2	HYDROGEN GAS
3	VAN DE GRAAFF ACCELERATOR
4	ACCELERATION TUBE
5	VALVE
6	DIFFUSION PUMP AND BAFFLE
7	ANALYZER MAGNET
8	QUADRAPOLE LENS ADAPTER
9	BEAM MONITOR
10	BELLOWS
11	DIFFERENTIALLY PUMPORFICE SECTION
12	DIFFERENTIAL ION BOOSTIVAC PUMP
13	EUV SOURCE PORT
14	UV BEAM PORT
15	DEFLECTION PLATES
16	MIRROR
17	ULTRA-HIGH VACUUM CHAMBER
18	SAMPLE HOLDER
19	TRANSFER ARM
20	INTEGRATING SPHERE
21	DETECTOR PORT

REVISIONS				
ZONE	LTR	DESCRIPTION	DATE	APPROVED

D

D

C

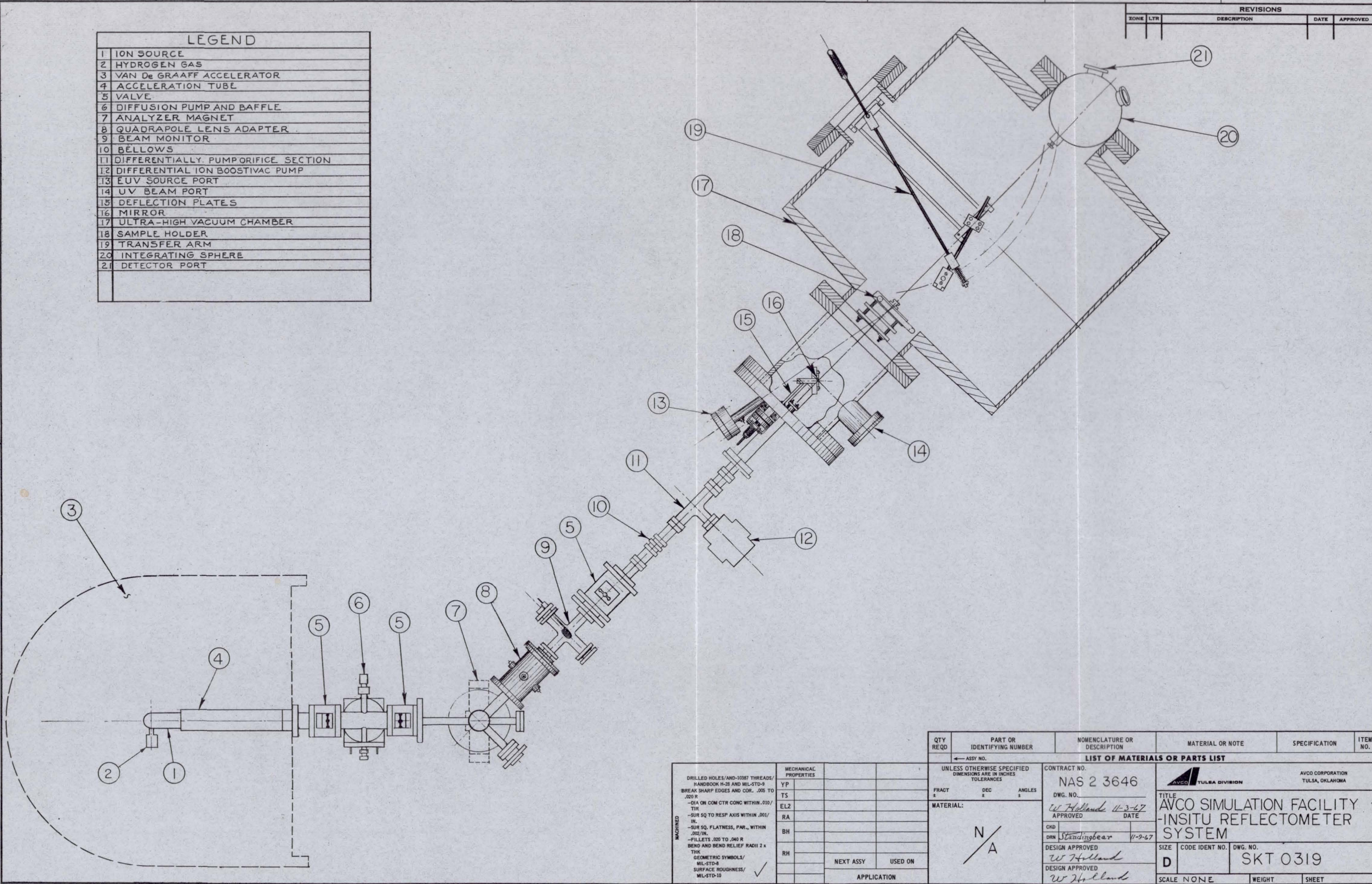
C

B

B

A

A



MACHINED

DRILLED HOLES/AND-10387 THREADS/
HANDBOOK H-28 AND MIL-STD-9
BREAK SHARP EDGES AND COR. .005 TO
.020 R
-DIA ON COM CTR CONC WITHIN .010/
TIR
-SUR SQ TO RESP AXIS WITHIN .001/
IN.
-SUR SQ. FLATNESS, PAR., WITHIN
.002/IN.
-FILLETS .020 TO .040 R
BEND AND BEND RELIEF RADI 2 x
TRK
GEOMETRIC SYMBOLS/
MIL-STD-8
SURFACE ROUGHNESS/
MIL-STD-10

MECHANICAL PROPERTIES	
YP	
TS	
EL2	
RA	
BH	
RH	

NEXT ASSY USED ON

APPLICATION

QTY REQD	PART OR IDENTIFYING NUMBER	NOMENCLATURE OR DESCRIPTION	MATERIAL OR NOTE	SPECIFICATION	ITEM NO.
← ASSY NO. LIST OF MATERIALS OR PARTS LIST					
UNLESS OTHERWISE SPECIFIED DIMENSIONS ARE IN INCHES TOLERANCES		CONTRACT NO. NAS 2 3646		AVCO CORPORATION TULSA, OKLAHOMA	
FRACT	DEC	ANGLES	DWG. NO. <i>W Holland 11-3-67</i>	TITLE AVCO SIMULATION FACILITY -INSITU REFLECTOMETER SYSTEM	
MATERIAL: N/A			APPROVED DATE	AVCO TULSA DIVISION	
			DRN <i>Standingbear 11-9-67</i>	AVCO CORPORATION TULSA, OKLAHOMA	
			DESIGN APPROVED <i>W Holland</i>	SIZE D	CODE IDENT NO. SKT 0319
			DESIGN APPROVED <i>W Holland</i>	DWG. NO.	
			SCALE NONE	WEIGHT	SHEET

DO NOT SCALE DRAWING

FIGURE 1

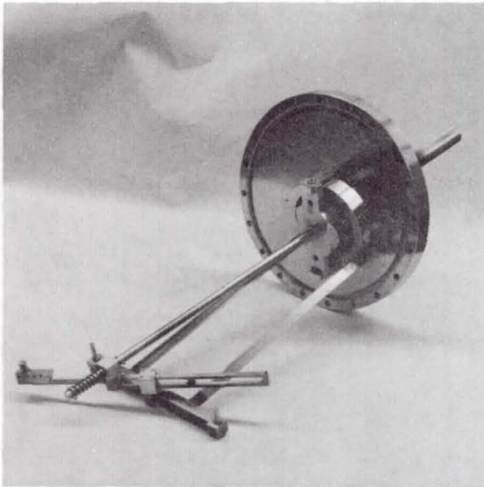


Fig 2 - Transfer Arm

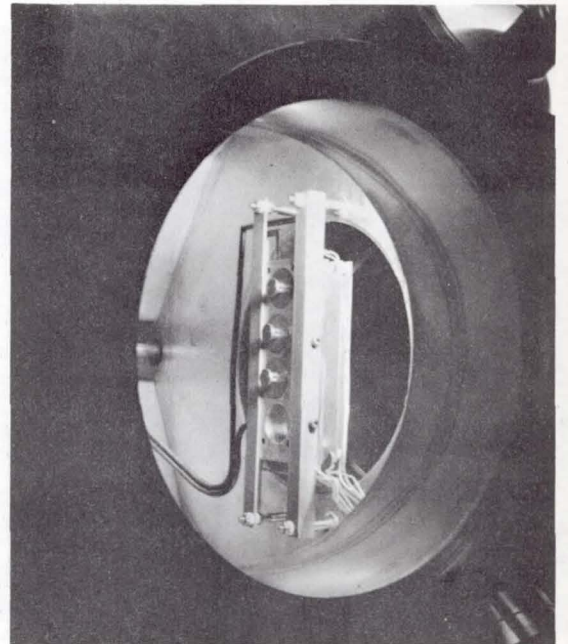


Fig 3 - Sample Rack, Mounted In Chamber

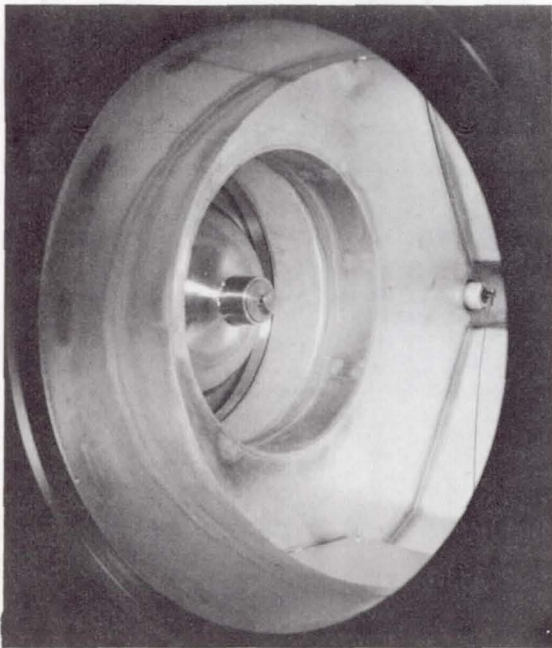


Fig 4 - Integrating Sphere - Vacuum View

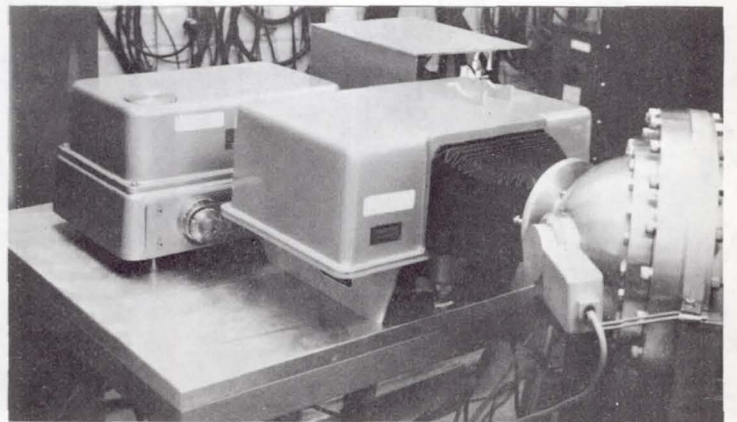


Fig 5 - Integrating Sphere - Atmosphere View

conical shaped holes arranged in a slight vertical arc because of the motion of the transfer arm. The samples can be clamped to conical plugs which fit in the holder. Three samples face the sources of radiation and one, mounted in the bottom of the holder, is shielded from these sources. Coolant fluids can be circulated through the sample holder via stainless steel tubing running through an insulated feedthrough which isolates the holder from ground. A cartridge heater is installed in the holder for maintaining higher temperatures. A thermocouple is spring loaded against the back of the sample which is irradiated by both particulate and electromagnetic radiation.

The samples tested are nominally 15/16-inch in diameter. The sample area which is exposed to radiation is 13/16-inch in diameter, since the samples are clamped at the edge. Two plates are mounted on insulating standoffs from the face of the sample holder. The plate farthest from the holder faces serves to collimate the particle beam and thus define the area of sample and sample holder which is irradiated. Two 15/16-inch diameter holes in this plate are centered over the samples. The charged particle beam as it is incident on this plate is rectangular, approximately 1-1/8-inches long x 3/16-inch wide. The beam is rastered across the appropriate collimating hole in the plates by the sawtooth voltage applied to the deflection plates. The collimating plate is connected to an insulated feedthrough in the four-inch vacuum-flange and may be grounded or biased as necessary. The purpose of the intermediate plate is to serve as a secondary electron suppressor. The charged particle beam passes through a short section of tubing in this plate. The plate (and tubing) is biased negatively with respect to the sample holder and collimating plate to force secondary electrons arising from particle bombardment back to their respective sources. Target current is read directly by connecting a meter to the insulated feedthrough which supports the sample holder. When samples which are good insulators, such as the paints, are being irradiated, a grid consisting

of five parallel strands of one mil stainless wire is mounted in contact with the sample surface. This grid masks less than one percent of the sample area and serves to prevent the sample surface from becoming electrically charged with consequent "chasing" of the particle beam and inaccurate beam current readings.

3. Integrating Sphere

The integrating sphere is shown in figures 4 and 5 (Item 20, Figure 1). It was fabricated from two stainless steel hemispheres to which were welded mounting flanges to mount on the chamber. It has three ports, one for the sample, one for the detector and one for the light from the Perkin-Elmer Model 112U spectrophotometer. It is coated inside with magnesium oxide and a baffle is mounted inside the sphere to prevent the light from the sample from seeing the detector directly.

B. Vacuum Chamber

The Avco ultra-high vacuum chamber is shown schematically in Figure 6 (Item 17, Figure 1). It has a normal working volume of 24" x 24" in the form of a right circular cylinder. This chamber has a ratio of total volume to useful volume of approximately 90%. The chamber was fabricated and welded with low carbon stainless steel. Ports entering into the vacuum chamber itself are metal gasketed and are 10.75" in diameter for access purposes or 1.5" in diameter for instrumentation. In addition, a four-inch port is provided for electrical feed-throughs. The chamber is pumped with 900 liters/sec of cold cathode ion getter pumping system. The system is comprised of a high voltage source, a magnet assembly, and two active pumping element assemblies. The magnetic field in the region of the pump cells is approximately two kilogauss provided by the magnet assembly. The chamber is a double wall chamber and the annulus between the cylinders, except in regions taken up by feedthroughs and flanges, serves as a passage for liquid nitrogen or other coolants to provide cold surrounds and some cryogenic pumping if desired.

C. Van de Graaff Accelerator

The accelerator (Item 3, Figure 1) is capable of accelerating positive ions or electrons in the energy range from about

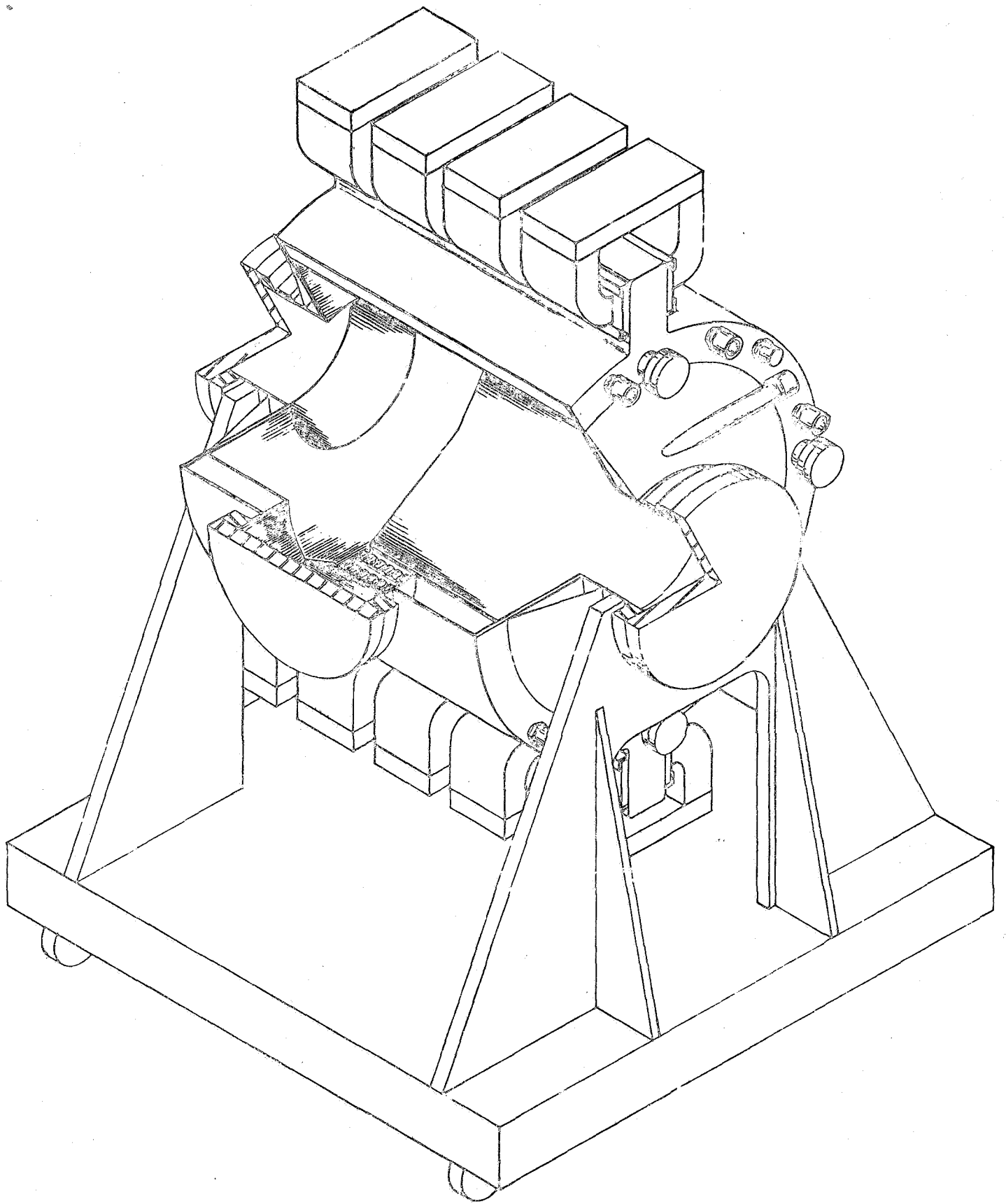


Figure 6 - WALL-PUMP ULTRA-HIGH VACUUM SYSTEM

10 Kev to 500 Kev. The Van de Graaff voltage generator is used from about 500 Kev down to 100 Kev, below which point the voltage stability becomes poor. Energies below 100 Kev are provided by disabling the Van de Graaff voltage generator in the accelerator and connecting an auxiliary 0 - 100 kilovolts power supply across the acceleration tube. Positive ions are generated by an R.F. ion source. The accelerator is pumped by a four-inch oil diffusion pump containing Dow Corning 705 diffusion pump oil. A Freon cooled baffle prevents migration of oil into the system. Basic pressure in the accelerator is about 10^{-6} torr as measured by a Phillips ionization gauge and pressure during operation is in the $0.6 - 1 \times 10^{-5}$ torr range.

The accelerator is equipped with an analyzing magnet to provide mass analysis of the ion beams. The analyzed beam which is used is bent at an angle of 45° to the accelerator axis.

D. Transition Section and Beam Scanner

After leaving the analyzing magnet, (Item 7, Figure 1), the beam passes through a glass cross (Item 9, Figure 2). Within the cross a monitor, consisting of a Vycor disc covered with a stainless steel screen, can be positioned to intercept the beam. This provides a beam current readout at that point and also a visual observation, since the glass fluoresces when the ions or electrons impinge upon it.

The accelerator and chamber are separated by a differentially pumped section to isolate the ultra-high vacuum region of the chamber from the moderately high vacuum region of the accelerator. The differentially pumped section is terminated at either end by rectangular slit orifices which help to limit gas conductance, and also serve to collimate the charged particle beam prior to entrance into the beam scanner. Pressure in the differential section is normally about 1.5 orders of magnitude lower than that in the accelerator. Pressures in the chamber are normally in the 10^{-8} to 10^{-10} torr range during operation.

The beam scanner consists of a pair of electrostatic deflection plates. The collimated beam passes between these plates and is moved to sample center by application of a d. c. bias and then "rastered" across the required area by means of a low frequency sawtooth voltage applied to the plates.

E. Solar Simulator

The solar simulator utilizes a 5 kilowatt short-arc lamp, either xenon or xenon-mercury to simulate the solar spectrum. The light from the simulator is beamed through a quartz window in the port (Item 14, Figure 1), and reflected from an aluminized front face mirror onto the samples. The lens system in the simulator provides for focusing the light such that with the end of the simulator barrel about one-fourth inch from the quartz window flange, a uniform three-inch diameter beam is obtained at a distance of 14 inches from the mirror. Total intensity was expected to be in excess of ten solar constants with either type tube. However, it was not possible to achieve ten solar equivalents in the 0.2 - 0.4 micron range with the Xe lamp so that the Xe-Hg lamp was used for the balance of the study.

F. Lyman-Alpha Source

The vacuum ultraviolet source of Avco design is essentially a Penning discharge tube with water-cooled anode and cathodes. Light from this source is beamed through a lithium fluoride window onto the samples. The source provides energy in the 0.105 to 0.2 micron range. With hydrogen gas it is essentially a line source with the Lyman-alpha line at 1216 \AA as the most prominent. The port for the source is shown in Figure 1, Item 13.

G. Reflectance Measuring Apparatus

Reflectance measurements are made with a Perkin-Elmer Model 112-U spectrophotometer attached to the Avco designed integrating sphere. A-Pek Model X-75 xenon lamp and Gier-Dunkle Model RXS-1 power supply were obtained to provide sufficient intensity for reflectance measurements below 0.4 microns. A tungsten lamp is used for measurements at longer wavelengths.

H. Non-In Situ System

The system used for irradiation and measurement of samples for non-in situ testing has been used in performance of other contracts and is adequately described in previous reports. (1)

IV. EQUIPMENT CALIBRATION AND EVALUATION

A. In Situ Reflectometer System

Evaluation of the in situ reflectometer was performed by comparing spectral reflectance measurements in the in situ integrating sphere with measurements in the Gier-Dunkle AIS-6 integrating sphere for a ZnO/K_2SiO_3 sample and for SiO_x on vapor deposited aluminum. Five sets of spectral reflectance measurements were made on each sample to check repeatability of the equipment. The attached tables show the measured values obtained in the Gier-Dunkle sphere and in each of the five sets of measurements in the in situ sphere, the averages of the five sets of measurements, and the maximum deviation from the average at each wavelength. Measurements are presented only over the wavelength range measureable with a tungsten lamp because of problems with the xenon lamp power supply.

Figures 7 and 8 present comparative spectral reflectance curves for the two spheres for the ZnO/K_2SiO_3 and SiO_x on vapor deposited aluminum respectfully.

B. Particle Energy and Flux

Particle energy is essentially determined by the potential drop across the acceleration tube in the accelerator. When the Van de Graaff voltage generator is being used, the generating voltmeter on the Van de Graaff has been calibrated to read directly the particle energy. The calibration was performed as follows:

The particle beam from the accelerator after collimation by the orifice slits passes between the electrostatic deflection plates of the beam scanner. The beam was permitted to fall on a Pyrex window and the resultant fluorescence marked the position of the beam. By applying a d. c. potential to the deflection plates the beam was moved to a different position. The accelerating potential was determined from the well known equation

$$V_A = \frac{ld}{2tx} V_d$$

TABLE II
 Comparison of Measurements in
 In Situ Sphere With Those in Gier-
 Dunkle Sphere at Atmosphere
 for ZnO/K₂SiO₃

Wavelength (Millimicrons)	Spectral Reflectance							Max. Deviation From Average
	Gier- Dunkle	1	2	In Situ Sphere		5	Ave.	
				3	4			
390	63.5	63.4	63.0	64.6	64.3	62.9	63.6	1.0
400	78.4	77.1	75.7	76.4	76.2	76.5	76.4	0.7
410	82.6	81.7	81.7	81.6	80.7	81.5	81.4	0.7
420	86.0	85.5	84.4	84.4	81.7	85.1	84.2	1.3
430	88.0	85.8	86.3	86.4	89.1	87.2	87.0	2.1
440	89.8	88.2	87.7	89.3	88.4	87.7	88.3	1.0
450	90.6	89.7	89.2	89.4	88.1	89.3	89.1	1.0
460	91.8	90.4	89.6	90.1	91.2	89.7	90.2	1.0
470	92.1	91.0	89.9	90.4	90.8	90.0	90.4	0.6
480	92.5	90.3	90.3	90.7	91.2	90.7	90.6	0.6
490	93.6	91.1	91.7	91.9	90.9	91.5	91.4	0.5
500	94.6	91.2	91.5	92.0	91.9	91.6	91.6	0.4
510	93.8	92.4	91.8	92.8	93.3	92.2	92.5	0.8
520	94.1	93.1	93.2	93.5	92.6	93.1	93.1	0.5
530	94.5	91.7	93.5	93.0	91.8	93.2	92.6	0.9
540	94.5	92.8	92.1	92.8	92.7	93.8	92.8	1.0
550	94.3	91.3	92.0	93.5	93.2	93.5	92.7	1.4
560	94.6	91.7	93.2	93.8	92.3	93.6	92.9	1.2
570	94.6	92.8	93.5	93.2	93.7	93.9	93.4	0.6
580	94.8	93.2	93.9	92.5	93.8	94.1	93.3	0.8
600	94.4	93.3	92.9	93.3	92.7	93.7	93.2	0.5
630	94.8	93.4	93.8	94.3	93.9	94.7	94.0	0.7
660	95.3	92.5	93.5	93.7	94.4	92.9	93.4	1.0
600	95.9	92.2	92.4	93.2	92.8	93.4	92.8	0.6
630	95.1	92.4	91.9	92.5	93.5	93.0	92.7	0.8
660	95.1	92.4	92.1	92.9	92.3	93.4	92.6	0.8
700	95.3	93.4	92.4	92.4	93.2	94.1	93.1	1.0
750	94.9	92.9	92.8	93.7	92.7	93.2	93.1	0.6
800	94.4	93.1	92.3	93.6	92.3	93.9	93.0	0.9
900	94.1	92.0	92.4	93.1	92.4	92.9	92.6	0.6
1000	93.4	89.6	92.0	93.5	91.2	91.7	91.6	2.0
1100	92.5	91.7	91.7	92.2	91.8	92.3	91.9	0.4
1200	91.8	92.3	91.0	91.7	91.9	90.5	91.5	1.0
1300	91.2	90.4	91.2	90.0	90.1	90.4	90.4	0.8
1400	90.3	89.2	88.5	88.9	88.6	88.5	88.7	0.5
1500	87.9	87.5	88.2	88.3	88.4	87.7	88.0	0.5
1600	86.7	86.7	87.0	86.4	87.4	86.2	86.7	0.7
1700	85.2	84.9	85.0	85.2	85.9	85.5	85.3	0.6
1800	82.5	82.5	83.0	83.4	82.7	83.7	83.1	0.6
1900	78.9	78.9	79.4	79.1	78.7	79.5	79.1	0.4
2000	75.7	75.4	75.4	75.8	76.3	75.2	75.6	0.7
2100	74.6	74.8	74.9	74.9	74.4	75.8	75.0	0.8
2200	73.0	73.2	73.3	73.2	73.5	74.1	73.5	0.6
2300	68.8	68.6	68.7	68.7	68.3	68.8	68.6	0.3
2400	64.2	64.1	63.7	63.9	63.4	63.8	63.8	0.4

↑ P.M. Tube
↓
↑ Pb S Cell
↓

TABLE III
 Comparison of Measurements in
 In Situ Sphere With Those in Gier-
 Dunkle Sphere at Atmosphere
 for SiO_x on Vapor Deposited Aluminum

Wavelength (Millimicrons)	Spectral Reflectance							Max. Deviation From Average
	Gier- Dunkle	1	2	In Situ Sphere			Ave.	
390	47.5	45.1	43.9	44.6	44.1	44.4	44.4	0.7
400	50.2	46.2	45.3	46.6	46.2	46.2	46.1	0.8
410	51.4	47.2	47.9	47.9	48.2	48.0	47.8	0.6
420	52.9	49.5	49.9	50.4	49.6	50.2	49.9	0.5
430	52.9	51.8	52.0	51.5	51.1	53.5	52.0	1.5
440	54.7	52.9	53.5	53.6	53.3	53.7	53.4	0.5
450	56.4	54.0	55.2	54.7	55.2	54.5	54.7	0.7
460	57.8	55.8	55.8	56.4	56.5	56.5	56.2	0.4
470	58.8	56.4	57.2	57.3	56.9	57.6	57.1	0.7
480	60.5	57.5	58.5	59.1	59.0	58.8	58.6	1.1
490	62.2	60.0	59.9	60.5	60.3	60.1	60.2	0.3
500	64.6	61.2	61.9	61.8	61.4	62.3	61.7	0.5
510	66.3	63.0	63.2	63.3	63.3	63.7	63.3	0.4
520	66.6	64.4	65.0	64.4	64.8	64.4	64.6	0.4
530	66.8	64.8	65.4	66.0	65.3	65.8	65.5	0.7
540	67.9	65.4	66.7	66.0	65.8	66.6	66.1	0.7
550	68.1	66.4	67.0	66.6	67.1	66.7	66.8	0.4
560	68.9	67.5	68.2	67.0	67.7	66.9	67.5	0.7
570	69.4	67.5	68.0	68.1	67.8	68.5	68.0	0.5
580	70.2	68.4	69.5	68.8	68.9	68.6	68.8	0.7
600	71.1	68.7	69.2	68.6	69.8	69.1	69.1	0.7
630	72.5	69.6	70.0	70.3	70.1	70.3	70.1	0.5
660	73.7	69.7	71.3	70.7	70.4	71.1	70.6	0.9
600	71.3	67.2	69.2	67.3	67.4	68.2	67.9	1.3
630	72.3	67.9	68.7	69.2	68.6	68.7	68.6	0.7
660	73.8	69.1	69.1	70.2	69.7	70.9	69.8	1.1
700	74.3	69.3	70.0	70.1	69.4	70.3	69.8	0.5
750	72.9	68.5	69.7	69.2	69.2	68.4	69.0	0.7
800	71.4	66.5	67.3	67.4	67.4	67.3	67.2	0.7
900	80.0	75.6	75.6	75.8	75.6	75.2	75.6	0.4
1000	87.9	82.3	82.9	83.2	82.6	83.5	82.9	0.6
1100	90.9	84.0	84.9	85.9	85.0	85.4	85.0	0.9
1200	93.0	85.8	87.8	87.7	86.4	87.4	87.0	1.2
1300	93.8	88.7	89.0	88.1	87.8	87.8	88.3	0.7
1400	93.9	88.0	88.4	88.4	87.4	87.2	87.9	0.7
1500	94.8	88.0	89.0	88.9	89.4	88.8	88.8	0.8
1600	95.3	89.8	90.2	90.8	89.8	90.3	90.2	0.6
1700	95.2	90.7	91.5	91.0	90.5	90.8	90.9	0.6
1800	95.4	90.1	91.0	91.7	91.4	91.6	91.2	1.1
1900	95.3	91.0	91.8	92.0	91.9	91.5	91.6	0.6
2000	95.4	90.5	92.0	91.9	92.0	91.9	91.7	1.2
2100	95.8	91.8	93.1	92.9	92.2	92.2	92.4	0.9
2200	95.9	92.2	92.4	92.4	91.7	91.3	92.0	0.7
2300	95.5	89.5	90.1	89.9	89.8	90.6	90.0	0.6
2400	94.9	89.8	90.4	90.1	89.8	90.0	90.0	0.4

P. M. Tube
 ↓
 Pb S Cell

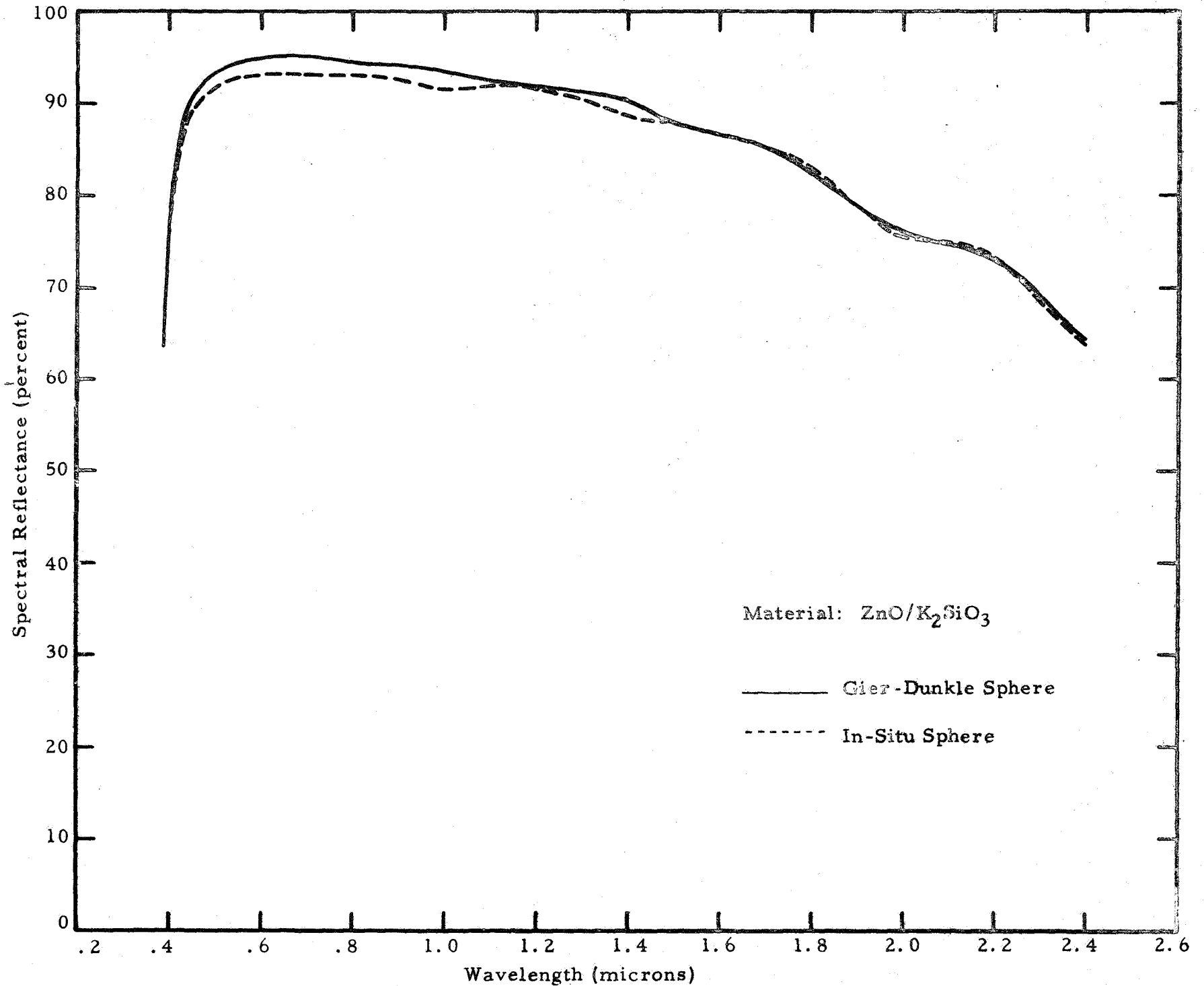


Figure 7 -- Comparison (In Air) of In Situ Integrating Sphere with Gier-Dunkle Sphere

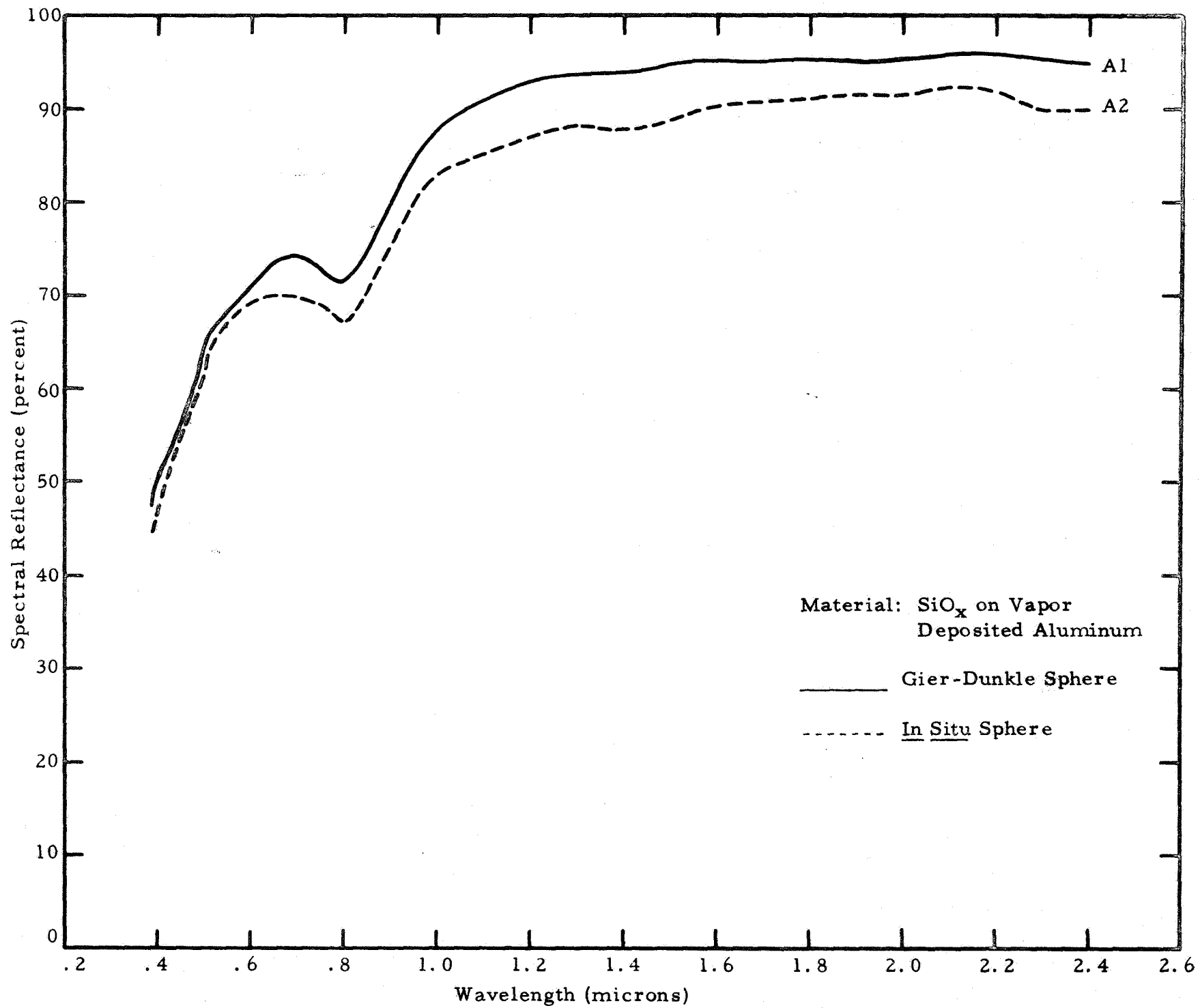


Figure 8 -- Comparison (In Air) of In Situ Integrating Sphere with Gier-Dunkle Sphere

where V_A is the acceleration voltage, l is the length of the deflection plates, d is the distance from the center of the plates to the glass window, V_d is the applied deflection voltage, t is the spacing between the plates, and x is the distance the beam was moved on the window.

The calibration was made at several accelerating potentials to accurately calibrate the readout meter.

When the auxiliary power supply is used, the reading from the meter on its control panel is used to determine the particle energy, i. e., a 10 kilovolt potential produces 10 Kev particles. This is not strictly true in the case of positive ions since in addition to the potential across the acceleration tube, the ions are given an initial acceleration to extract them from the R. F. ion source by application of a relatively low potential to the source probe. However, the total energy of the particles is known to within ten percent.

Charged particle flux is readily determined due to the geometry of the sample holder. As described in Section III. A. 2, the collimating plate mounted in front of the sample holder defines the area, A , of the sample and sample holder which is irradiated. The average current striking this area is directly measured by connecting a meter from the sample holder to ground. If this current, I , is noted in amperes, the flux is given by

$$\frac{I}{A} \times 6.25 \times 10^{18}, \text{ particles/cm}^2/\text{sec}$$

When a certain flux is required it is, therefore, simple to determine the required beam current and adjust the accelerator accordingly. The method used in adjusting for the desired current is to adjust for a current on the monitor in the glass cross section which will yield approximately the proper target current and to make final minor corrections after the beam is on target.

The target current is recorded on a strip chart recorder throughout the tests. The current is sufficiently stable that the total integrated flux in particles/cm² striking the samples during a test is known within an estimated fifteen percent.

C. Solar Simulator Calibration

The solar simulator was calibrated by duplicating the vacuum chamber geometry on a work bench. Spectral calibrations were made using a monochromator calibrated with an NBS standard quartz-iodine lamp, thus providing quantitative spectral intensity data. The ellipsoidal collecting mirror which was provided for the simulator was coated with an aluminized coating. Figure 9 compares plots of simulator spectral intensity with a Hg Xe lamp and using the aluminized collector with a plot of solar extraterrestrial spectral intensity according to Johnson.⁽⁸⁾ An analysis of the curve for the aluminized collector in Figure 9 shows that with 10 solar equivalents below 0.4 microns there were approximately 2.5 equivalents between 0.26 and 0.28, and 15 equivalents in the 0.26 to 0.30 micron range. These measurements were made with a new Xe-Hg lamp in the simulator.

D. Vacuum Ultraviolet Calibration

The vacuum ultraviolet light calibration was made with one centimeter nickel discs mounted at the sample positions in the sample holder, and with a nitric oxide ionization cell with a lithium fluoride window also at sample position. The nickel discs serve as photoelectric detectors. With a negative bias applied to the discs, the photoelectrons, which are generated primarily by Lyman-alpha photons, are ejected and the current is proportional to the light intensity. A quantum efficiency of 2.5 percent was assumed for the nickel based on data of Hinteregger and Watanabe.⁽⁹⁾ The overall quantum efficiency of the NO cell obtained from G. B. L. Associates was not known. Dunkleman⁽¹⁰⁾ states that efficiencies range from 10 to 50% for similar detectors.

A loop of 10 mil nickel wire permanently mounted close to the light source was cross calibrated to provide continuous monitoring of light intensity during the tests.

E. Non-In Situ System

Calibration of this system is adequately described in previous reports.⁽¹⁾

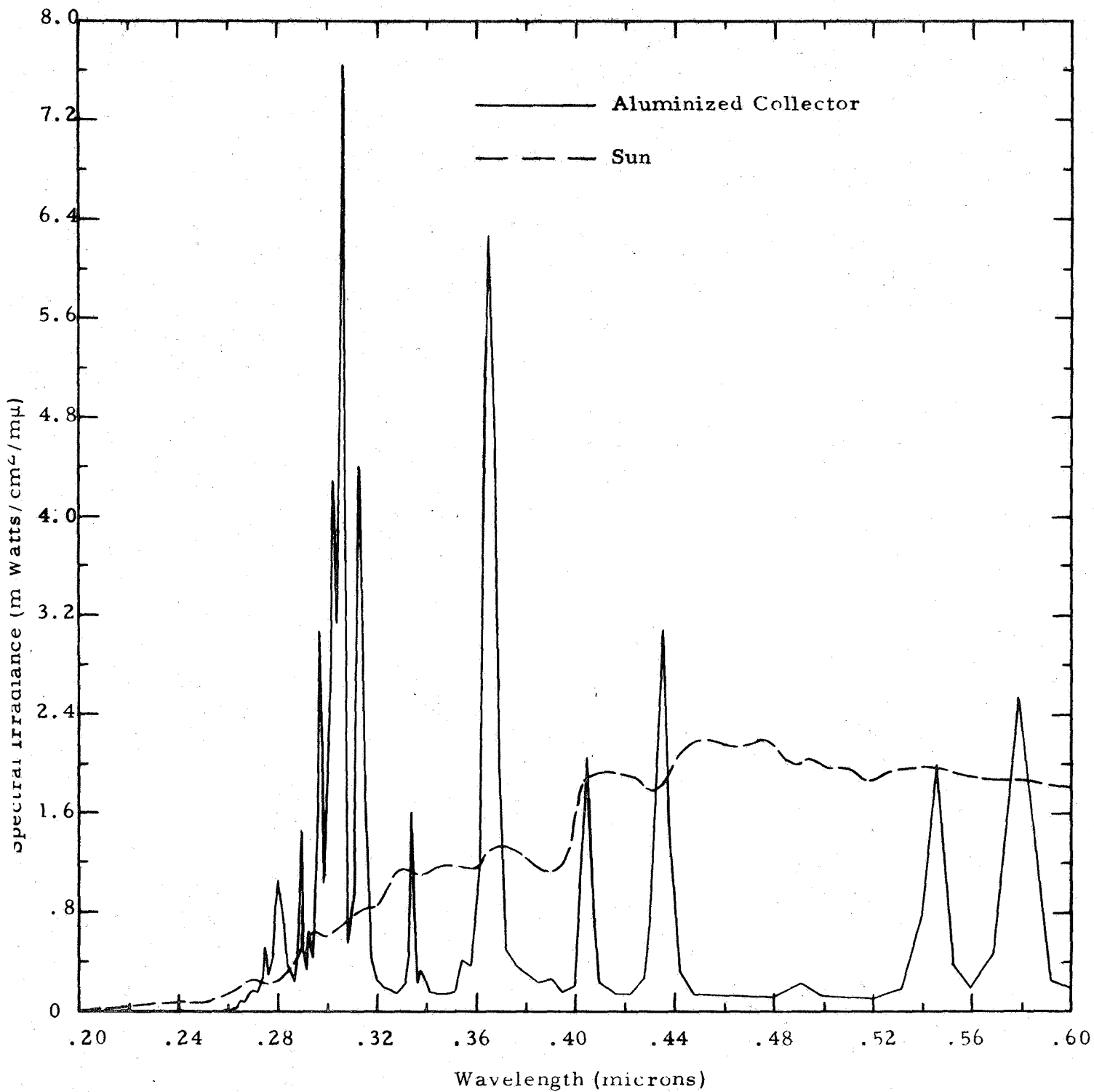


Figure 9 - SPECTRAL IRRADIANCE OF SOLAR SIMULATOR AT 10 SOLAR EQUIVALENTS

V. TEST PARAMETERS AND RESULTS

A compilation of all the sample materials, environmental parameters and values of α_s and $\Delta\alpha_s$ of the in situ tests are included in Table IV. Two values of $\Delta\alpha_s$ are presented, $\Delta\alpha_{s1}$ is the change at the end of the accelerated radiation, and $\Delta\alpha_{s2}$ is the change at the end of the test. The proton energy for each test was 10 Kev, the sample temperature was maintained at room temperature and the chamber pressure was 10^{-7} torr or less for every test. These items are not tabulated. Except in the tests with the xenon lamp which is given the near and vacuum, ultraviolet was applied at a rate of 10 solar equivalents for a total of 750 sun hours of electromagnetic radiation. This was chosen because it had been previously shown in non-in situ testing that this was about the minimum necessary to cause measurable optical damage to ZnO_2/K_2SiO_3 samples.

A total integrated proton flux of 2×10^{15} p/cm² was selected in the majority of the tests. In one test a total integrated flux of 1×10^{16} p/cm² was selected in order to determine if additional proton damage could be detected. In order to determine if a rate effect existed, some tests were conducted at an accelerated rate approximately 100 times the continuous rate. In the accelerated tests, the flux was applied for approximately one hour in order to obtain the same total integrated flux as in the continuous irradiation tests. Reflectance measurements were made on the samples in situ and were made at various times during the irradiation. The reflectance measurements were made over the range .34 to 2.4 microns.

TABLE IV

TEST PARAMETERS AND RESULTS

Test No.	Material	Batch & Sample No.	Near UV Sun Hrs.	Lyman- α Sun Hrs.	Protons		Initial a_s	Δa_{s_1}	Δa_{s_2}
					p/cm^2 sec	p/cm^2			
1	ZnO/K ₂ SiO ₃	1-11-9-13 #5			-----	-----	----	----	----
		1-11-9-13 #6			1.1×10^{12}	5.3×10^{15}	.181	----	.063
		1-11-9-13 #7			1.1×10^{12}	5.3×10^{15}	.180	----	.082
		1-11-9-13 #8			-----	-----	----	----	----
2	ZnO/K ₂ SiO ₃	1-11-9-13 #9			-----	-----	----	----	----
		1-11-9-13 #10			5.5×10^{11}	2×10^{15}	.190	.046	.041
		1-11-9-13 #11			5.5×10^{11}	2×10^{15}	.179	.043	.035
		1-11-9-13 #12			-----	-----	----	----	----
3	ZnO/K ₂ SiO ₃	1-11-9-13 #13			-----	-----	----	----	----
		1-11-9-13 #14			3.2×10^9	2×10^{15}	.183	----	.233
		1-11-9-13 #15			3.2×10^9	2×10^{15}	.192	----	.224
		1-11-9-13 #16			-----	-----	----	----	----
Hg Xe Lamp									
4	ZnO/K ₂ SiO ₃	F-1-47-D #1	750	750	-----	-----	.287	----	.020
		F-1-47-D #2	750	750	5.2×10^{11}	2×10^{15}	.287	.027	.035
		F-1-47-D #3	---	---	5.2×10^{11}	2×10^{15}	.291	.035	.031
		F-1-47-D #4	---	---	-----	-----	----	----	----
5	ZnO/K ₂ SiO ₃	F-1-47-D #5	750	750	-----	-----	.295	----	.023
		F-1-47-D #6	750	750	7.35×10^9	2×10^{15}	.287	----	.043
		F-1-47-D #7	---	---	7.35×10^9	2×10^{15}	.286	----	.048
		F-1-47-D #8	---	---	-----	-----	----	----	----

Test No.	Material	Batch & Sample No.	Near UV Sun Hrs.	Lyman- α Sun Hrs.	Protons		Initial a_s	Δa_s	
					p/cm^2 sec	p/cm^2		Δa_{s1}	Δa_{s2}
6	La ₂ O ₃ /K ₂ SiO ₃	F-1-53-A #1	750	750	-----	-----	.373	----	.036
		F-1-53-A #2	750	750	5.2×10^{11}	2×10^{15}	.346	.003	.025
		F-1-53-A #3	---	---	5.2×10^{11}	2×10^{15}	.339	.006	.002
		F-1-53-A #4	---	---	-----	-----	----	----	----
7	ZnO/Silicone	F-1-55 #1	750	750	-----	-----	.210	----	.021
		F-1-55 #2	750	750	7.35×10^9	2×10^{15}	.214	----	.083
		F-1-55 #3	---	---	7.35×10^9	2×10^{15}	.217	----	.047
		F-1-55 #4	---	---	-----	-----	----	----	----
8	ZnO/Silicone	F-1-55 #5	750	750	-----	-----	.213	----	.016
		F-1-55 #6	750	750	5.5×10^{11}	2×10^{15}	.211	.028	.044
		F-1-55 #7	---	---	5.5×10^{11}	2×10^{15}	.211	.038	.030
		F-1-55 #8	---	---	-----	-----	----	----	----
9	La ₂ O ₃ /K ₂ SiO ₃	F-1-38 #1	750	750	-----	-----	.201	----	.086
		F-1-38 #2	750	750	5.2×10^{11}	2×10^{15}	.194	.006	.086
		F-1-38 #3	---	---	5.2×10^{11}	2×10^{15}	.194	.010	.009
		F-1-38 #4	---	---	-----	-----	----	----	----
10	La ₂ O ₃ /K ₂ SiO ₃ ZnO/Silicone ³	F-1-38 #5	----	---	5.5×10^{11}	1×10^{16}	.189	----	.012
		F-1-55 #9	---	---	5.5×10^{11}	1×10^{16}	.218	----	.015
11	S-13G	A275 #1	750	750	-----	-----	.224	----	.012
		A275 #2	750	750	7.35×10^9	2×10^{15}	.227	----	.075
		A275 #3	---	---	7.35×10^9	2×10^{15}	.232	----	.047
		A275 #4	---	---	-----	-----	----	----	----
12	TiO ₂ /Silicone	F-1-56 #1	190	190	-----	-----	.212	----	.017
		F-1-56 #2	190	190	5.5×10^{11}	3×10^{15}	.209	----	.080
		F-1-56 #3	---	---	5.5×10^{11}	3×10^{15}	.212	----	.085
		F-1-56 #4	----	---	-----	-----	----	----	----

Test No.	Material	Batch & Sample No.	Near UV Sun Hrs.	Lyman- α Sun Hrs.	Protons		Initial a_s	a_s	
					$p/cm^2/sec$	p/cm^2		Δa_{s1}	Δa_{s2}
13	MgO (powdered)	-----	---	---	5.5×10^{11}	5×10^{15}	.158	----	.009
	TiO ₂ (powdered)	-----	---	---	5.5×10^{11}	5×10^{15}	.172	----	.108
14	SiO ₂ (powdered)	-----	---	---	5.5×10^{11}	5×10^{15}	.108	----	.004
	AL ₂ O ₃ (powdered)	-----	---	---	5.5×10^{11}	5×10^{15}	.096	----	.006
15	ZnO/K ₂ SiO ₃	1-11-9-13 #17	---	---	5.5×10^{11}	5×10^{15}	.184	.074	.058
16	LaO ₃ (powdered)	-----	---	---	5.5×10^{11}	5×10^{15}	.114	----	.007
	ZnO/K ₂ SiO ₃	F-1-47-D #9	---	---	5.5×10^{11}	5×10^{15}	.287	.077	.046

NON-IN SITU TESTS

Test No.	Material	Batch & Sample No.	Near UV Sun Hrs.	Lyman- α Sun Hrs.	Protons		Initial a_s	Δa_s
					$p/cm^2/sec$	p/cm^2		
1	ZnO Powder	-----	---	---	5.5×10^{11}	2×10^{15}	.124	.035
2	ZnO powder	-----	750	750	7.4×10^9	2×10^{15}	.120	.023
		-----	750	750	-----	-----	.125	.004
		-----	---	---	-----	-----	.124	-.003
3	Vac. Dep. Ag on Fused Silica	-----	750	750	5.5×10^{11}	1.5×10^{17}	.064	.060
		-----	750	750	-----	-----	.064	.001
		-----	---	---	-----	-----	.065	----

VI. DISCUSSION OF RESULTS

A. In Situ Tests

Sixteen exposure tests were conducted on various samples in which reflectance measurements were made in situ. Four samples were included in each test.

1. A sample exposed to vacuum, controlled temperature, and solar simulation.
2. A sample exposed to vacuum, controlled temperature, solar simulation and protons.
3. A sample exposed to vacuum, controlled temperature and protons.
4. A control sample exposed to vacuum and controlled temperature.

Proton exposures were conducted with a pure beam of 10 Kev protons.

1. Xenon Lamp

Three exposure tests were conducted on $\text{ZnO/K}_2\text{SiO}_3$ samples in which reflectance measurements were made in situ. Solar simulation for the tests was provided by a simulator using a 5 kilowatt xenon lamp. Spectral irradiance was to have been at a level of 10 solar equivalents of near ultraviolet. However, this level could not be attained so the highest levels attainable were used. Proton exposures were conducted with a pure beam of 10 Kev protons. All tests were conducted at a nominal temperature of 298°K as measured by a thermocouple in contact with the sample rack.

For the first test, simulated solar irradiance at sample position was approximately 5.5 solar constants with 3 solar equivalents in the near ultraviolet. Proton flux was greater than planned because of an error in current readout and because the beam narrowly missed one edge of the samples due to a misalignment in the beam line.

Proton flux was approximately 1.1×10^{12} p/cm²/sec and the integrated flux was 5.3×10^{15} p/cm². Because of the error in the proton flux, the test was stopped immediately after the proton irradiation.

Figures 10 and 11 show the change in spectral absorptance for the sample irradiated only with protons and for the sample exposed to the combined environment. The change in solar absorptance was .082 for the former and .063 for the latter. Changes are based upon pre-exposure measurements made in vacuum.

For the second test spectral reflectance measurements were made on each of the four samples before evacuating the test chamber and again about 24 hours later at a pressure in the 10^{-9} torr range. The primary result of the vacuum environment was to increase the reflectance of the samples by approximately 2% in the wavelength range of 1.6 to 2.4 microns.

The solar irradiance was the same at the beginning of this test as in the first test. The proton flux was to have been 5.5×10^{11} p/cm²/sec for one hour to obtain an integrated flux of 2×10^{15} p/cm². However, a problem in the proton beam scanning supply caused the beam to miss the sample exposed only to protons for a part of the irradiation period. After stopping the test it was found that the aluminum surface had evaporated from the mirror which reflects the light from the solar simulator onto the samples. This mirror is located in the vacuum chamber and could not adequately dissipate the heat from the absorbed infrared radiation.

Figure 12 is plotted from data taken for the sample exposed to the combined environment, since this sample was uniformly irradiated even though the proton flux and solar exposure cannot be accurately evaluated. The curves in Figure 12 are based upon changes from the pre-exposure spectral reflectance measurements in vacuum. The solid curve shows the change in spectral absorptance induced by the radiation from data taken immediately following proton irradiation. An absorption

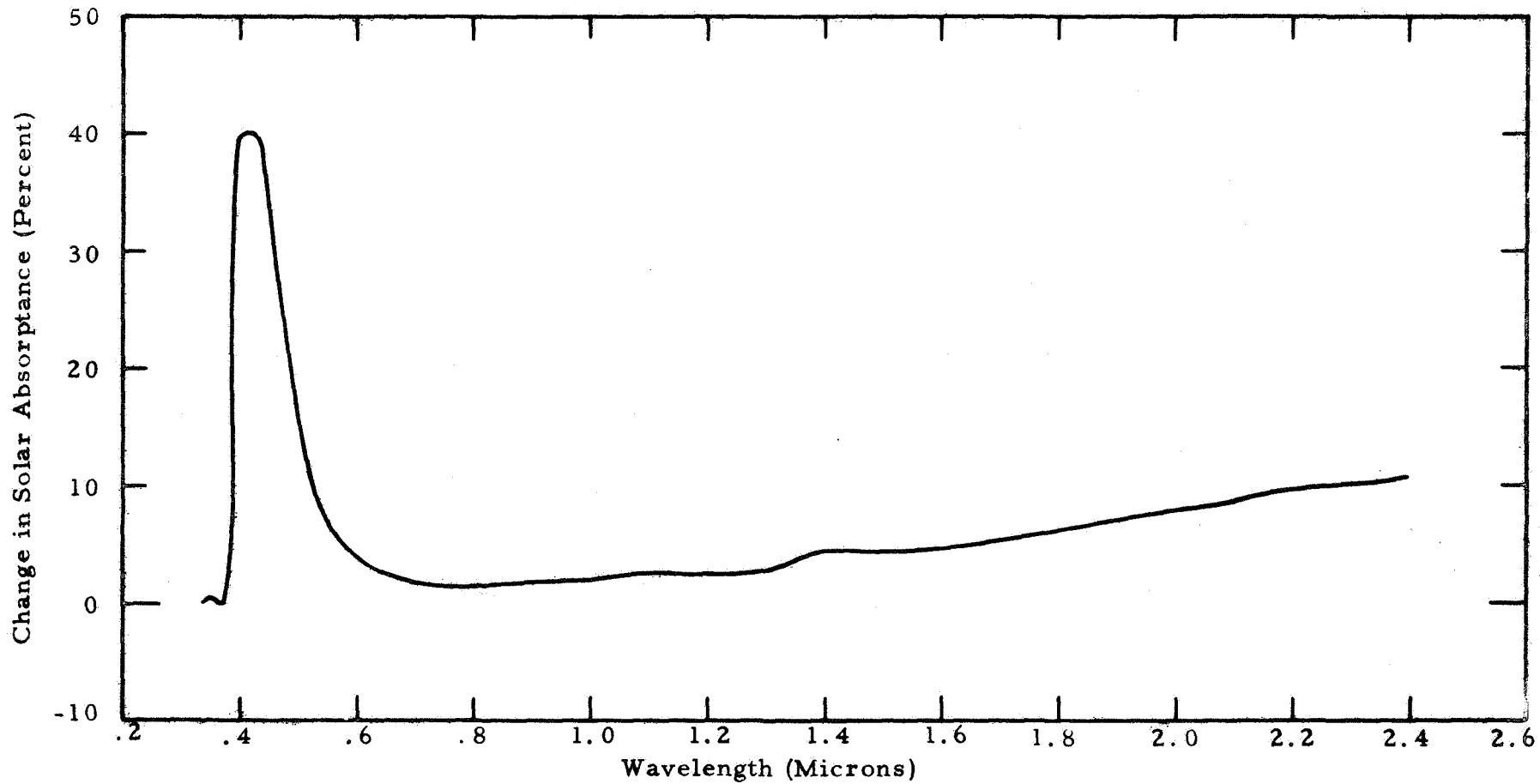


Figure 10-- Effect of 10 Kev protons on ZnO/K₂SiO₃ -
5.3 x 10¹⁵ p/cm² at 1.1 x 10¹² p/cm²/sec

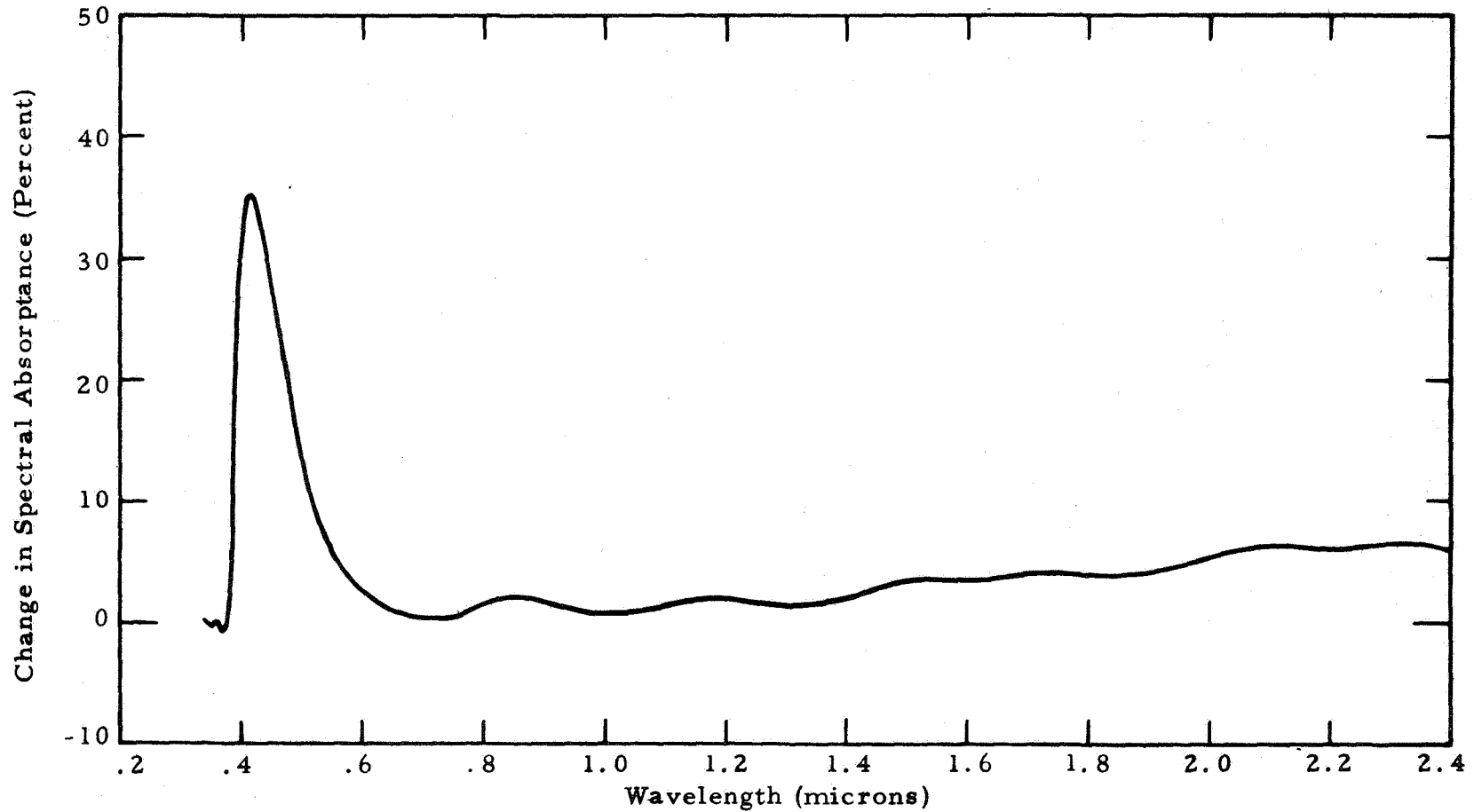


Figure 11-- Effect of combined environment exposure of ZnO/K₂SiO₃,
10 Kev protons - 5.3×10^{15} p/cm² at 1.1×10^{12} p/cm²/sec,
15 sun hours of near ultraviolet (Xenon) at 3 solar equivalents.

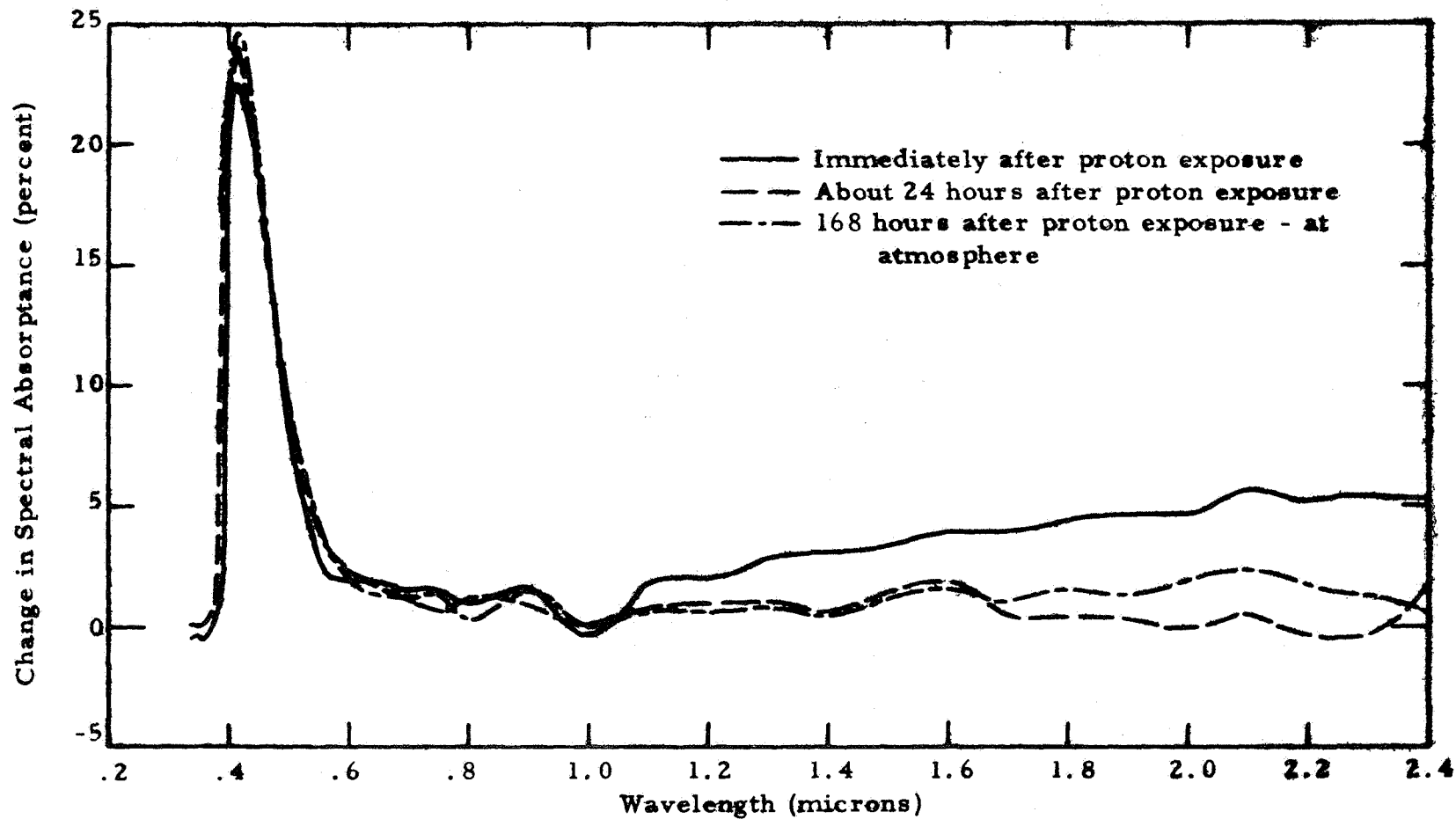


Figure 12 -- Transient proton damage in the infrared ZnO/K₂SiO₃

band was induced from .31 to .55 micron and another above 1 micron. The data taken about 24 hours later shows a recovery of infrared damage even though chamber pressure was less than 10^{-9} torr. The recovery is not an effect of the solar radiation since the sample which was exposed only to protons exhibited the same recovery; nor was it a continued effect of vacuum since the control sample did not exhibit any further change following the initial measurements in vacuum. The other curve shows an increase in infrared reflectance following return of the chamber to atmospheric pressure.

Pre-exposure spectral reflectance measurements were made both in air and vacuum for the samples used in the third test and they exhibited the same increase in reflectance in the infrared as had the previous group.

The test was set up for a proton flux of 3.2×10^9 p/cm²/sec and an integrated flux of 2×10^{15} p/cm². With a new mirror with a somewhat improved heat sink installed in the chamber the solar irradiance at sample position as measured with a pyrhelimeter was 7.5 solar constants with 4.3 solar equivalents in the near ultraviolet. When the test was stopped after what should have been 750 sun hours of ultraviolet exposure, it was found that the aluminum had evaporated off the new mirror.

Figure 13 shows an effect of the solar radiation. The solid curve is from spectral reflectance measurements made immediately after shutting the radiation off the samples after approximately 48 hours of exposure. The sample was exposed only to solar radiation. The dashed curve is from measurements made when the radiation had been off for 2 hours, on for 40 minutes, and then off for 3-1/2 hours. The radiation apparently caused a decrease in reflectance primarily around the absorption edge but in a short period of time after blocking off the radiation the absorption peak disappeared. At the end of the test, this sample exhibited considerable more optical damage than would have been expected even from a full 750 sun hours of near ultraviolet. A check showed that the samples

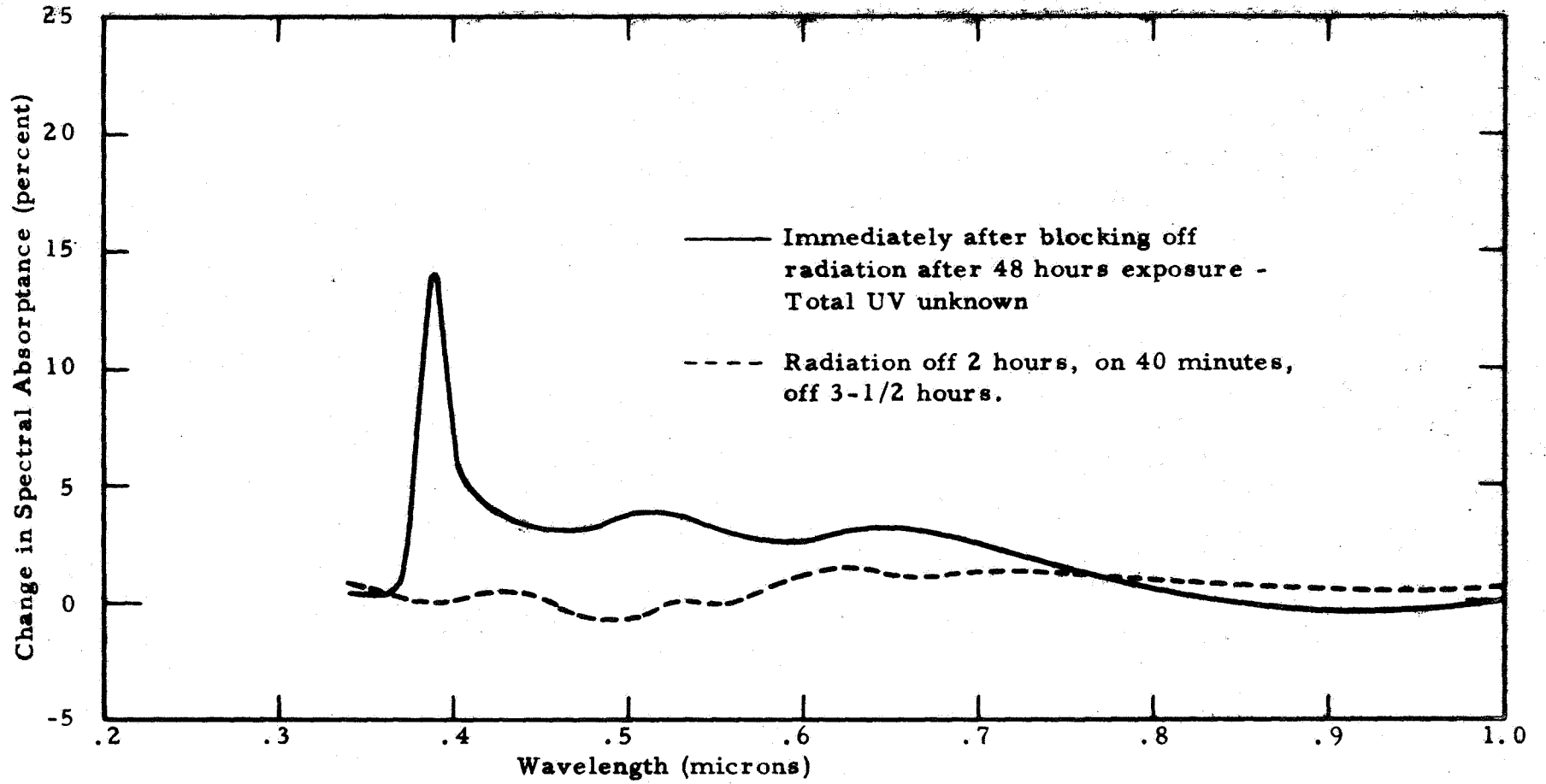


Figure 13 -- Effect of Solar Radiation on ZnO/K₂SiO₃

were not seating properly in the sample holders. Thermal transfer was probably inadequate to keep the samples exposed to the simulated solar radiation from heating. The transient absorption peak was an anomalous result and was never reproduced.

The sample which was exposed to the combined environment suffered more damage than the sample exposed to protons. This was in contradiction to the results of previous tests of $\text{ZnO}/\text{K}_2\text{SiO}_3$ when the samples were maintained at the same temperature and is a further indication that the samples exposed to the solar radiation may have been considerably warmer than the other two samples.

Figures 14 and 15 show changes in spectral absorp tance caused by proton exposure and by combined proton and solar radiation exposure respectively. The three curves represent the change which had occurred at various stages of exposure. Changes in solar absorptance are noted on the figures.

2. Mercury Xenon Lamp

Thirteen exposures were conducted on the various materials using a 5KW Mercury Xenon Lamp in the solar simulator. The results of these tests are discussed in the following paragraphs based upon the environmental parameters selected. The curves which accompany show only changes in spectral absorptance.

a. Zinc Oxide/Potassium Silicate

Two batches of zinc oxide potassium silicate were tested, F-1-47-D and 1-11-9-13. Effects of the individual irradiations as well as the combined environment are discussed below.

1. Proton Effects

The effects of proton radiation only are shown in Figures 16 and 17 for the F-1-47-D $\text{ZnO}/\text{K}_2\text{SiO}_3$ and Figure 18

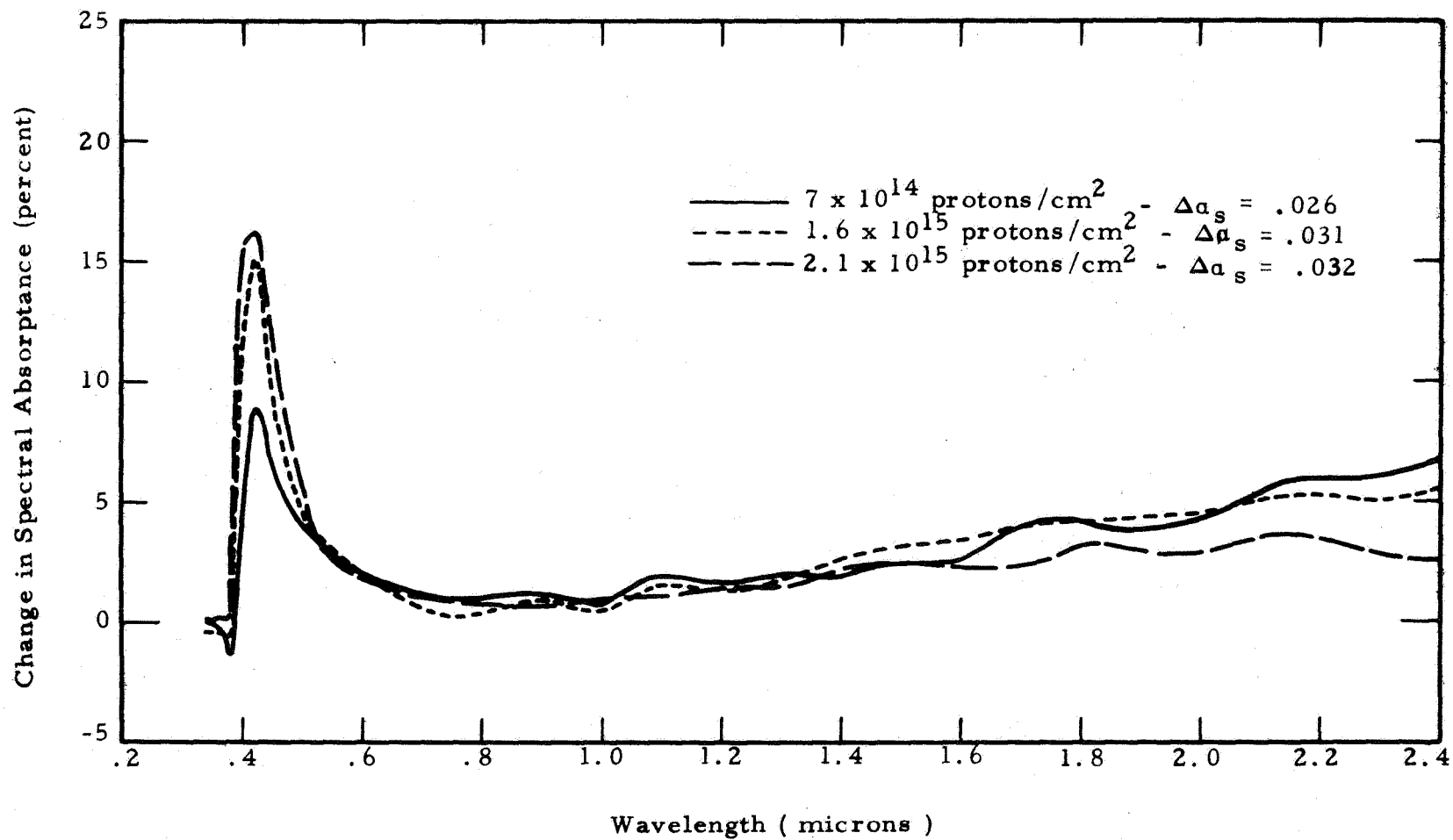


Figure 14 -- Effect of 10 KEV protons on ZnO/K₂SiO₃ at 298°K
Average proton flux 3.8 × 10⁹ p/cm²/sec

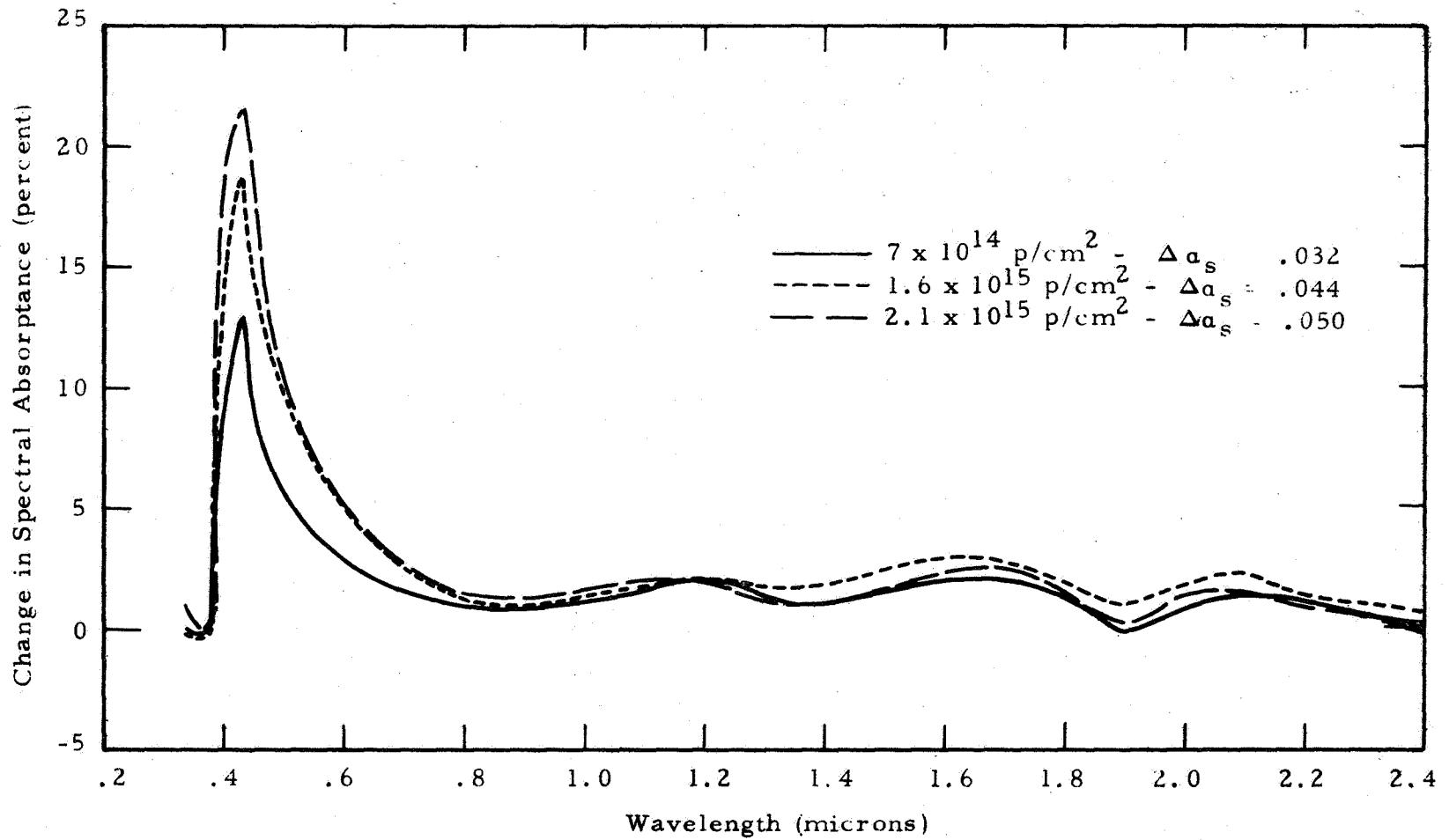


Figure 15 -- Effect of Combined Environment on ZnO/K_2SiO_3 at $298^\circ K$
Average proton flux $3.8 \times 10^9 p/cm^2/sec$ - Ultraviolet
unknown.

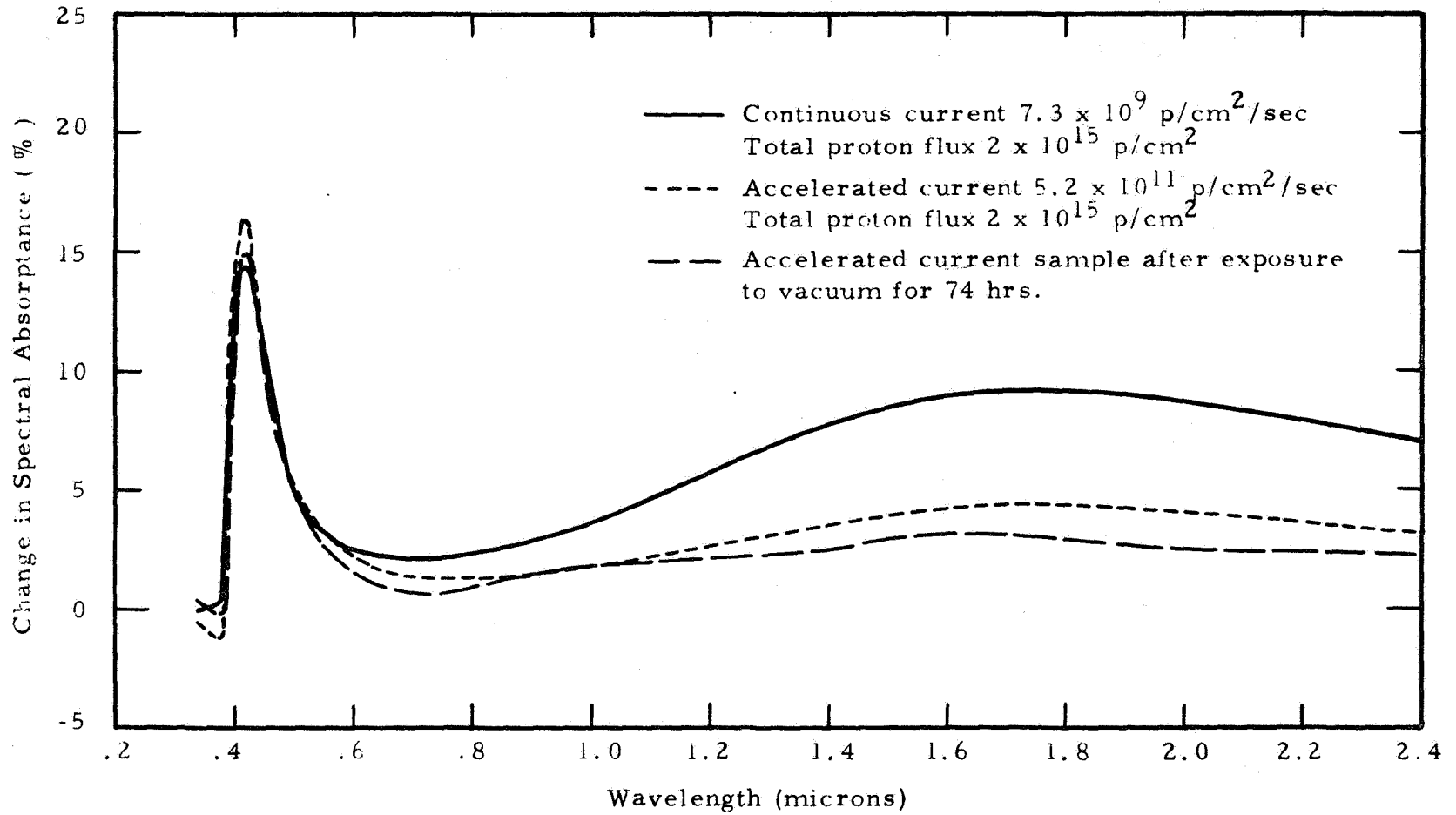


Figure 16 -- Rate and Vacuum effect of proton radiation only -
ZnO/K₂SiO₃ - (F-1-47-D)

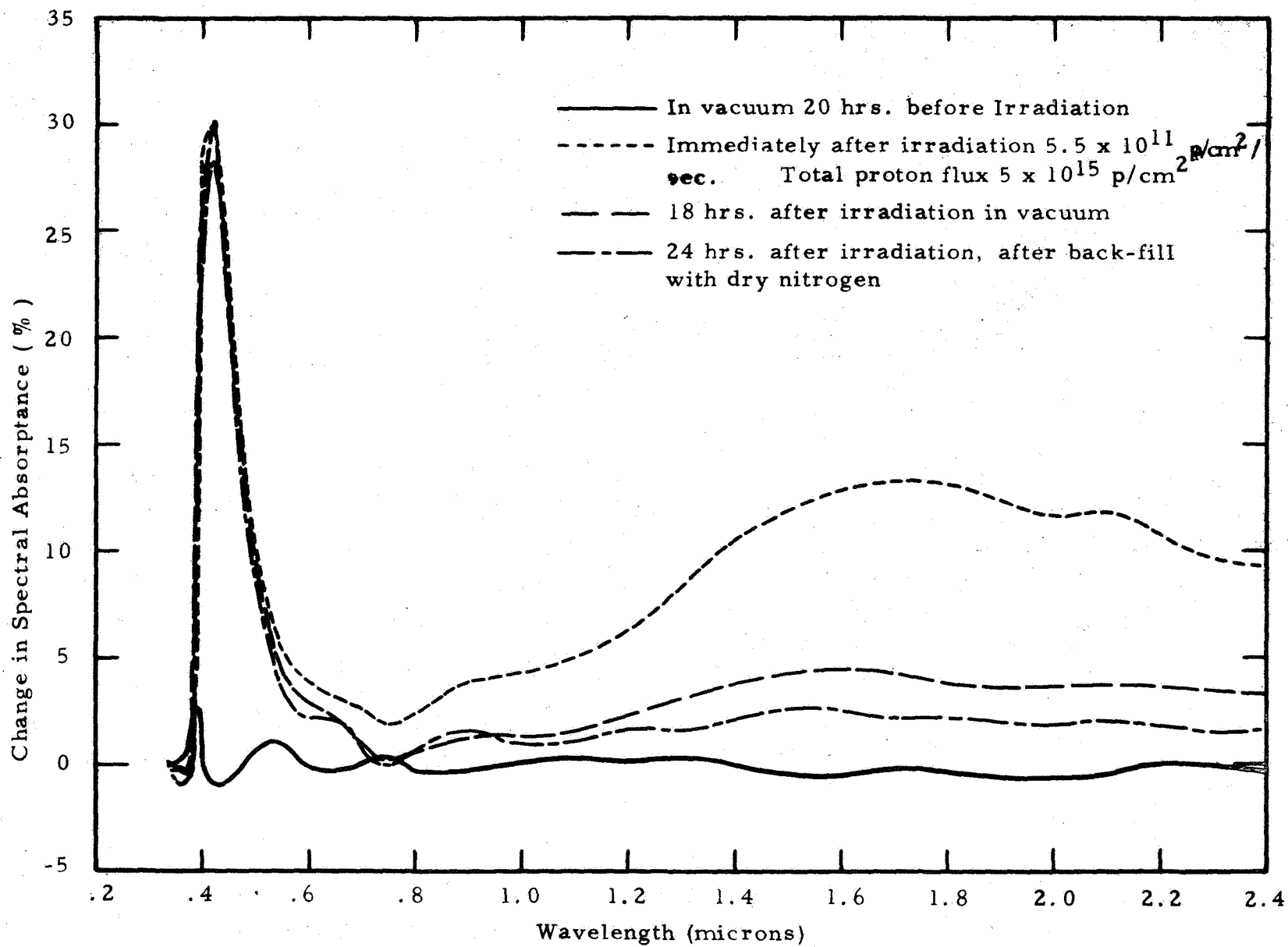


Figure 17 -- Effect of Total Proton Radiation to 5×10^{15} p/cm² - ZnO/K₂SiO₃ - (F-1-47-D)

shows the effect on the 1-11-9-13 ZnO/K₂SiO₃. Greater damage is observed in the infrared region due to the continuous proton radiation than with the accelerated flux indicating a rate effect. Also shown in Figure 16 is a slight bleaching effect in the infrared region for the sample which was irradiated at the beginning of the test and remained in vacuum while the other samples were irradiated with ultraviolet. Figure 17 also shows this effect. In Figure 17, the effect of increasing the proton flux 2-1/2 times is shown and allowing the sample to remain in vacuum for a specified period of time.

Figure 18 shows the effect of proton radiation only to the 1-11-9-13 material and again remaining in vacuum after irradiation. Again, the bleaching effect may be noted.

2. Ultraviolet Damage

Figure 19 shows the effect of ultraviolet radiation on the F-1-47-D ZnO/K₂SiO₃ material. In both tests the ultraviolet was applied at a rate of 10 suns. The damage was less than 5% in the near ultraviolet, visible and infrared region as may be seen from this figure. Results were essentially the same for two separate runs on this material.

3. Combined Effects

The combined effects of proton, vacuum and ultraviolet environment are shown in Figures 20, 21, 22, and 23.

Figures 20 and 21 show a comparison between the combined radiations on one

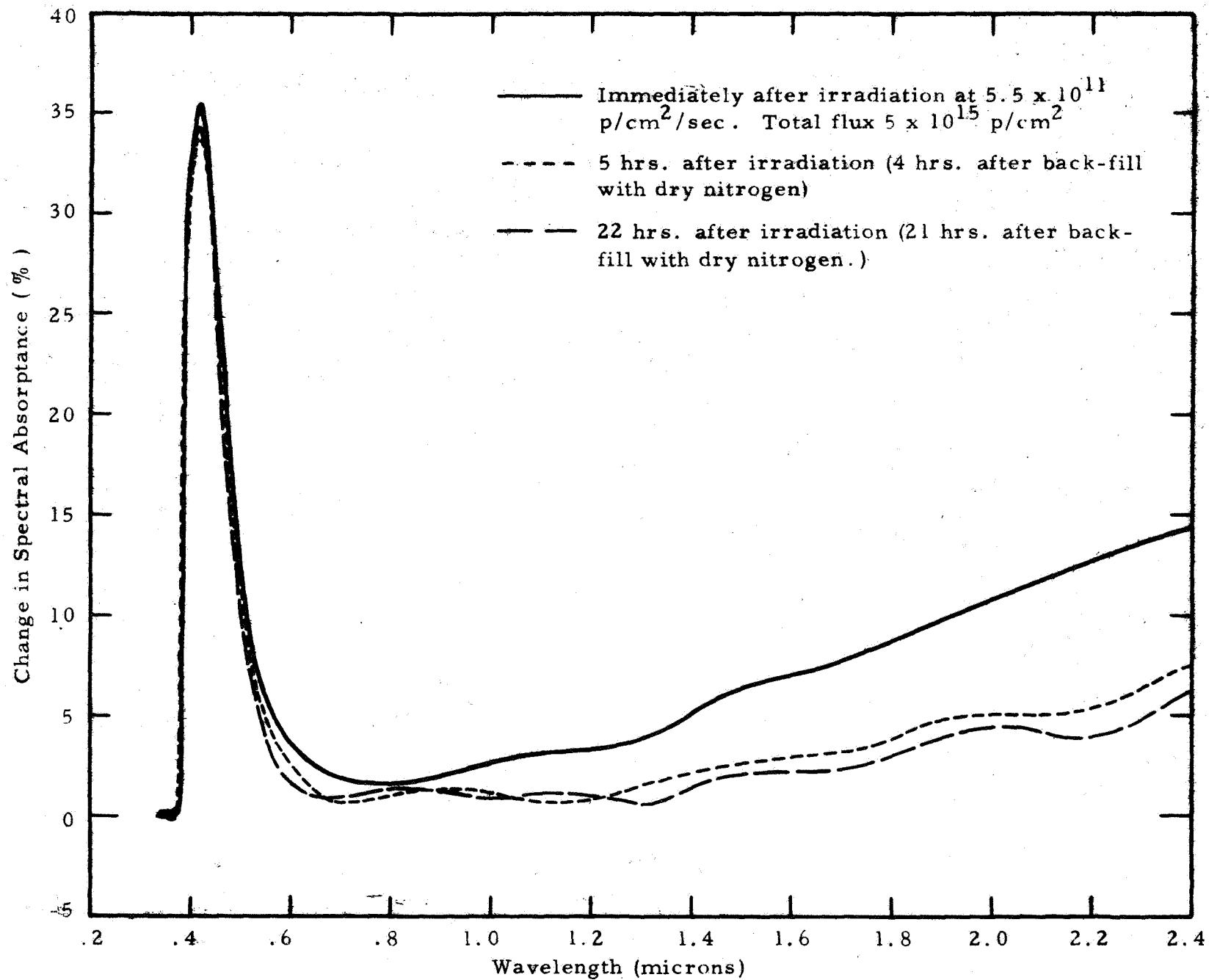


Figure 18--Effect of protons on 1-11-9-13 ZnO/K₂SiO₃.
Remaining in vacuum after irradiation

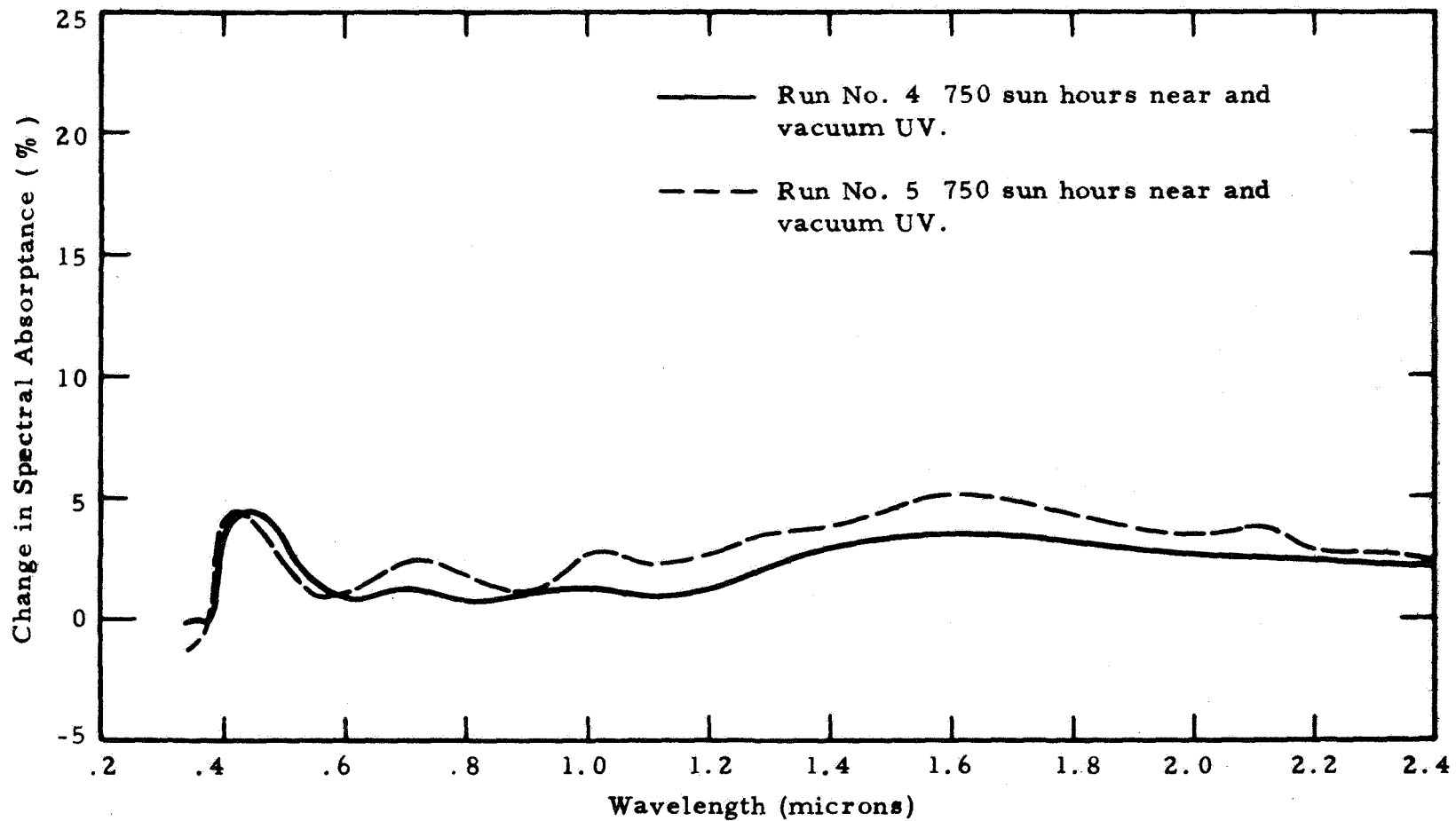


Figure 19--Effect of UV radiation only.
ZnO/K₂SiO₃ -(F-1-47-D)

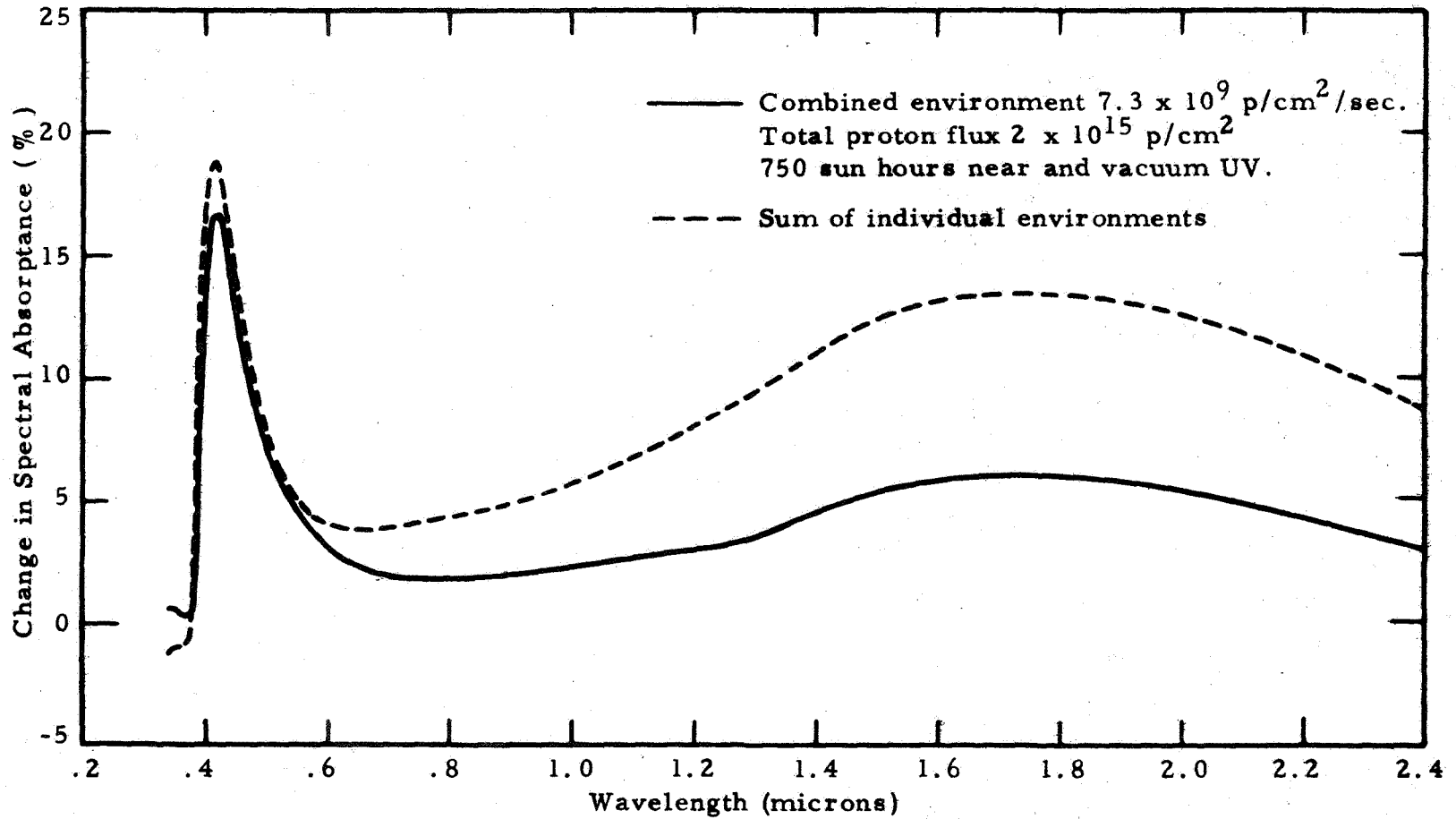


Figure 20 -- Combined effects versus sum of individual effects.
Continuous low current - ZnO/K₂SiO₃ (F-1-47-D)

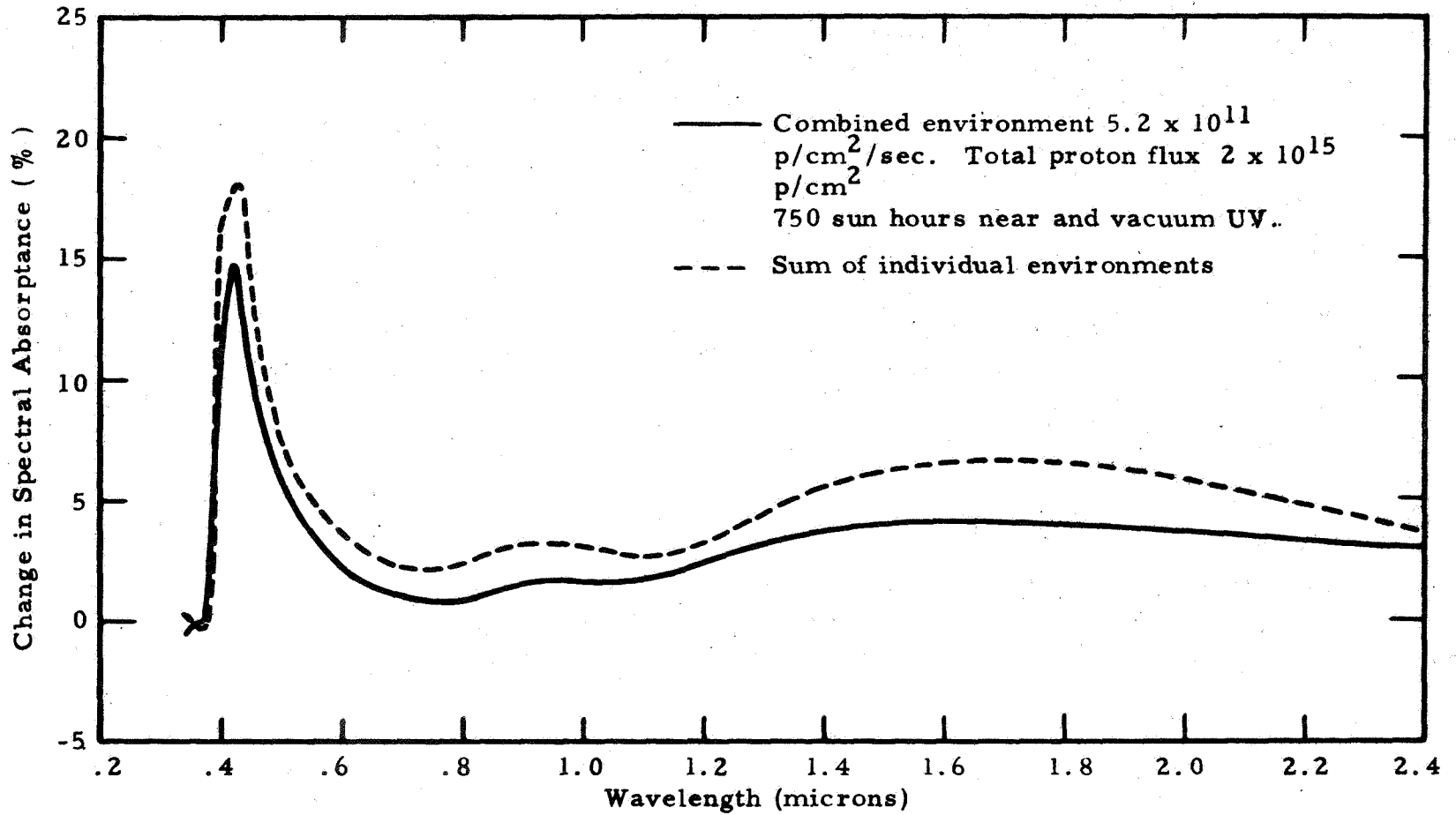


Figure 21 -- Combined effects versus sum of individual effects.
Accelerated current - ZnO/K₂SiO₃ (F-1-47-D)

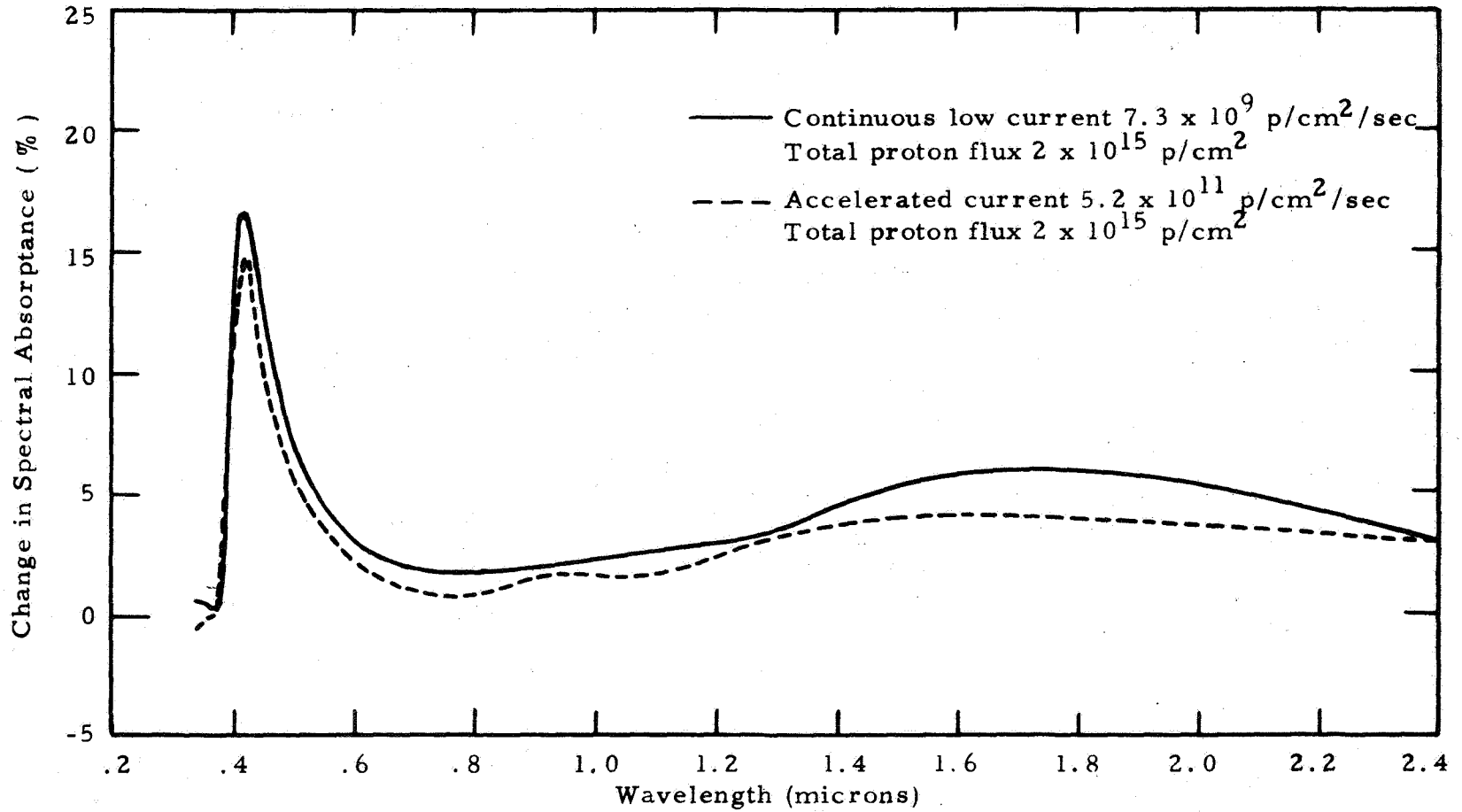


Figure 22 -- Combined effects with continuous current versus combined effects with accelerated current. ZnO/K₂SiO₃ (F-1-47-D)

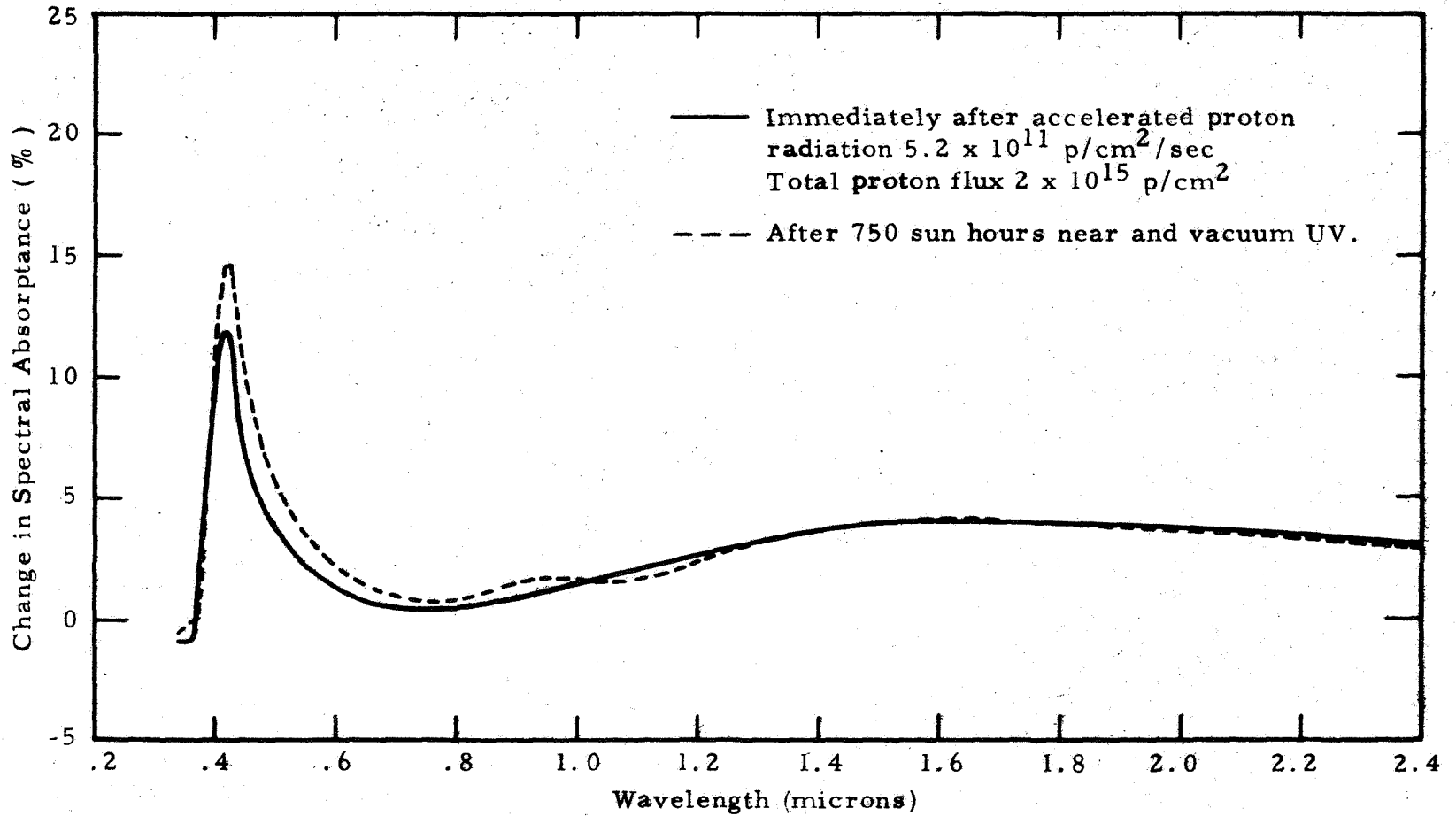


Figure 23 -- Effect of combined environment immediately after accelerated proton exposure and at the end of the test - ZnO/K₂SiO₃ (F-1-47D)

sample and the algebraic sum of the individual irradiations on the other two samples for two separate runs of high and low proton flux. Figure 22 shows a comparison between the combined environment of vacuum, ultraviolet and protons of low and high flux rate. Figure 23 shows the effect of ultraviolet radiation and vacuum on a sample irradiated with protons at the beginning of a test and comparing the change in spectral absorptance from the irradiation measurement to the end of the test.

b. ZnO/Silicone

1. Protons

The effects of proton radiation are shown in Figures 24 and 25. The characteristic curve for ZnO susceptibility to proton damage is depicted. The effect of the accelerated protons is almost identical to that produced by the continuous low current indicating no rate effect. A slight difference is observed in the height of the change of absorptance which is greater for the continuous current. Also shown by Figure 24 is that the ZnO/Silicone showed a bleaching in the IR due to remaining in the vacuum chamber for approximately 74 hours. The effect of increasing the total proton flux to 1×10^{16} p/cm² is shown in Figure 25. The peak change in absorptance was almost doubled with approximately 5% greater damage in the IR range.

2. Ultraviolet Effects

The effect of ultraviolet radiation on this material is shown in Figure 26. It shows very little damage with a slight absorptance peak near .4 μ and less in the infrared than the ZnO/K₂SiO₃. Both runs on the materials

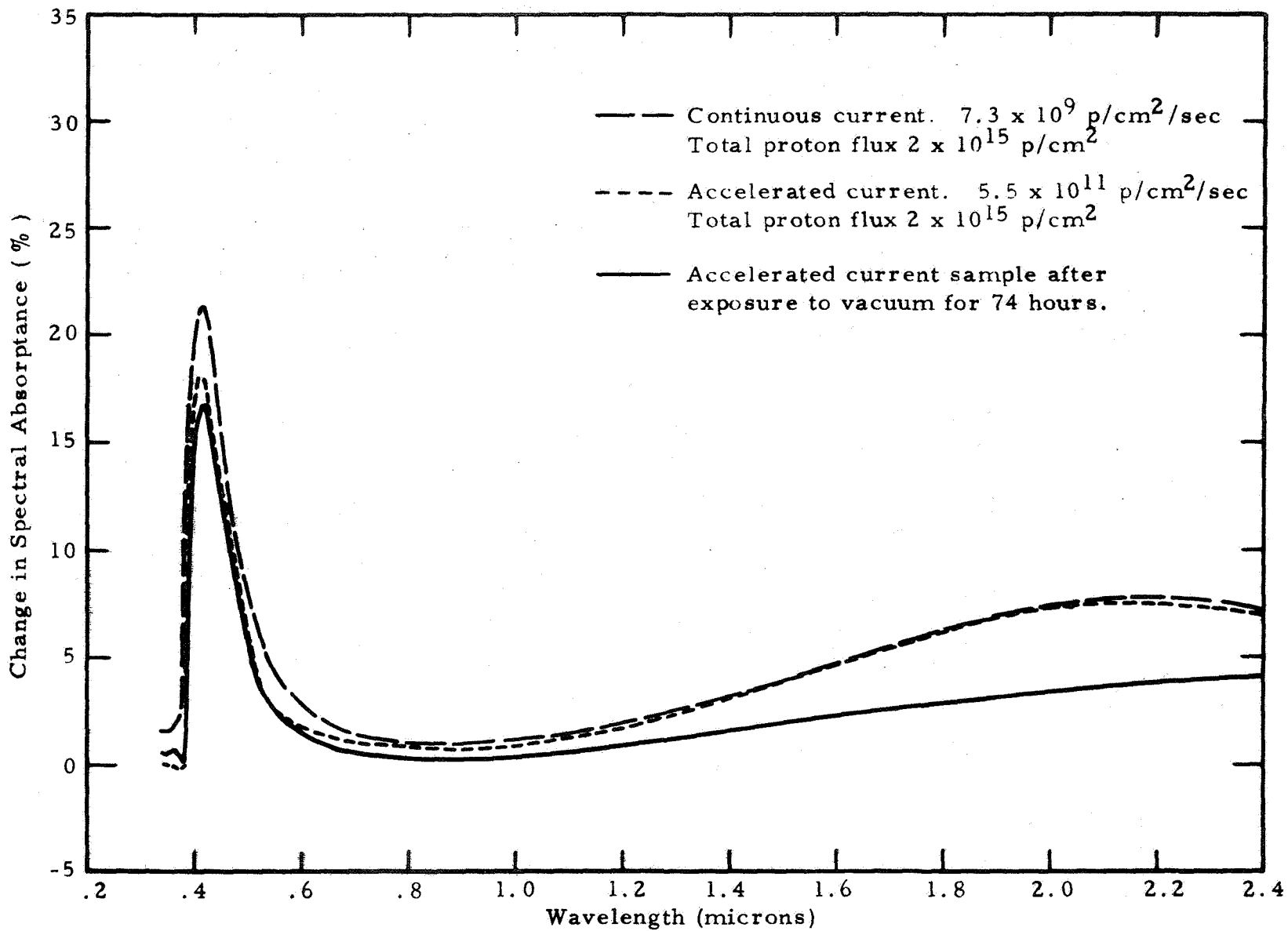


Figure 24 -- Rate and vacuum effect of proton radiation only - ZnO/Silicone (F-1-55)

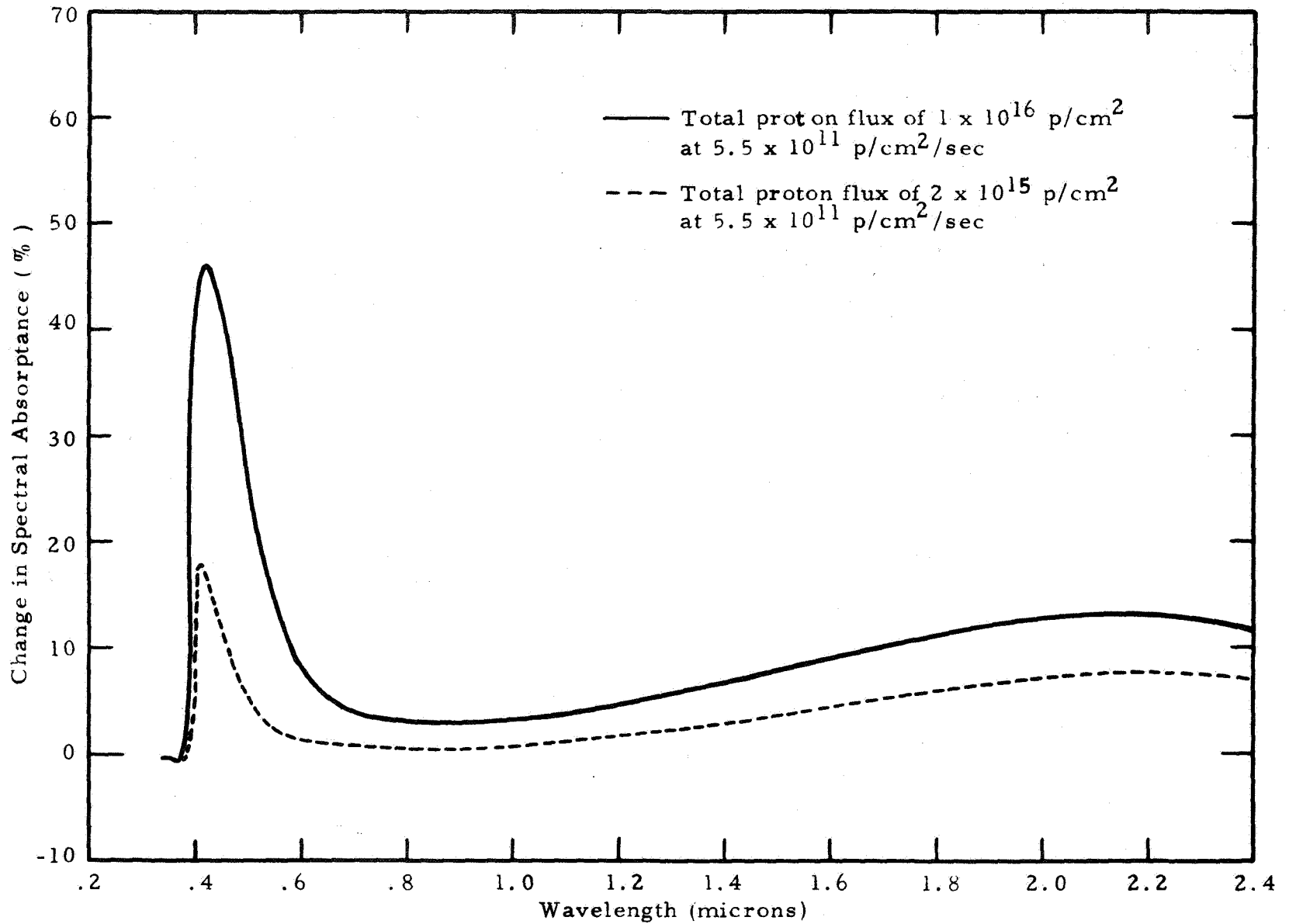


Figure 25 -- Effect of increasing total proton flux from 2×10^{15} p/cm² to 1×10^{16} p/cm² - ZnO/Silicone (F-1-55)

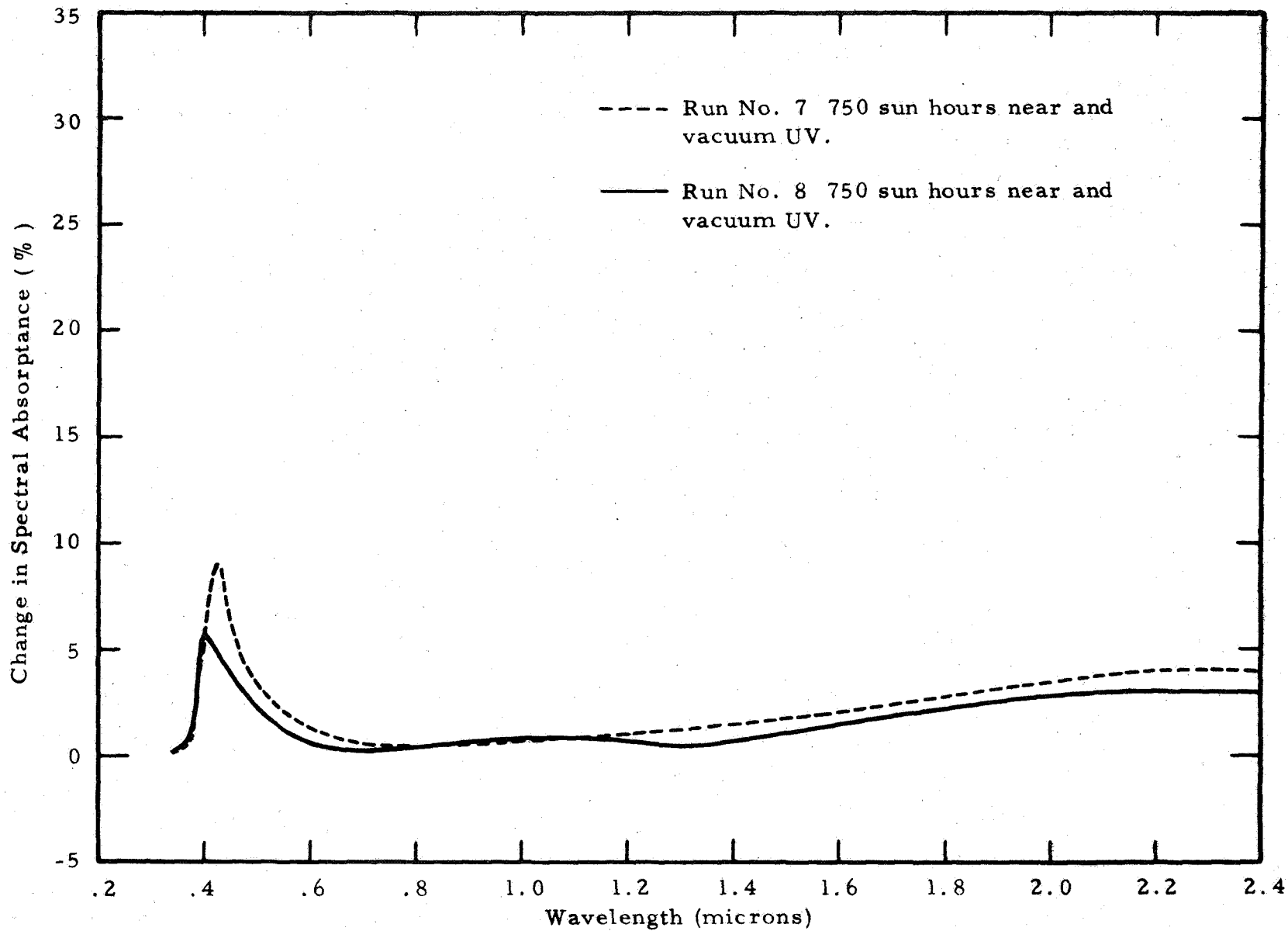


Figure 26 -- Effect of UV radiation only. ZnO/Silicone (F-1-55)

produced almost the same results as shown in this figure.

3. Combined Effects

The effects of the combined environment are shown in figures 27, 28, 29, and 30. Figures 27 and 28 show the comparison between the sum of the individual environment and the combined environments for both the high and low currents.

Figure 29 shows that the absorptance peak around $.4\mu$ was considerably greater for the continuous low current with approximately the same damage in the IR range.

Figure 30 shows a greater change in spectral absorptance around $.4\mu$ for the ultraviolet radiation than was effected in the ZnO/K_2SiO_3 .

c. Lanthanum Oxide/Potassium Silicate (F-1-53)

1. Protons

Figure 31 shows the effect of proton radiation on this material and the subsequent effect of exposure to a vacuum. Proton damage was very slight with practically no change due to vacuum exposure after irradiation.

2. Ultraviolet Effects

750 sun hours of ultraviolet and Lyman-alpha radiation produced the greatest damage to this material as shown by Figure 32. The effect was an absorptance peak in the near ultraviolet portion of the spectrum with a trailing off through the visible to practically no damage in the IR range.

3. Combined Effects

The effects of combined environment are shown in Figures 33 and 34. The algebraic

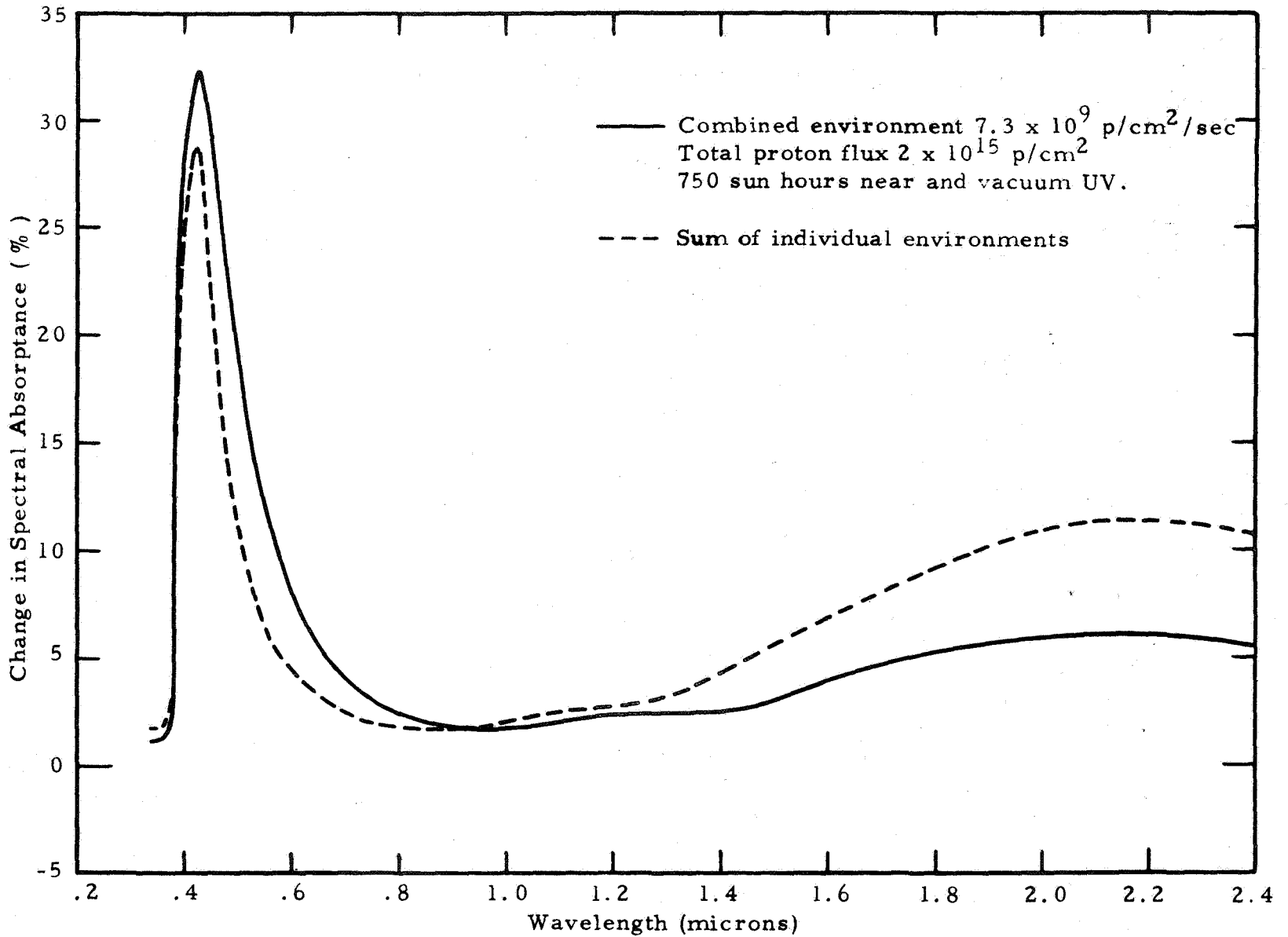


Figure 27 -- Combined effects versus sum of individual effects.
Continuous low current - ZnO/Silicone (F-1-55)

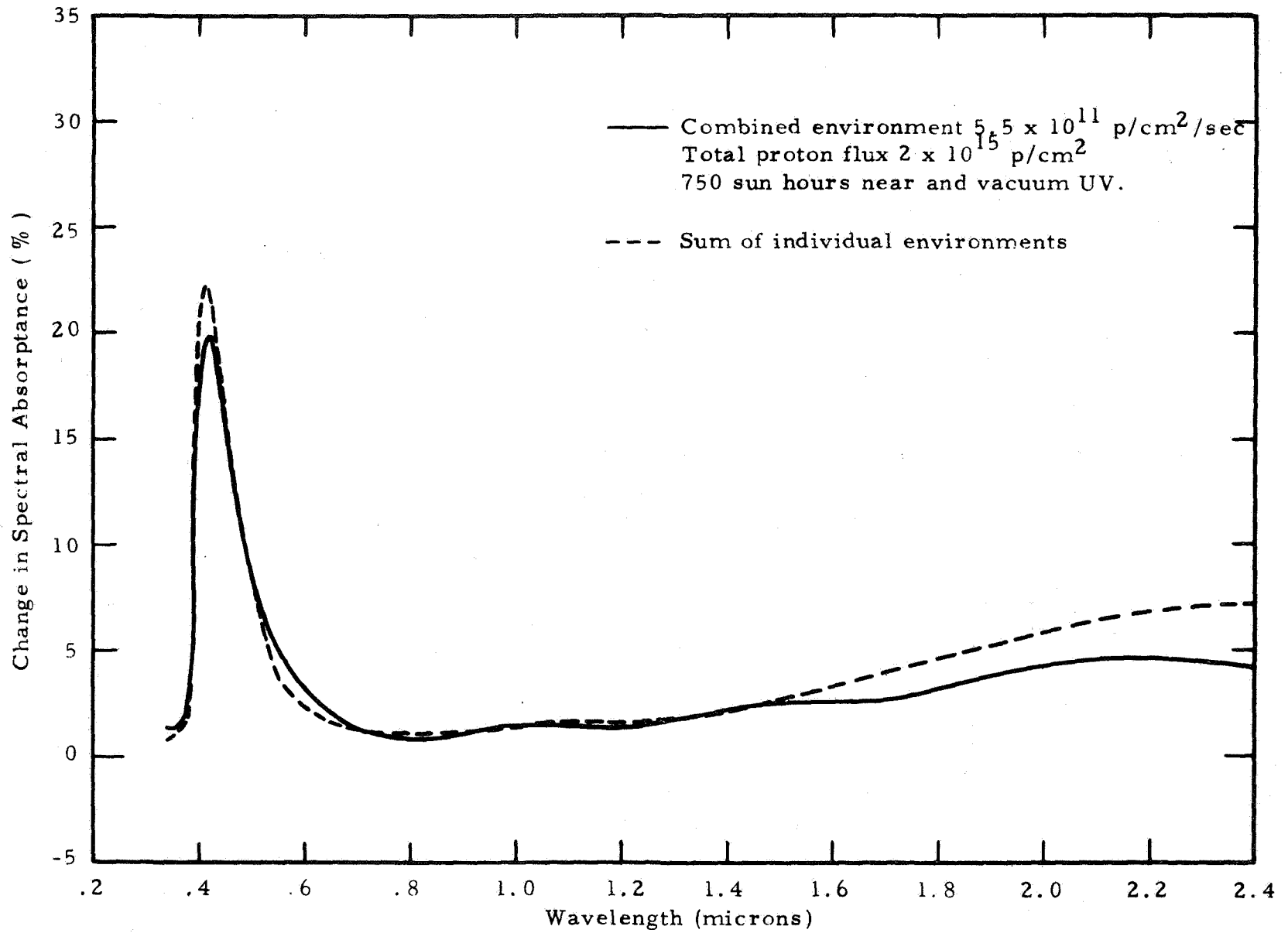


Figure 28 -- Combined effects versus sum of individual effects.
Accelerated current - ZnO/Silicone (F-1-55)

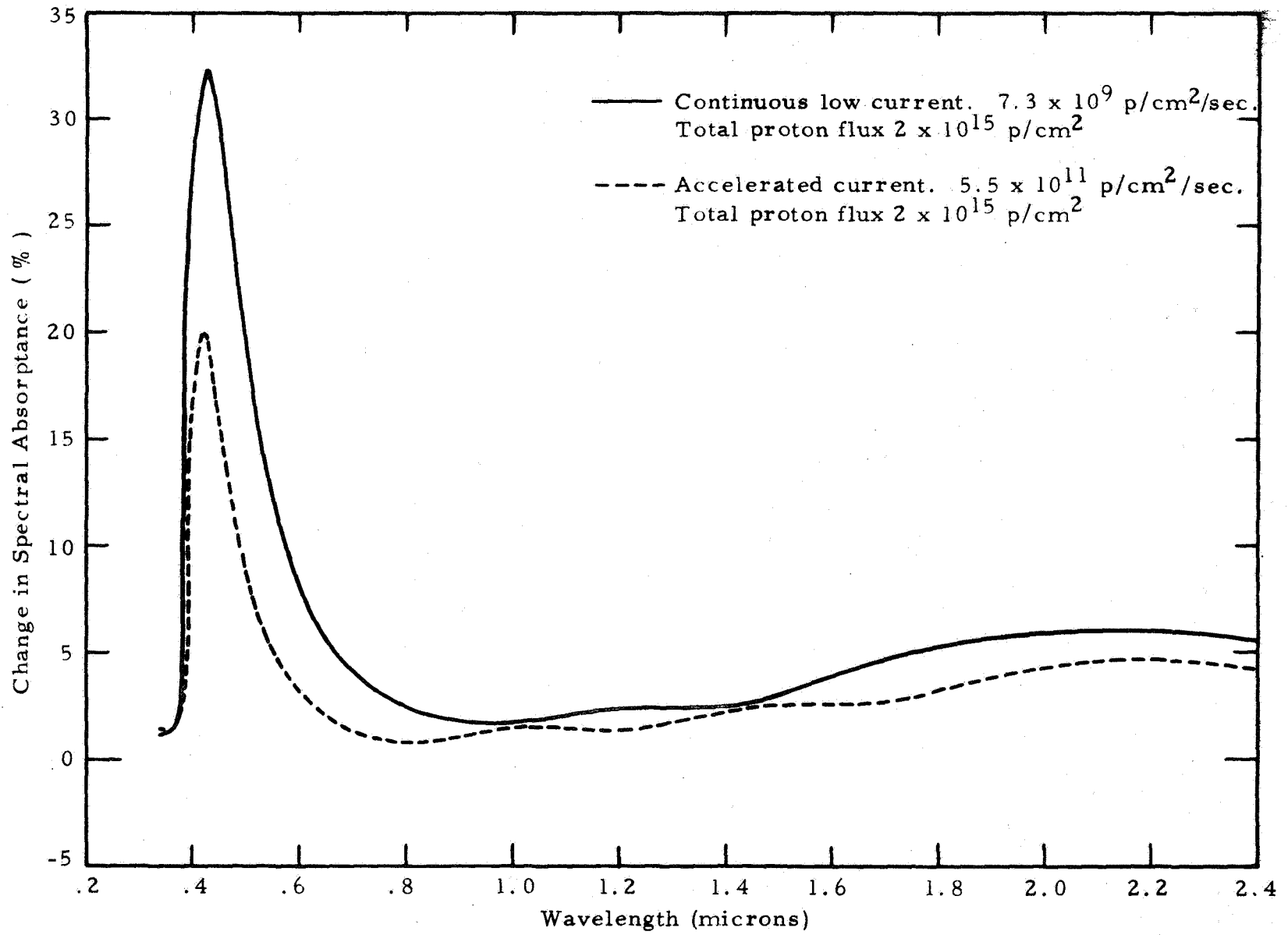


Figure 29 -- Combined effects with continuous current versus combined effects with accelerated current. ZnO/Silicone (F-1-55)

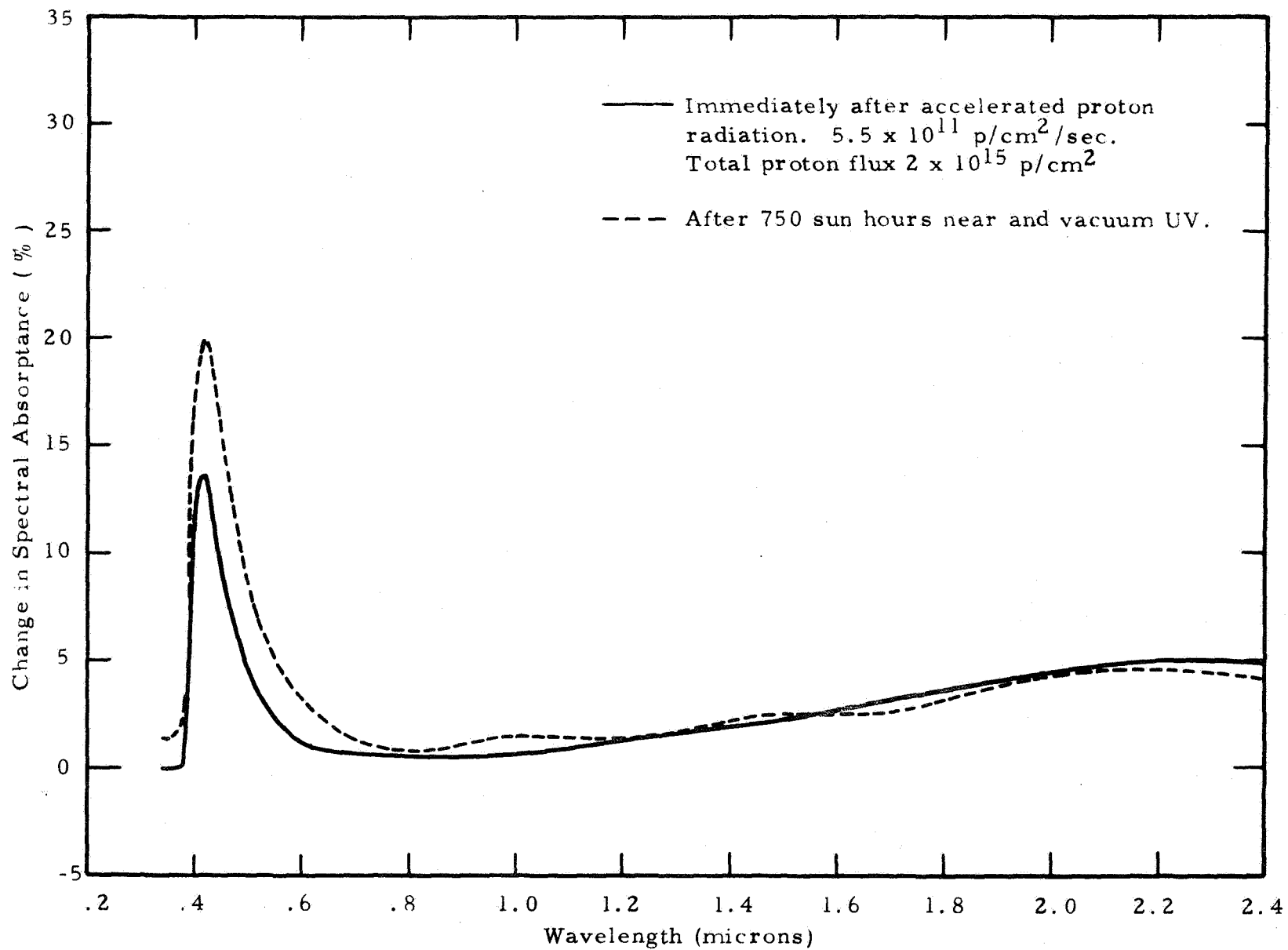


Figure 30 -- Effect of combined environment immediately after accelerated proton exposure and at end of test. ZnO/Silicone (F-1-55)

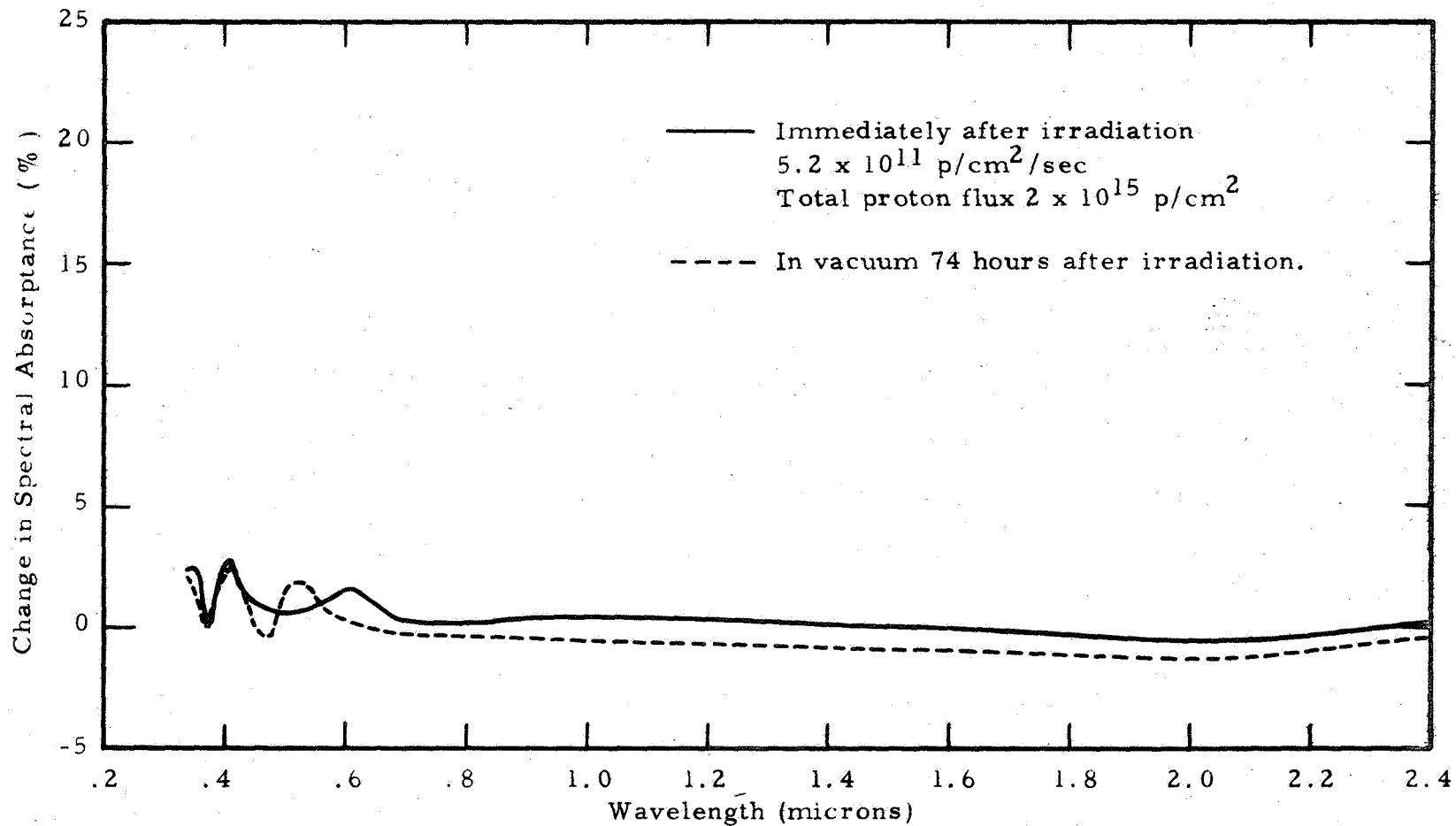


Figure 31 -- Effect of proton radiation only. Accelerated current - immediately after irradiation and at end of test
 $\text{La}_2\text{O}_3/\text{K}_2\text{SiO}_3$ (F-1-53A)

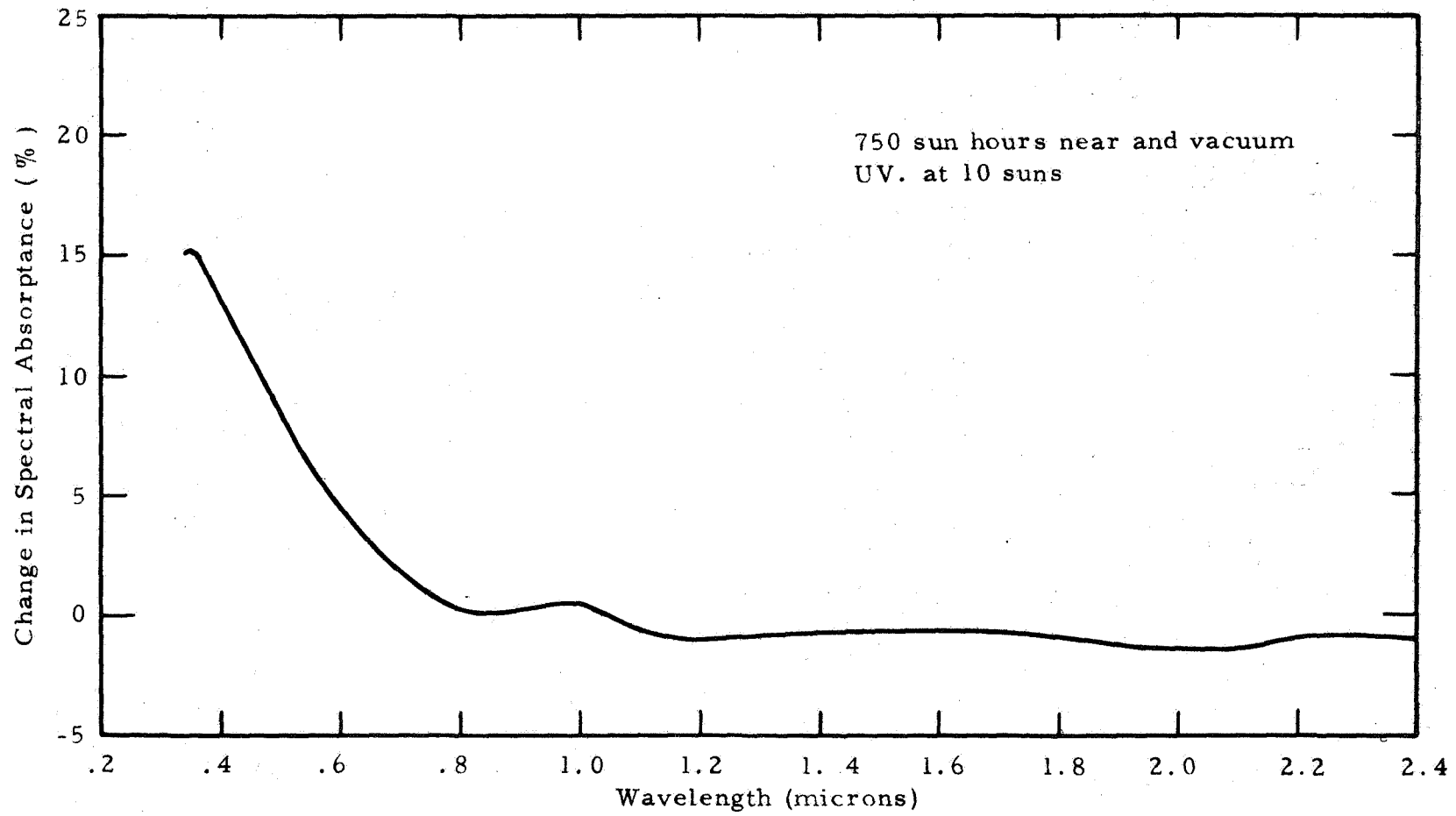


Figure 32 -- Effect of UV radiation only. $\text{La}_2\text{O}_3/\text{K}_2\text{SiO}_3$ (F-1-53A)

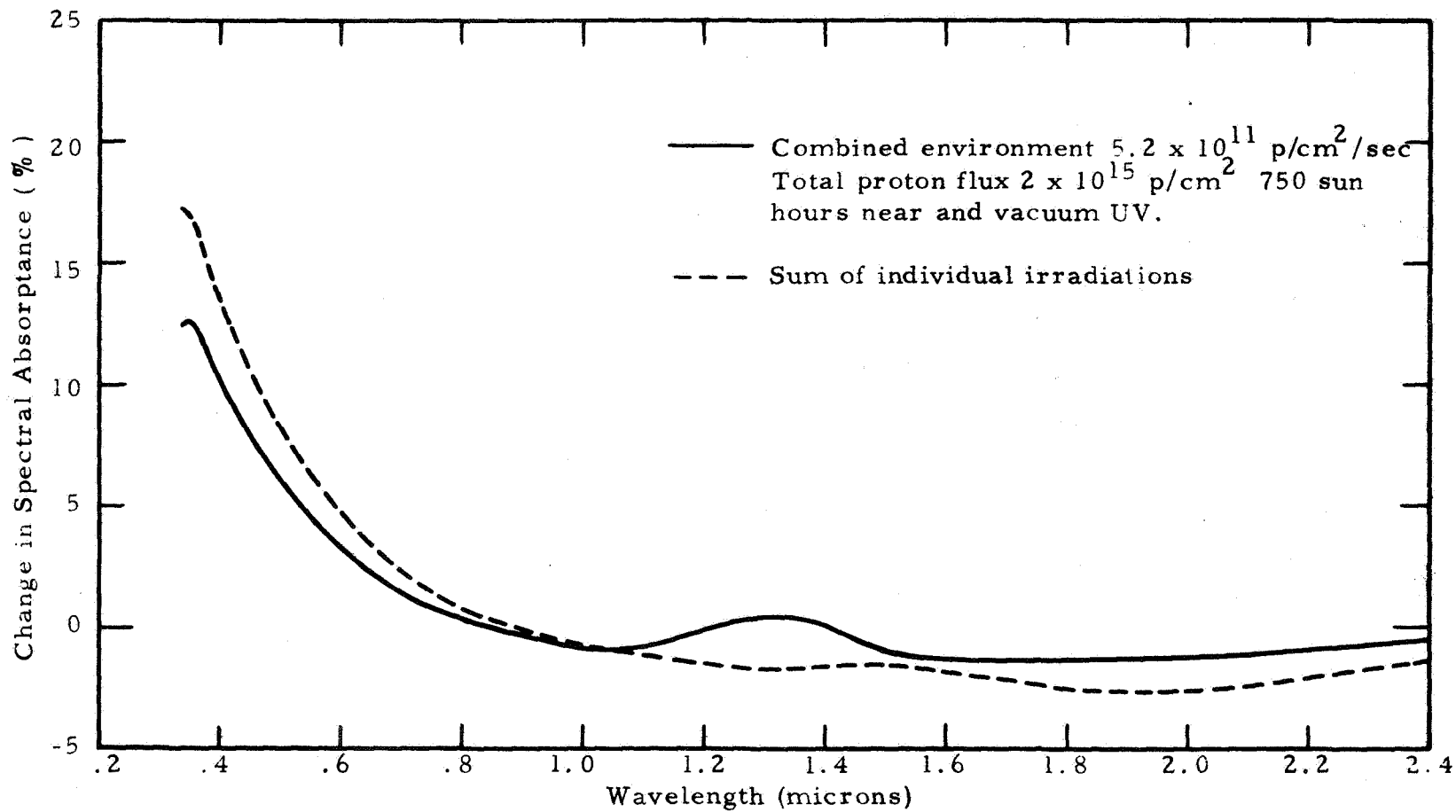


Figure 33 -- Combined effects versus sum of individual effects
 $\text{La}_2\text{O}_3/\text{K}_2\text{SiO}_3$ (F-1-53A)

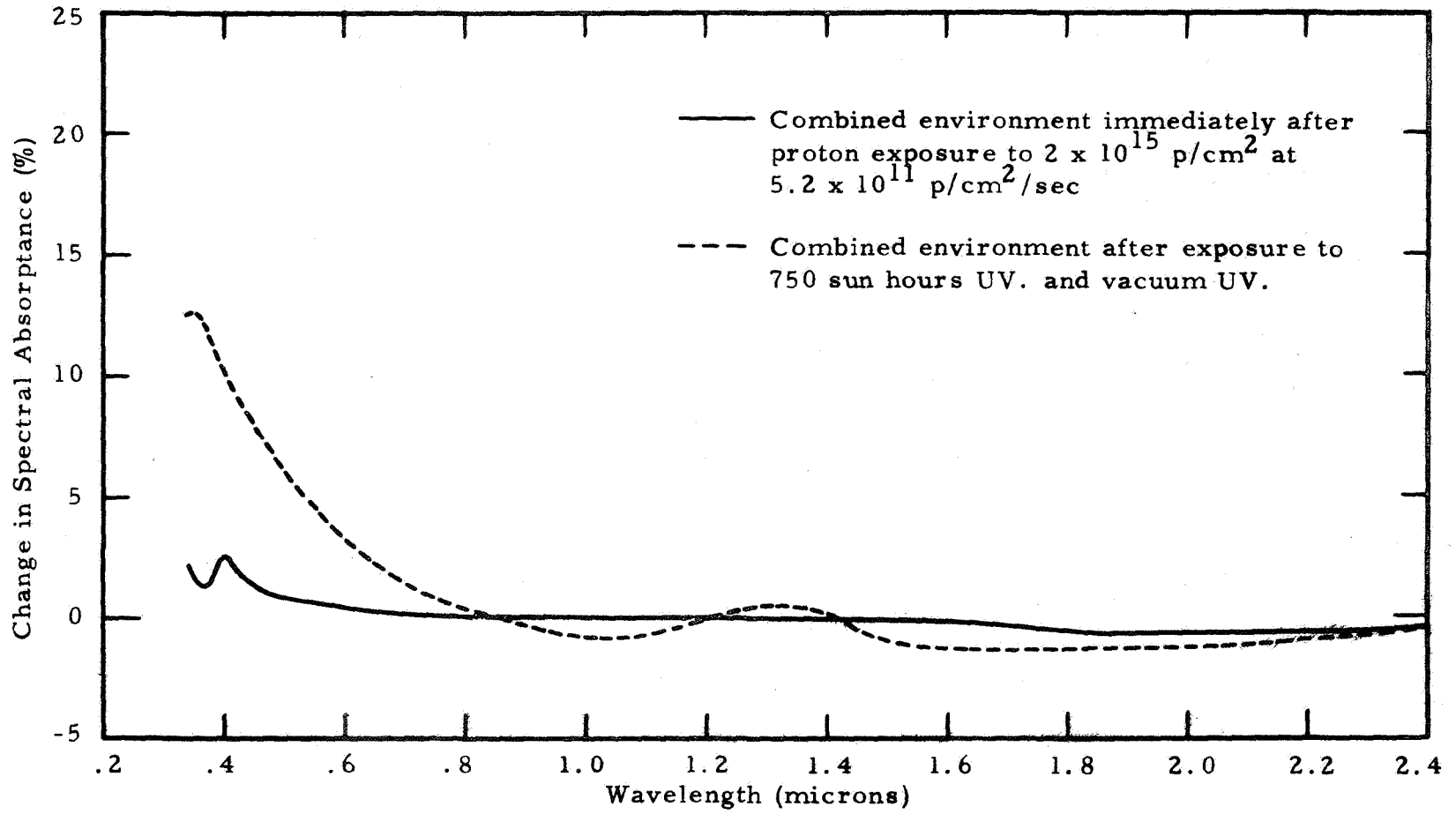


Figure 34 -- Effect of combined environment immediately after accelerated proton exposure and at end of test $\text{La}_2\text{O}_3/\text{K}_2\text{SiO}_3$ (F-1-53A)

sum of the individual damage very nearly equalled the combined environment damage. Figure 34 shows that practically all of the damage to the material in the combined environment was due to the solar electromagnetic radiation.

d. Lanthanum Oxide/Potassium Silicate (F-1-38)

1. Protons

The effect due to proton radiation only is shown in Figures 35 and 36. This was a different batch of Lanthanum Oxide/Potassium Silicate, however, it showed practically the same effect due to protons as did the F-1-53 material. Increasing the total proton flux by five times produced very little more damage as shown by Figure 36.

2. Ultraviolet Effect

The absorptance peak produced by the electromagnetic radiation was considerably greater in this batch of Lanthanum Oxide (F-1-38) than in that reported in the previous paragraph (F-1-53). This is shown in Figure 37. Damage in the IR range was again practically zero as before.

3. Combined Environment

The effects of combined environment are shown in Figures 38 and 39. The principal damage is seen to be due to the electromagnetic radiation with the algebraic sum very nearly equalling the combined damage.

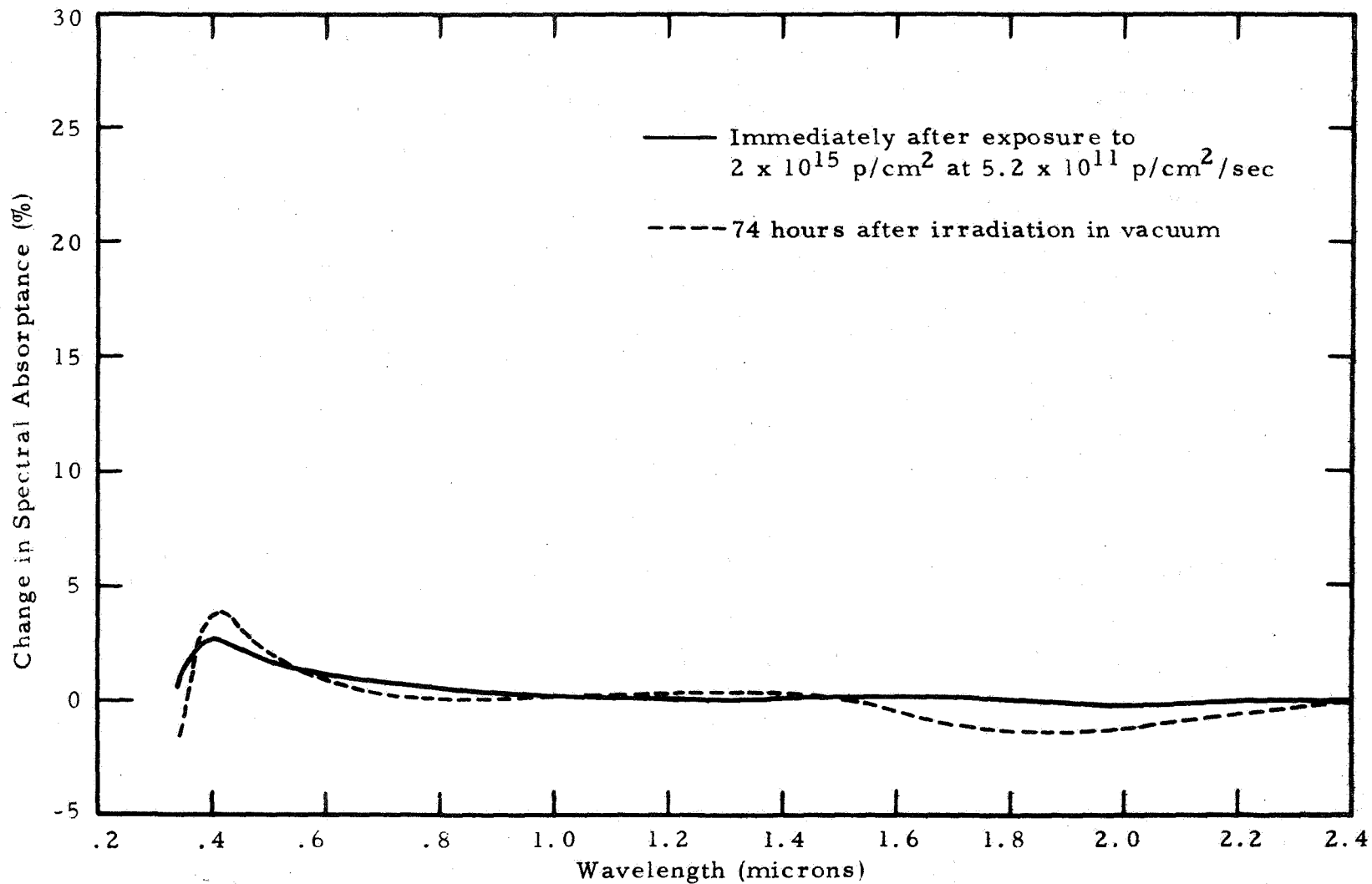


Figure 35 -- Effect of proton radiation only - Accelerated current - immediately after radiation and at end of test $\text{La}_2\text{O}_3/\text{K}_2\text{SiO}_3$ (F-1-38)

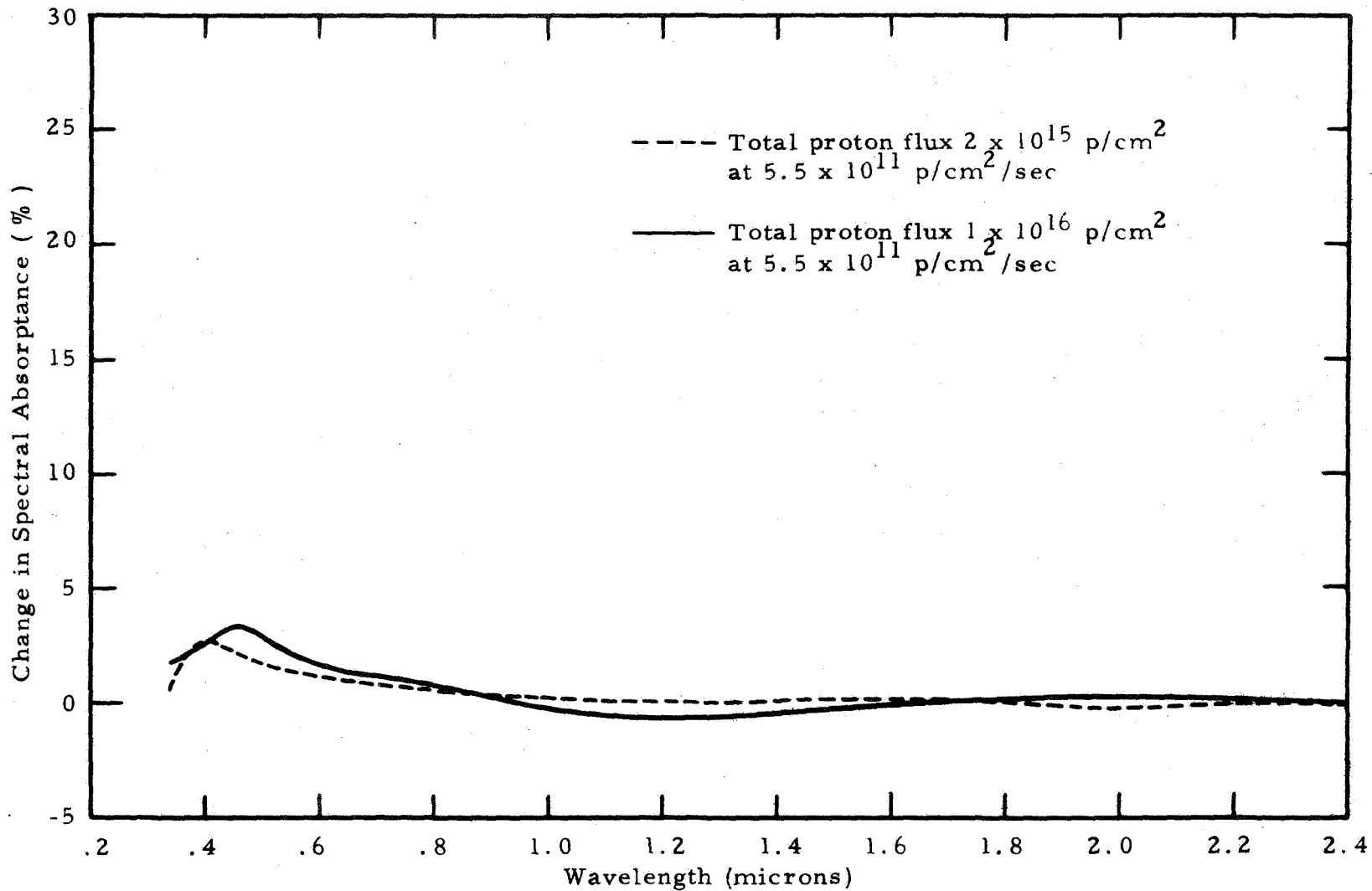


Figure 36 -- Effect of total proton flux of 1×10^{16} p/cm² -
La₂O₃/K₂SiO₃ (F-1-38)

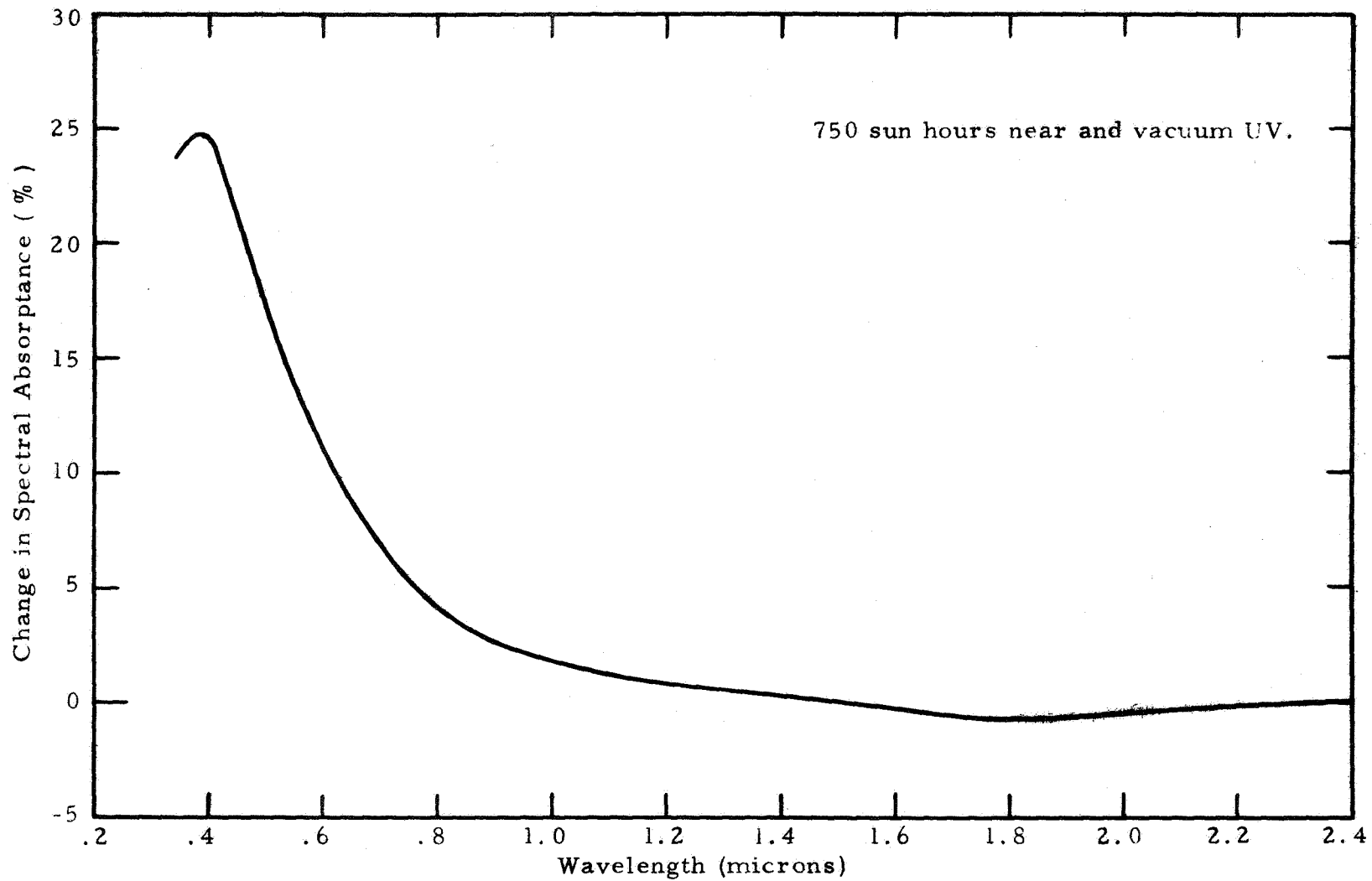


Figure 37 -- Effect of UV radiation only - $\text{La}_2\text{O}_3/\text{K}_2\text{SiO}_3$ (F-1-38)

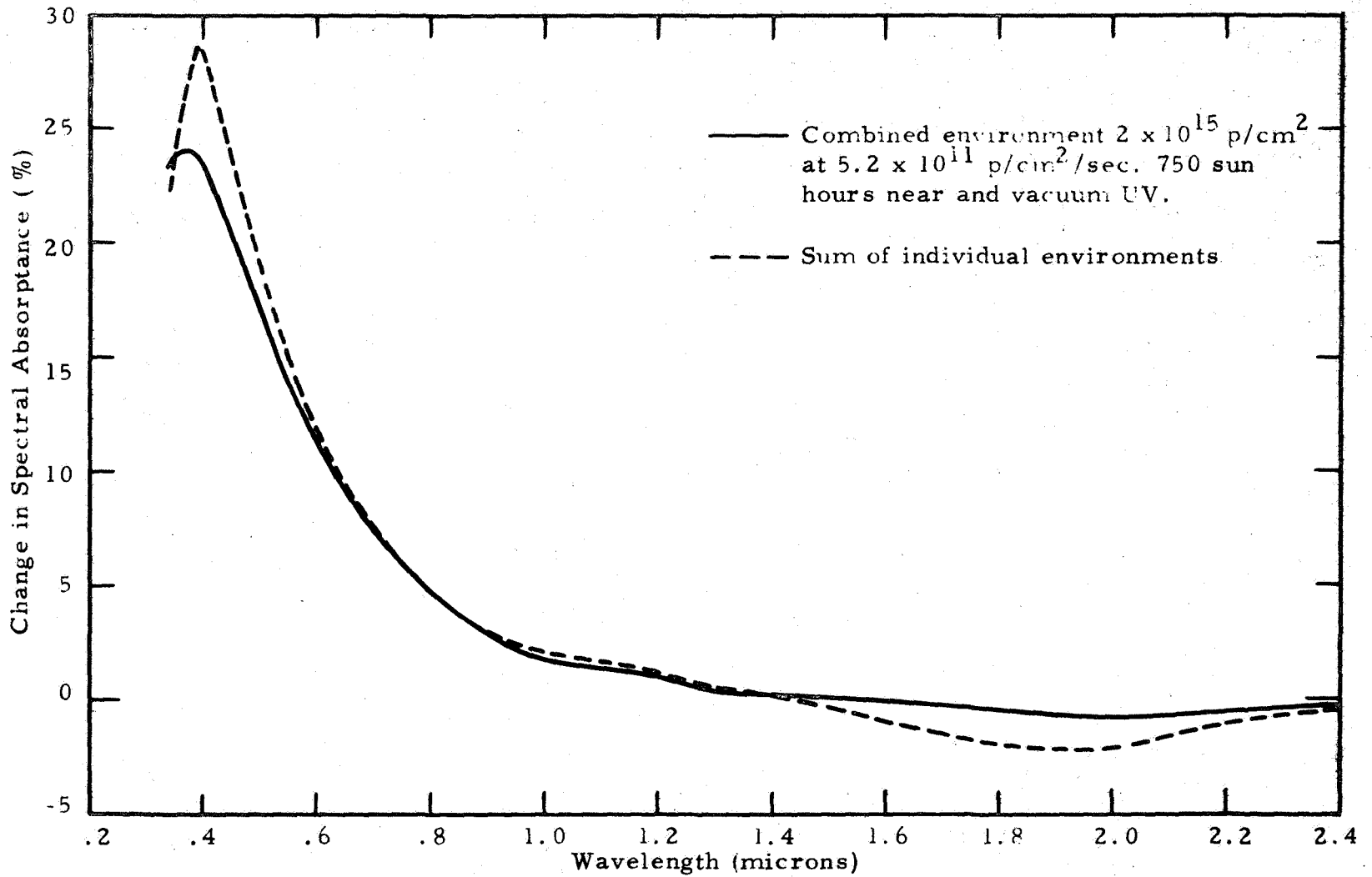


Figure 38 -- Combined effects versus sum of individual effects -
 $\text{La}_2\text{O}_3/\text{K}_2\text{SiO}_3$ (F-1-38)

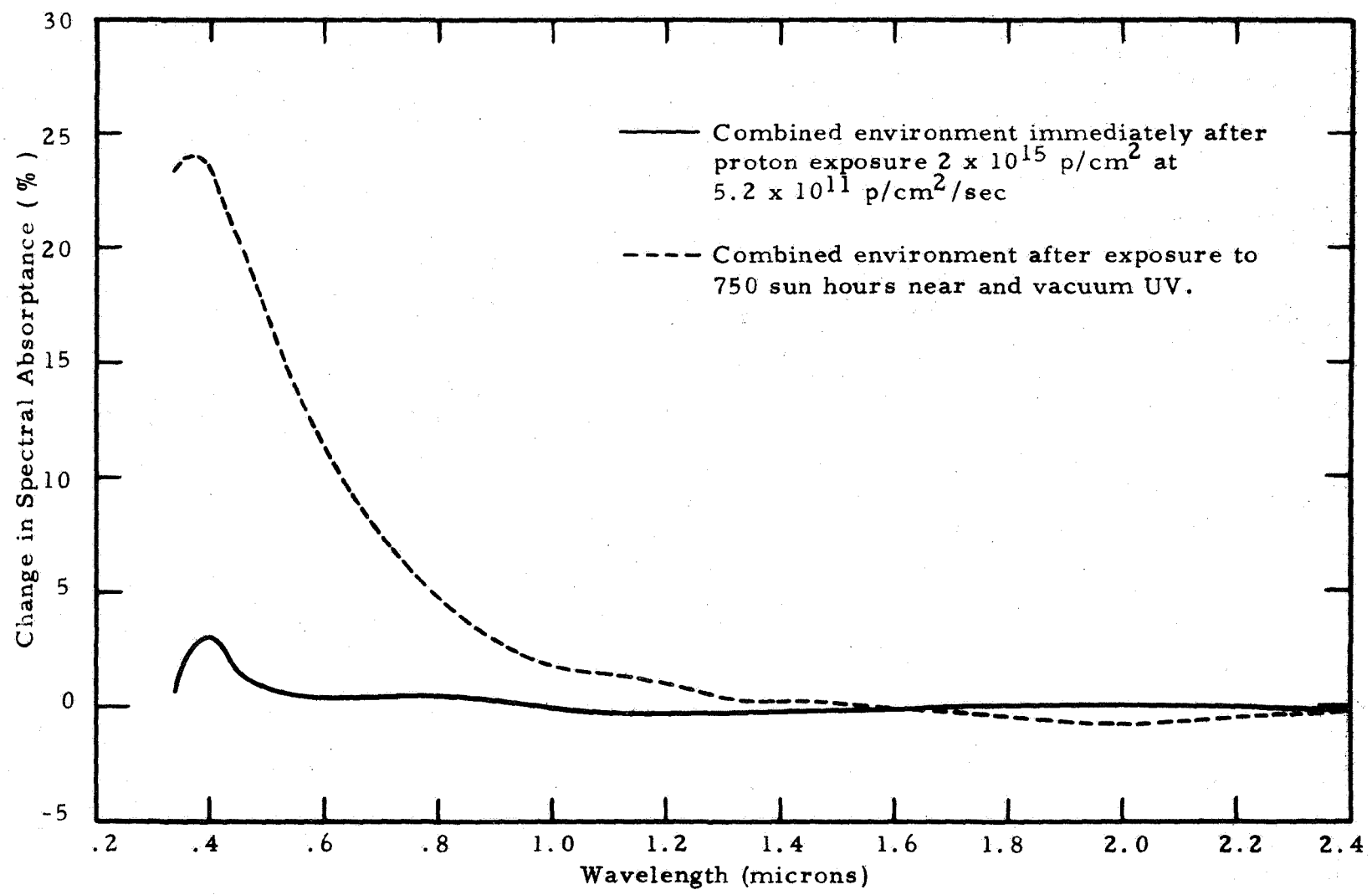


Figure 39 -- Effect of combined environment immediately after accelerated proton exposure and at end of test - $\text{La}_2\text{O}_3/\text{K}_2\text{SiO}_3$ (F-1-38)

e. S-13G

1. Proton Effects

The effect of proton radiation on this material is shown in Figure 40. The material showed the characteristic damage curve for ZnO with about the same effects as the ZnO/Silicone irradiated with continuous low current.

2. Ultraviolet Effects

The effect of ultraviolet radiation only is shown in Figure 41. The change in solar absorptance is greater around .4 micron than the ZnO/Silicone or the ZnO/K₂SiO₃ with virtually no damage again in the IR range.

3. Combined Environment Effect

The effect of combined environment simulation is shown in Figure 42. Bleaching of the proton damage in the IR range has apparently occurred.

f. TiO₂ Silicone

These tests were conducted in order to compare the results of in situ testing of TiO₂ Silicone with the work of Pinson⁽²⁾ which was conducted non-in situ.

1. Proton Effects

Figure 43 shows the effect of proton radiation on TiO₂/Silicone. It has the characteristic peak of ZnO but does not return to near zero in the visible range as does the ZnO. This material received 1-1/2 times more total proton flux than did the other materials.

-99-

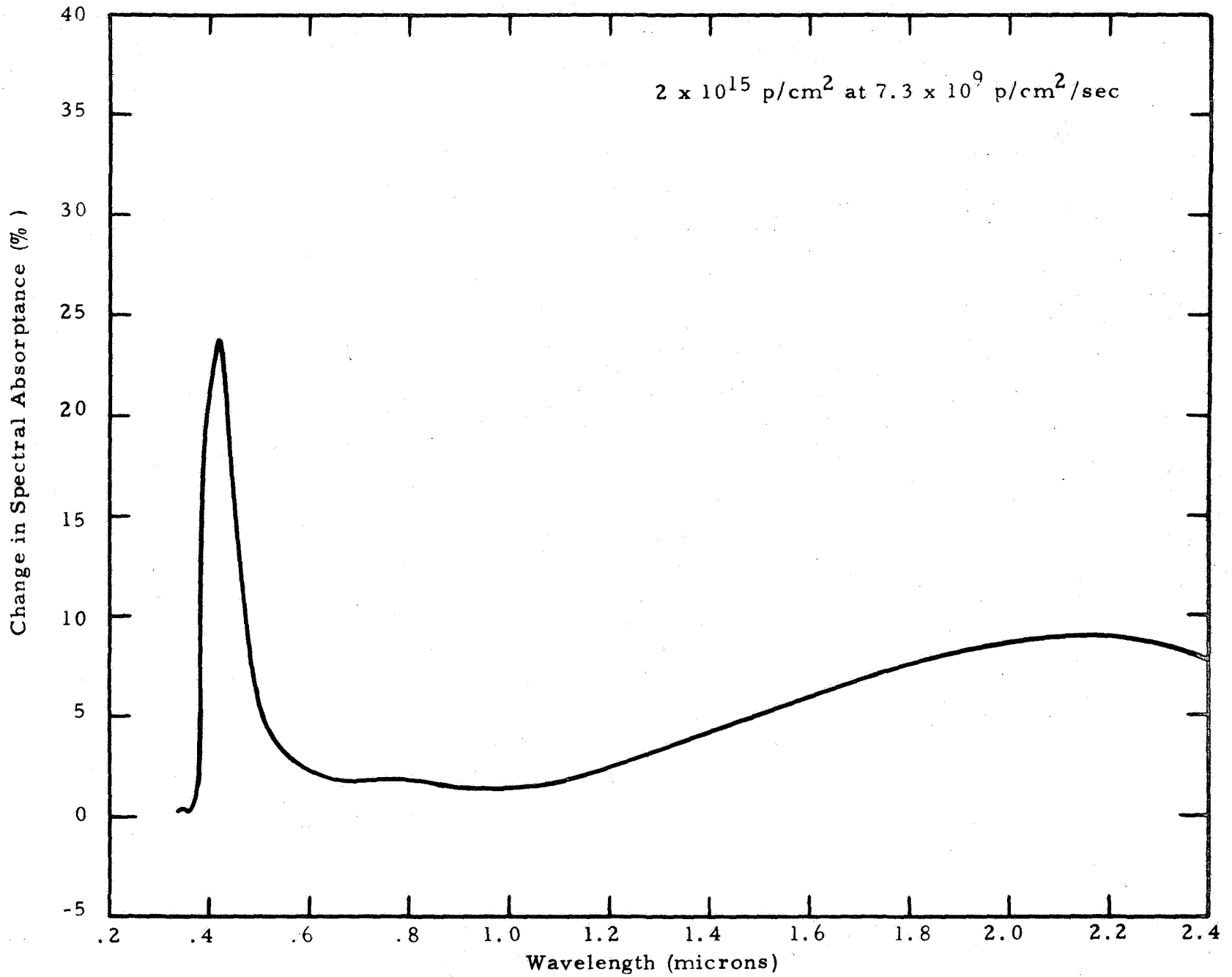


Figure 40 -- Effect of proton radiation only (S-13G)

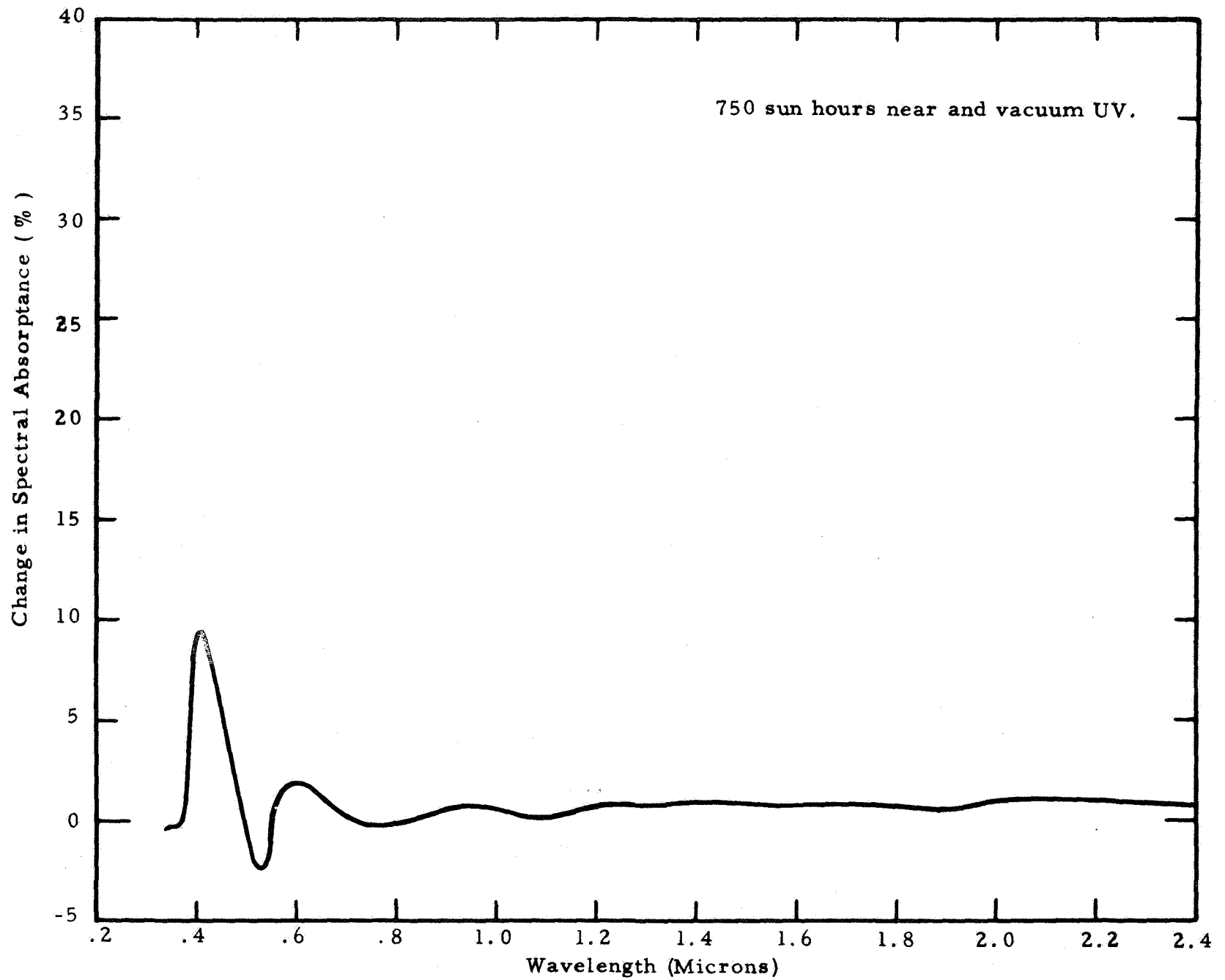


Figure 41 -- Effect of UV radiation only (S-13G)

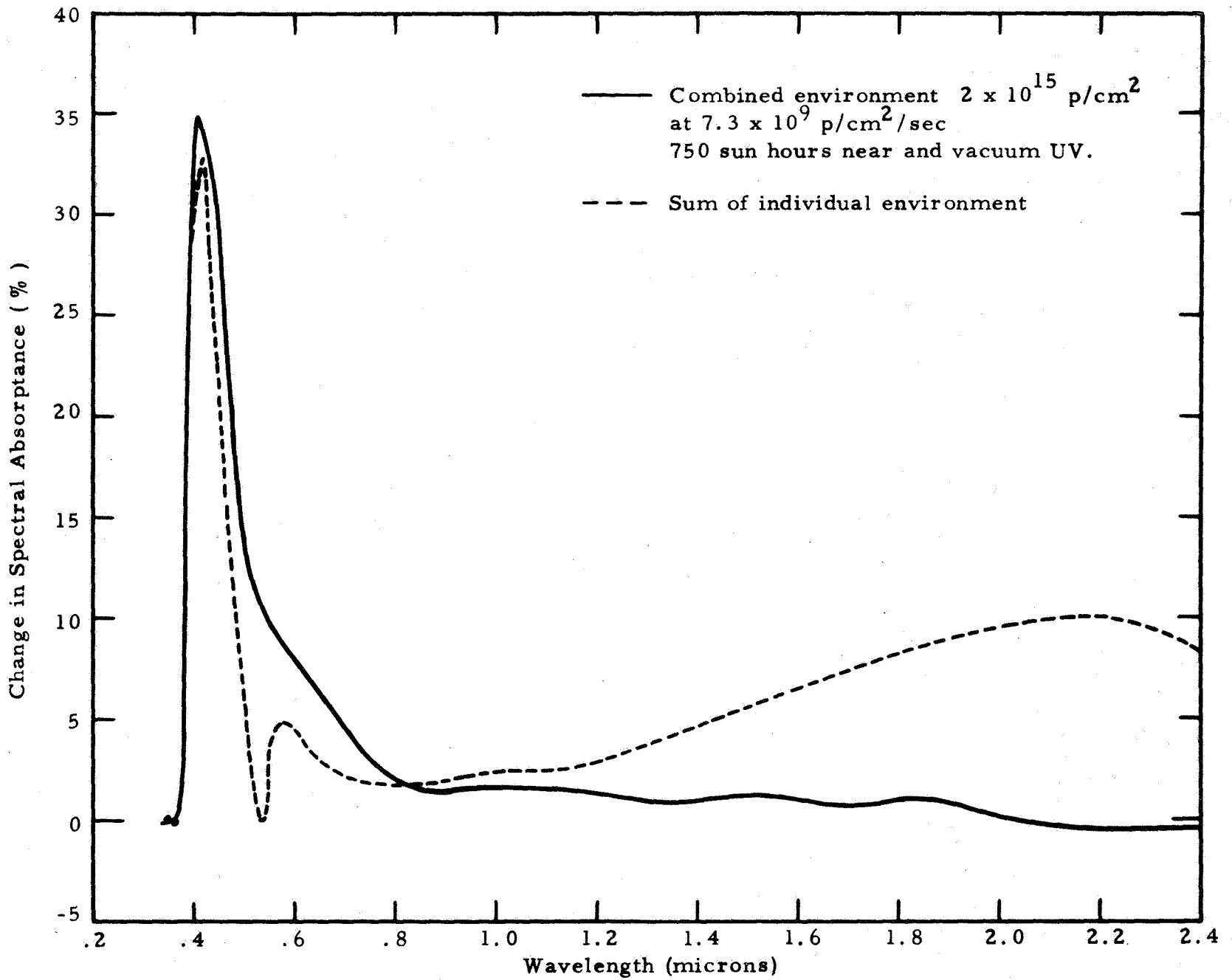


Figure 42 -- Combined effect versus sum of individual effects (S-13G)

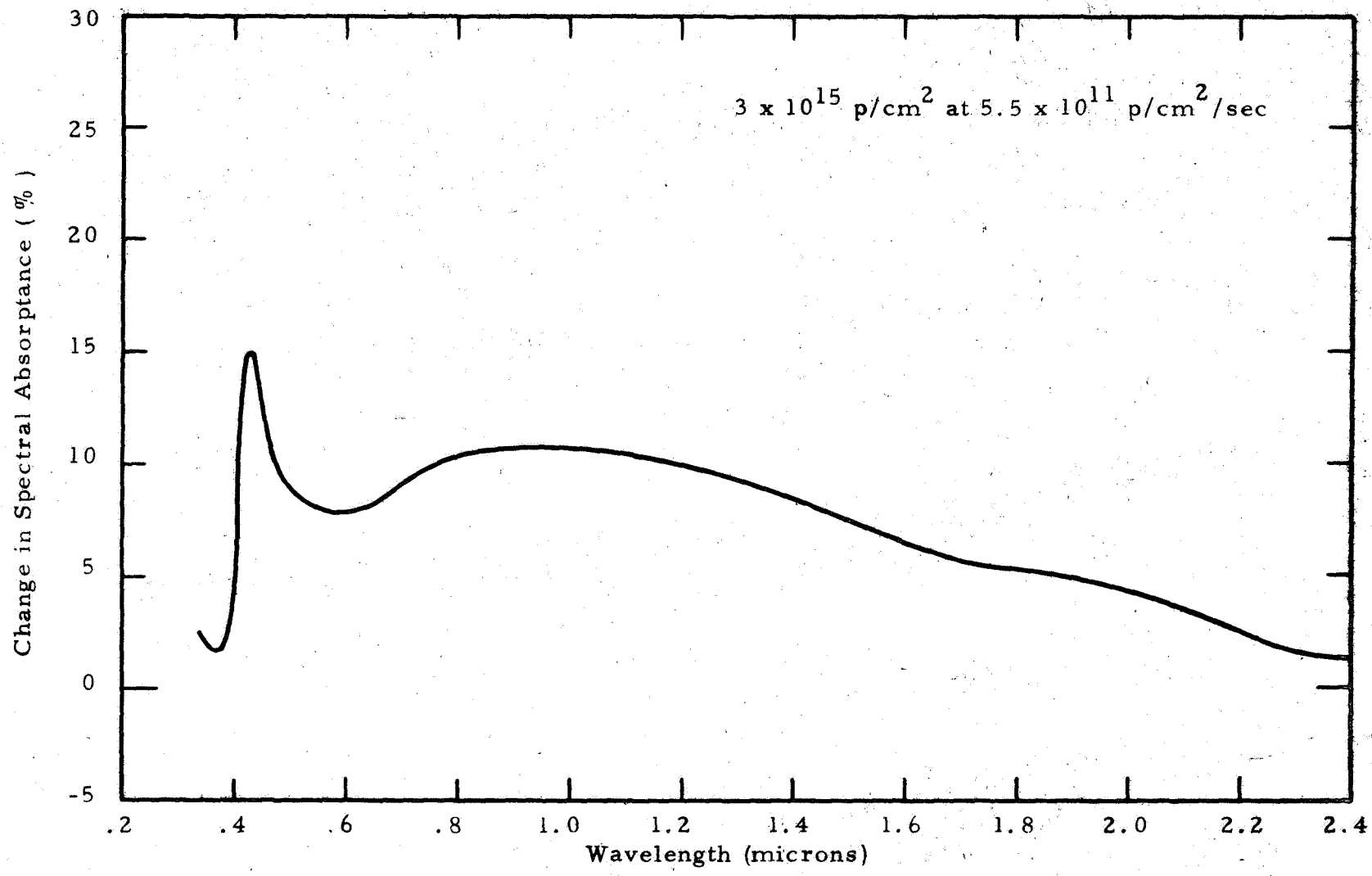


Figure 43 -- Effect of proton radiation only (TiO₂ Silicone)

2. Ultraviolet Radiation Effect

As shown by Figure 44, practically no damage was evident due to the near ultraviolet and vacuum ultraviolet radiation. This sample, however only received a total of 190 sun hours of electromagnetic radiations.

3. Combined Environment Effect

The effect of combined environment is shown in Figure 45. It may be seen that the combined damage is less than the proton damage alone which is just the opposite of the results obtained by Pinson.⁽²⁾ Synergistic effects were noted in Pinson's tests in which the combined damage was greater than the sum of the individual environments.

g. Powdered Samples

Powdered samples of SiO_2 , La_2O_3 , TiO_2 , Al_2O_3 and MgO were all irradiated with protons only for a total flux of 5×10^{15} p/cm^2 at a rate of 5.5×10^{11} $\text{p/cm}^2/\text{sec}$. The effects are shown in Figures 46 through 50. The only powdered sample which had significant damage is the TiO_2 . As may be seen from these figures, the other samples exhibited little or no damage.

B. Non-In Situ Tests

Three exposures were conducted non-in situ using a 5 KW mercury xenon lamp in the solar simulator. The results of these tests are discussed in the following paragraphs based upon the environmental parameters selected. The curves which accompany show only changes in spectral absorptance.

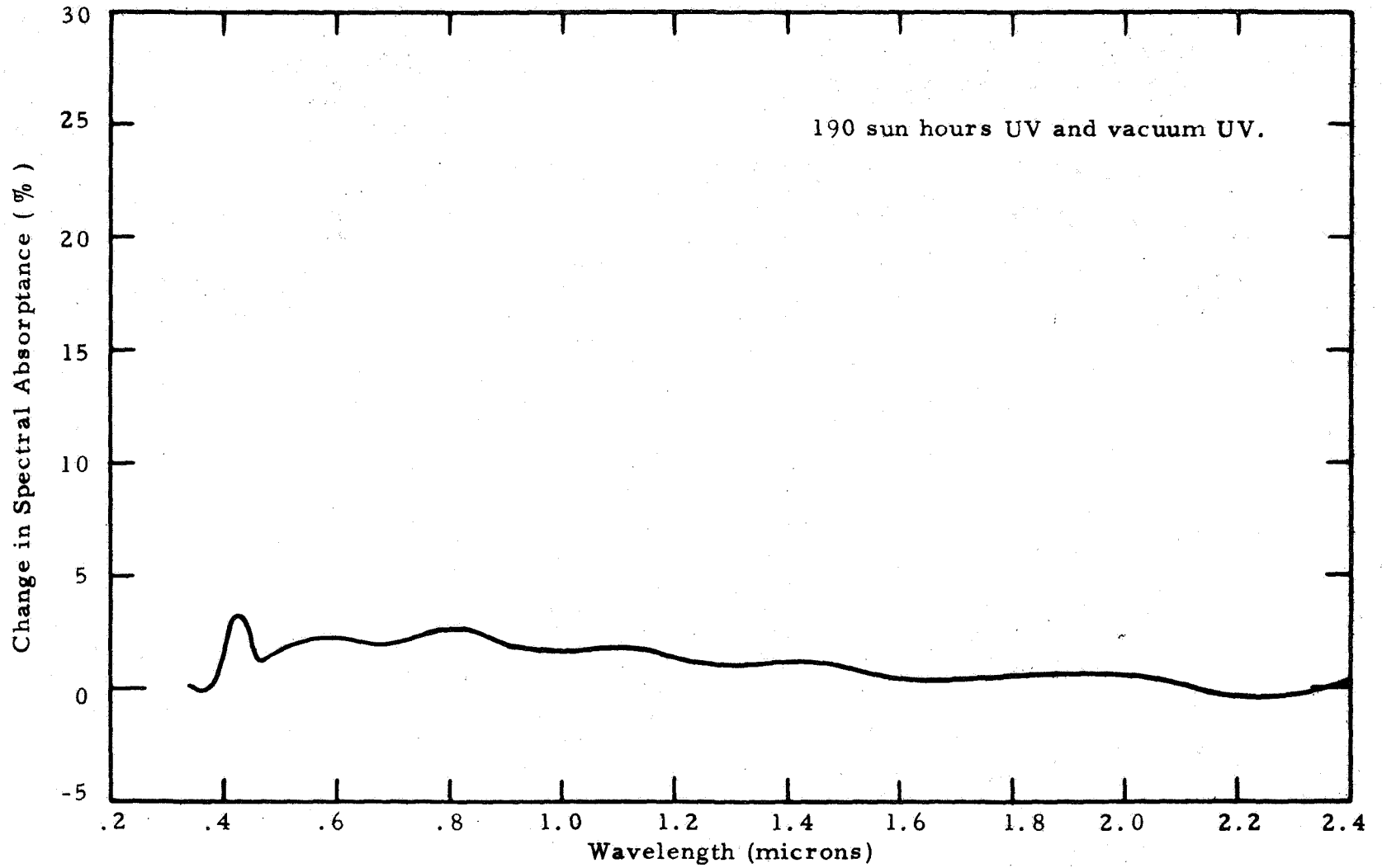


Figure 44 -- Effect of UV radiation only (TiO₂ Silicone)

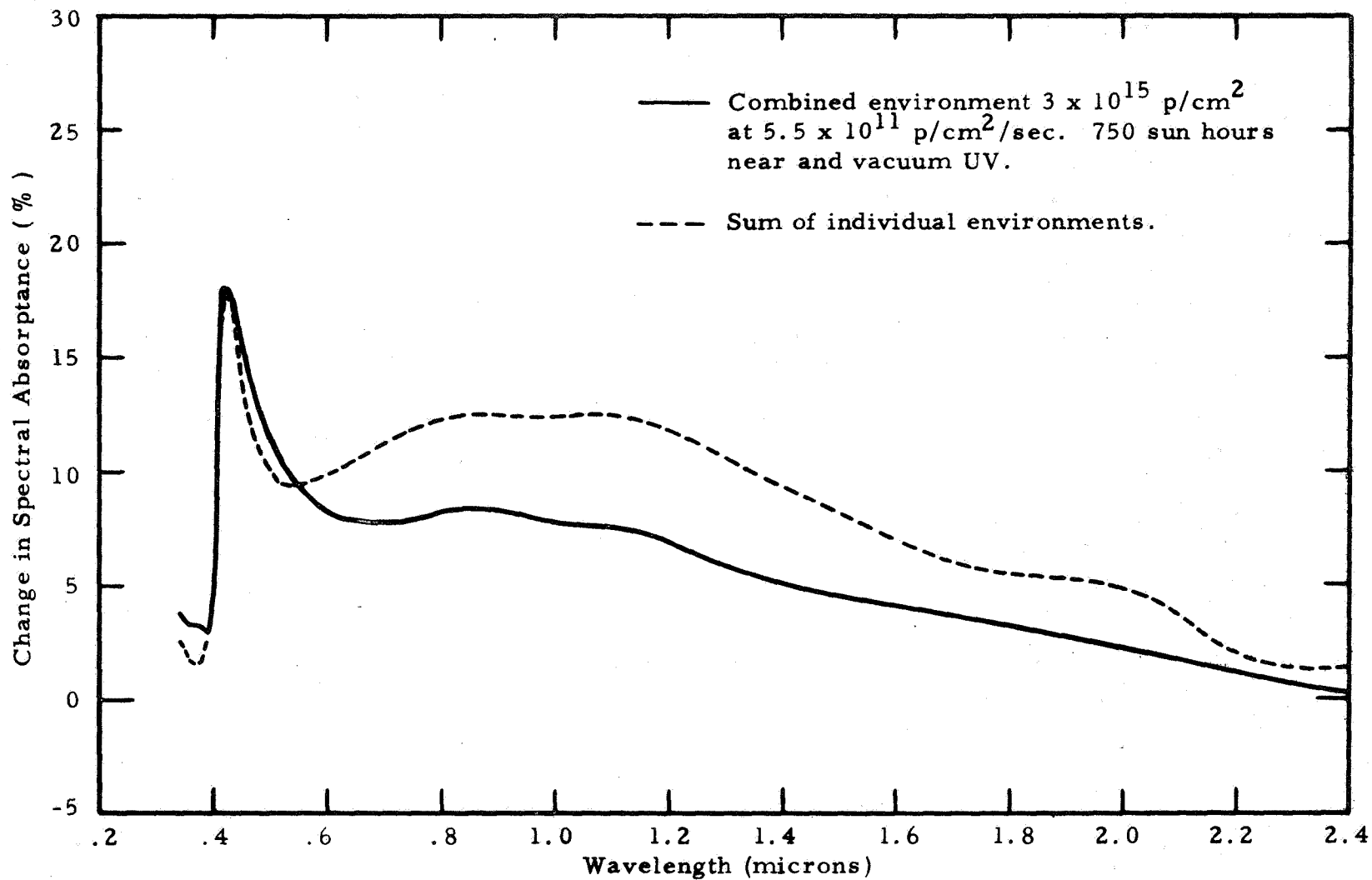


Figure 45 -- Combined effects versus sum of individual effects
(TiO₂ Silicone)

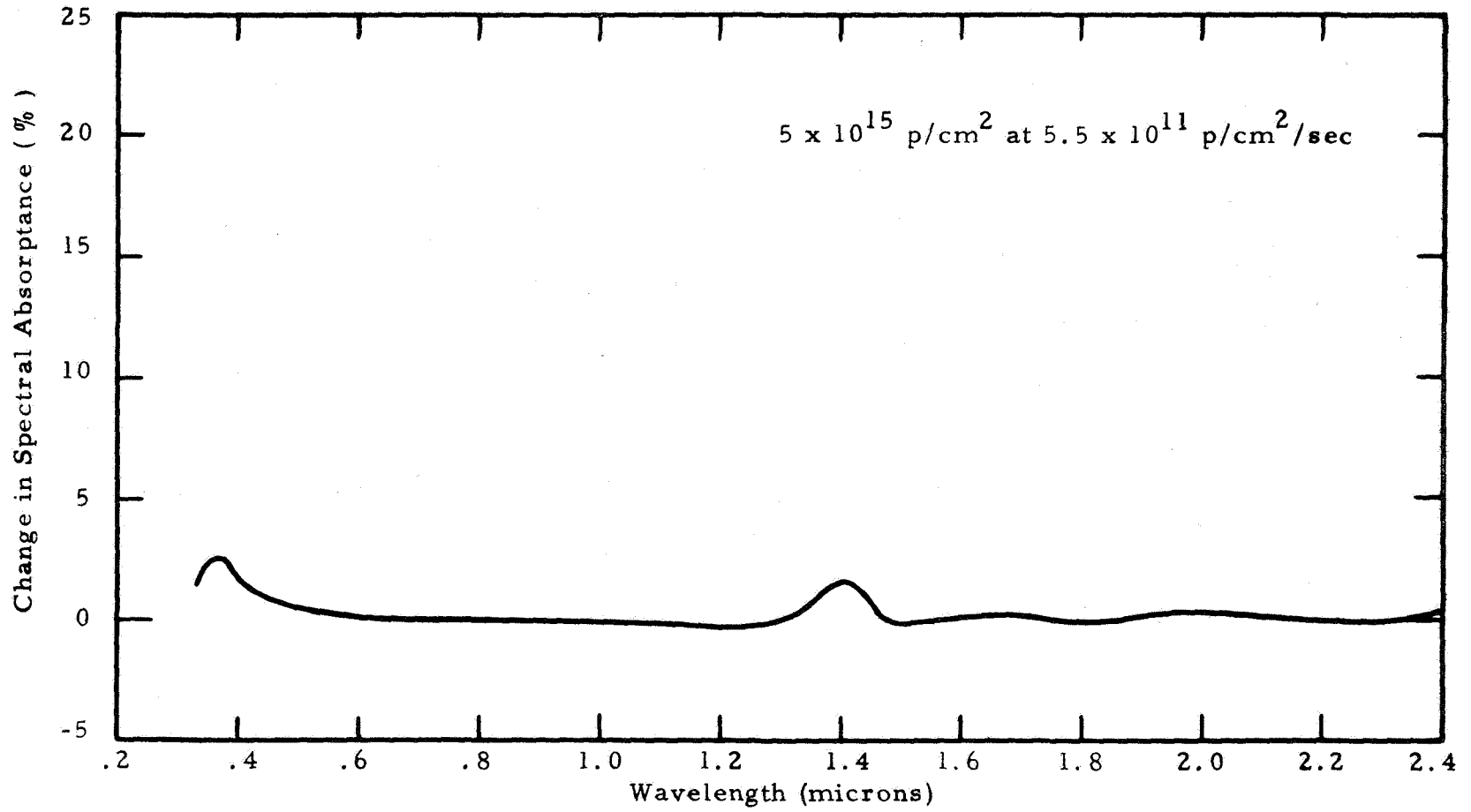


Figure 46 -- Effect of proton radiation only (SiO₂ powdered)

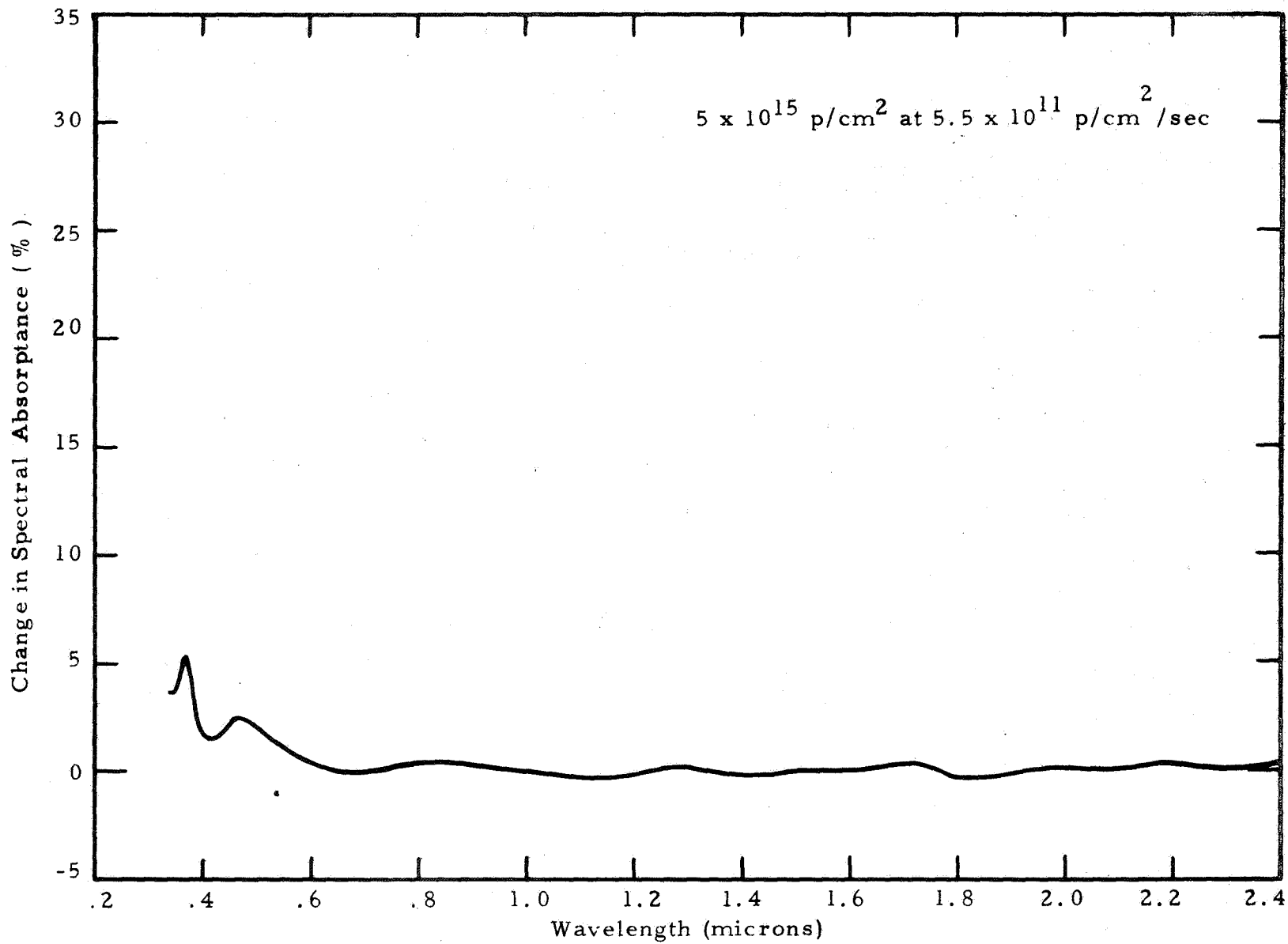


Figure 47 -- Effect of proton radiation only (La₂O₃ powdered)

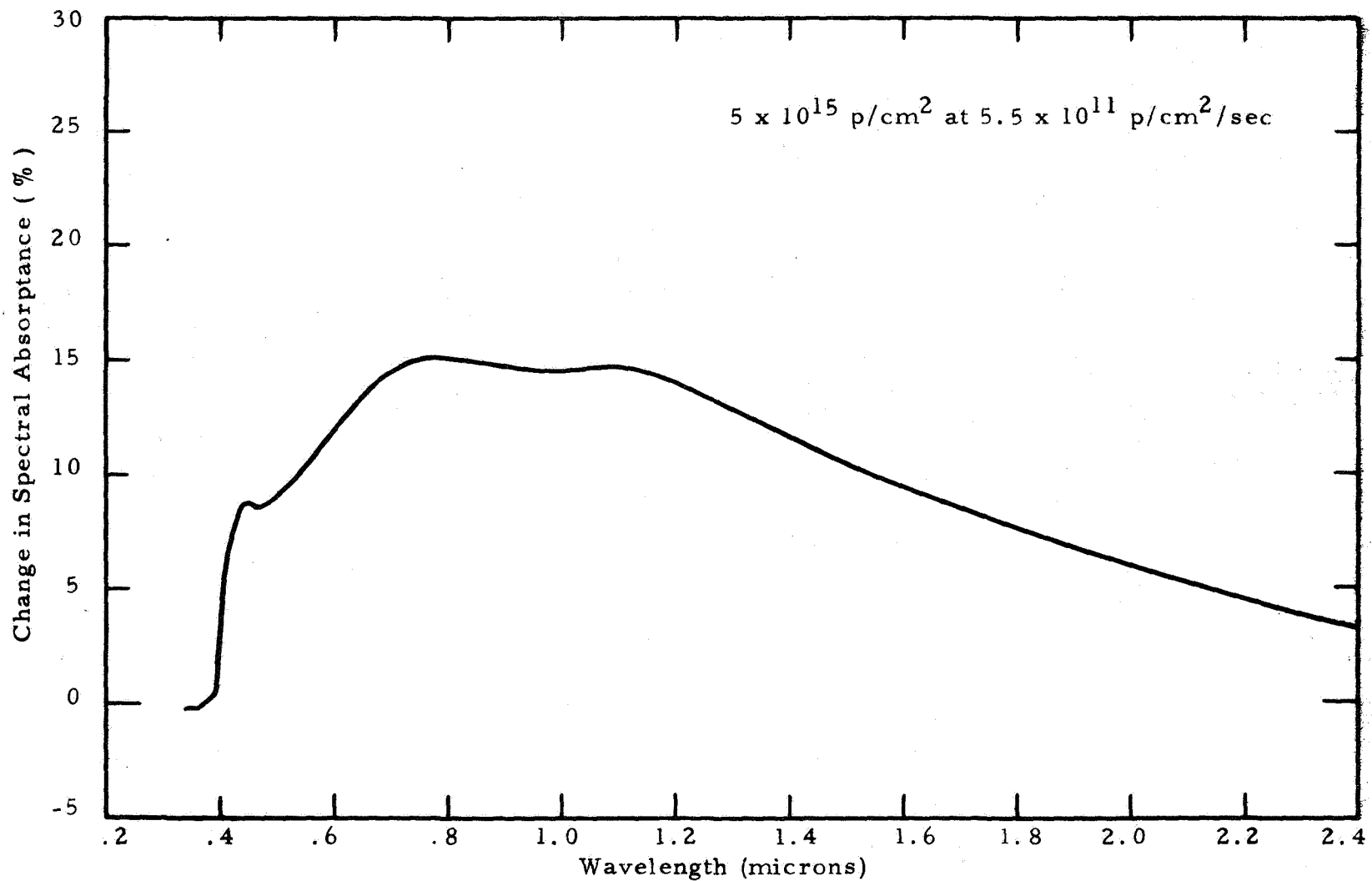


Figure 48 -- Effect of proton radiation only (TiO₂ powdered)

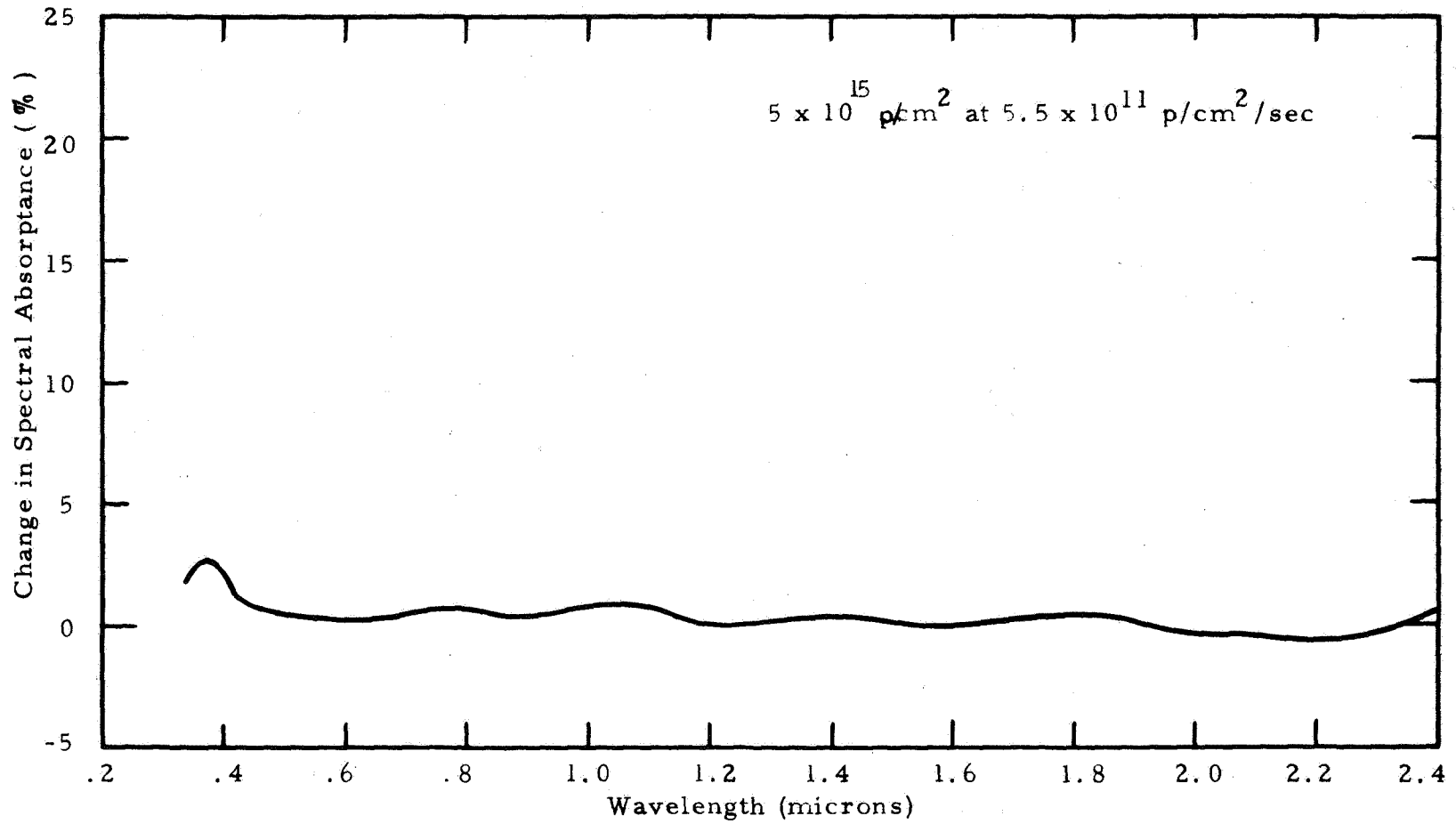


Figure 49 -- Effect of proton radiation only (AL₂O₃ powdered)

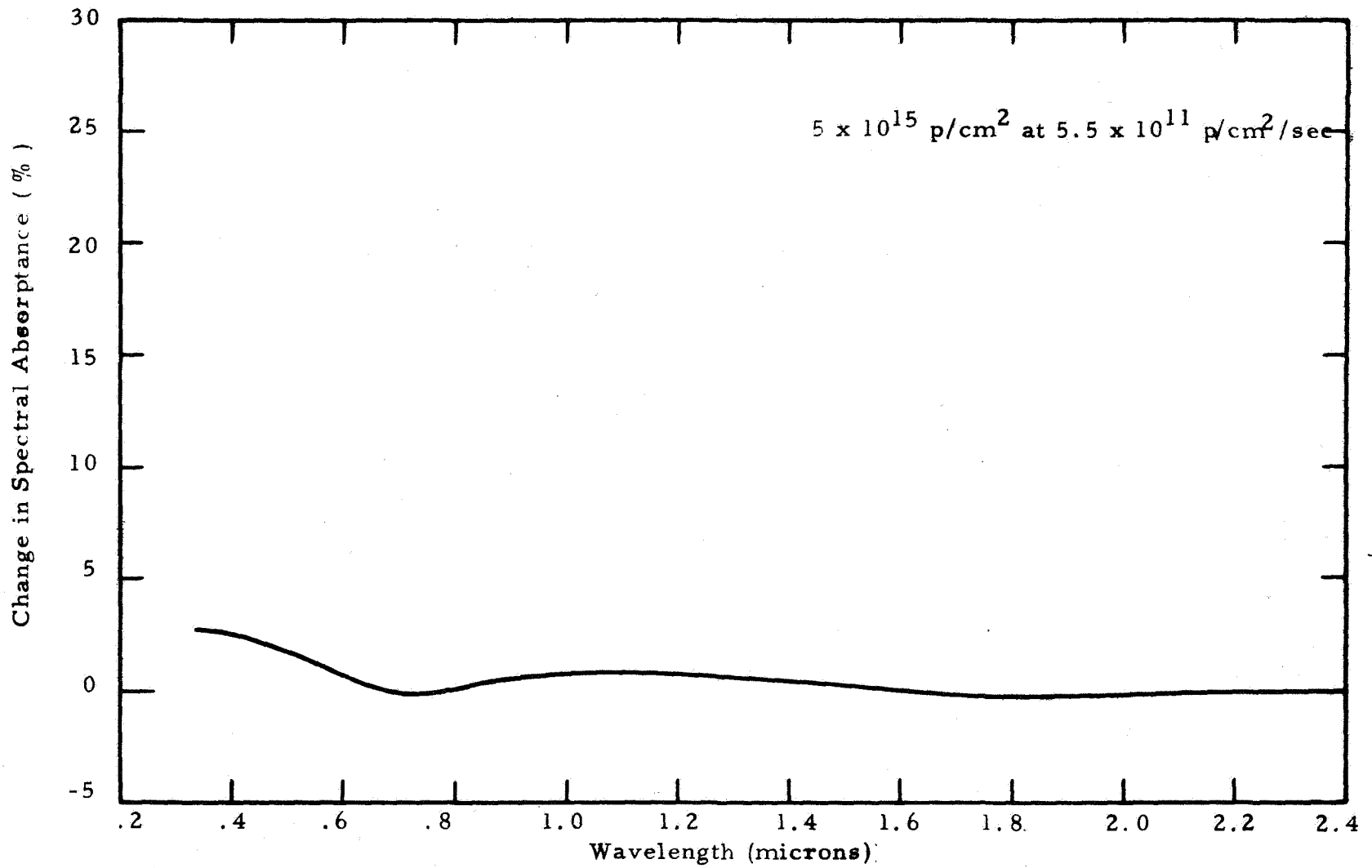


Figure 50 -- Effect of proton radiation only (MgO powdered)

1. SP 500 Zinc Oxide

Figure 51 shows the change in spectral absorbance for compressed zinc oxide powder following exposure to 10 Kev protons. Total flux was 2×10^{15} protons/cm² at 5.5×10^{11} p/cm²/sec. Sample temperature was 298°K. Damage in this case was comparable to that for ZnO/K₂SiO₃ in the same environment, from earlier work, indicating that the damage for the latter is occurring in the pigment.

Figure 52 shows the effect of a combined proton and ultraviolet environment on zinc oxide. The environment included a total 10 Kev proton flux of 2×10^{15} p/cm² at 7.4×10^9 p/cm²/sec and 750 sun hours of near and vacuum UV at 10 solar equivalents. The damage was substantially less than for the sample exposed to protons only, indicating proton damage bleaching by electromagnetic radiation.

Figure 53 shows the effect of exposure to 750 sun hours of near and vacuum UV at 10 solar equivalents. Measured damage was very small and essentially within the error of readings. Bleaching of damage undoubtedly occurred upon return of the sample to atmospheric conditions.

2. Vacuum Deposited Ag on Fused Silica

Figure 54 shows the effect of exposure to combined 10 Key protons (1.5×10^{17} p/cm² at 5.5×10^{11} p/cm²/sec) and 750 sun hours of near and vacuum UV on vacuum deposited silver on fused silica. Substantial damage incurred apparently from the proton exposure. The peak in the induced absorption band occurred at about 0.365 micron.

Figure 55 demonstrates the effect of 750 sun hours of near and vacuum UV at 10 solar equivalents to the vacuum deposited silver on fused silica. Changes were essentially within the errors in measurements,

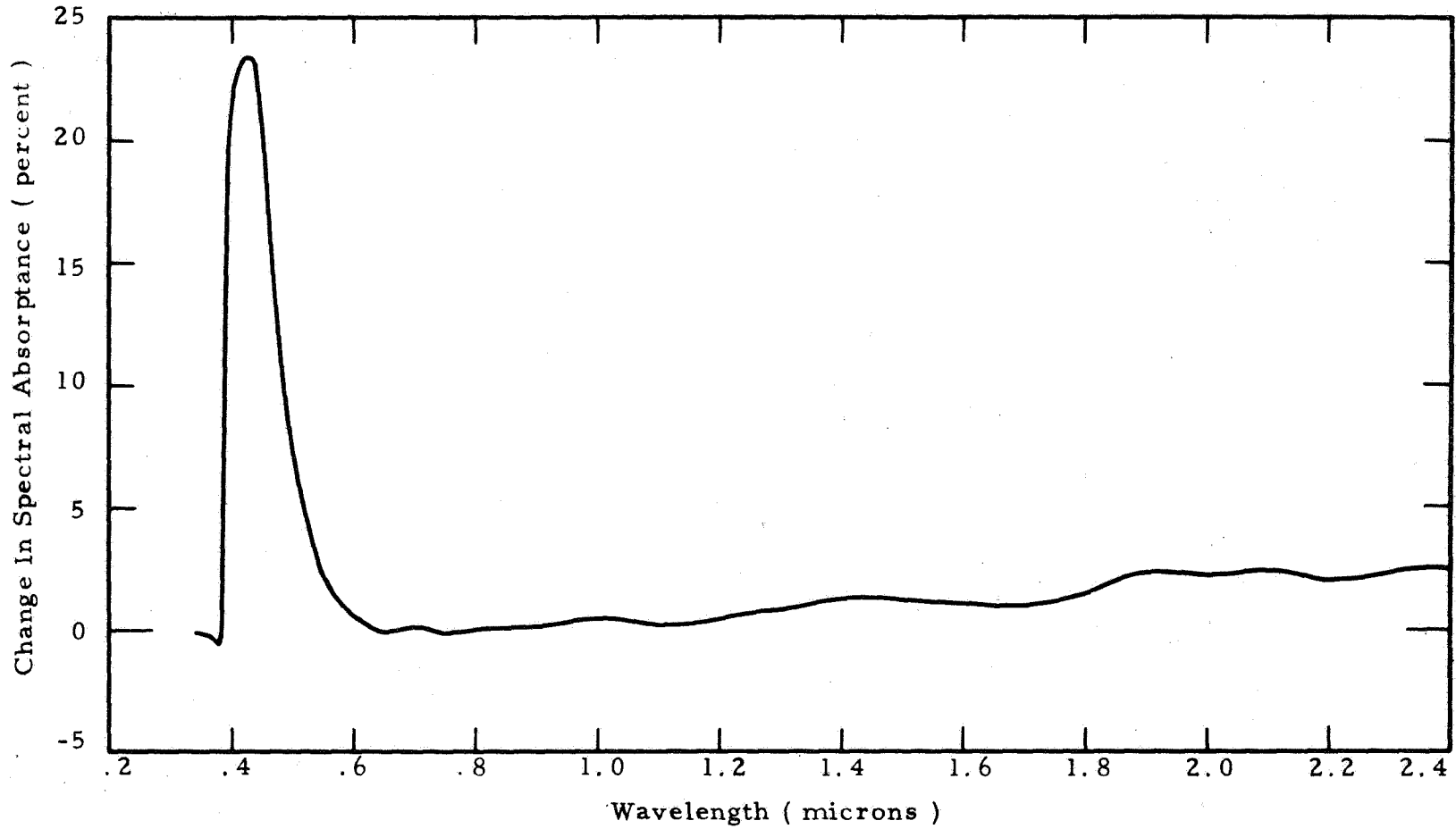


Figure 51-- Effect of proton exposure on SP 500 zinc oxide at 298°K. 10 Kev protons - 2×10^{15} p/cm² at 5.5×10^{11} p/cm²/sec.

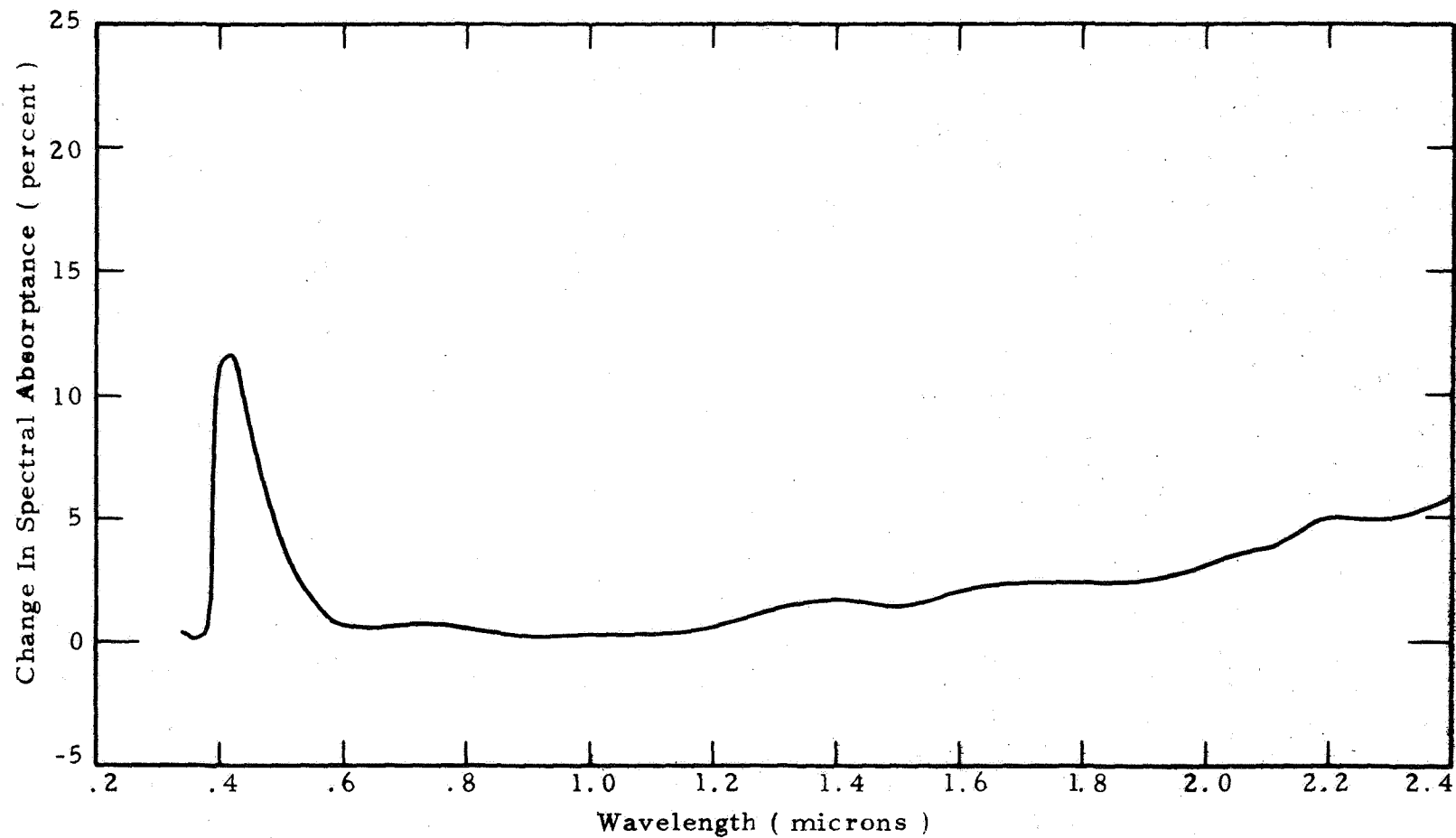


Figure 52-- Effect of combined environment exposure on SP 500 zinc oxide at 299°K. 10 Kev protons - 2×10^{15} p/cm² at 7.4×10^9 p/cm²/sec. 750 sun hours of near and vacuum UV at 10 solar equivalents.

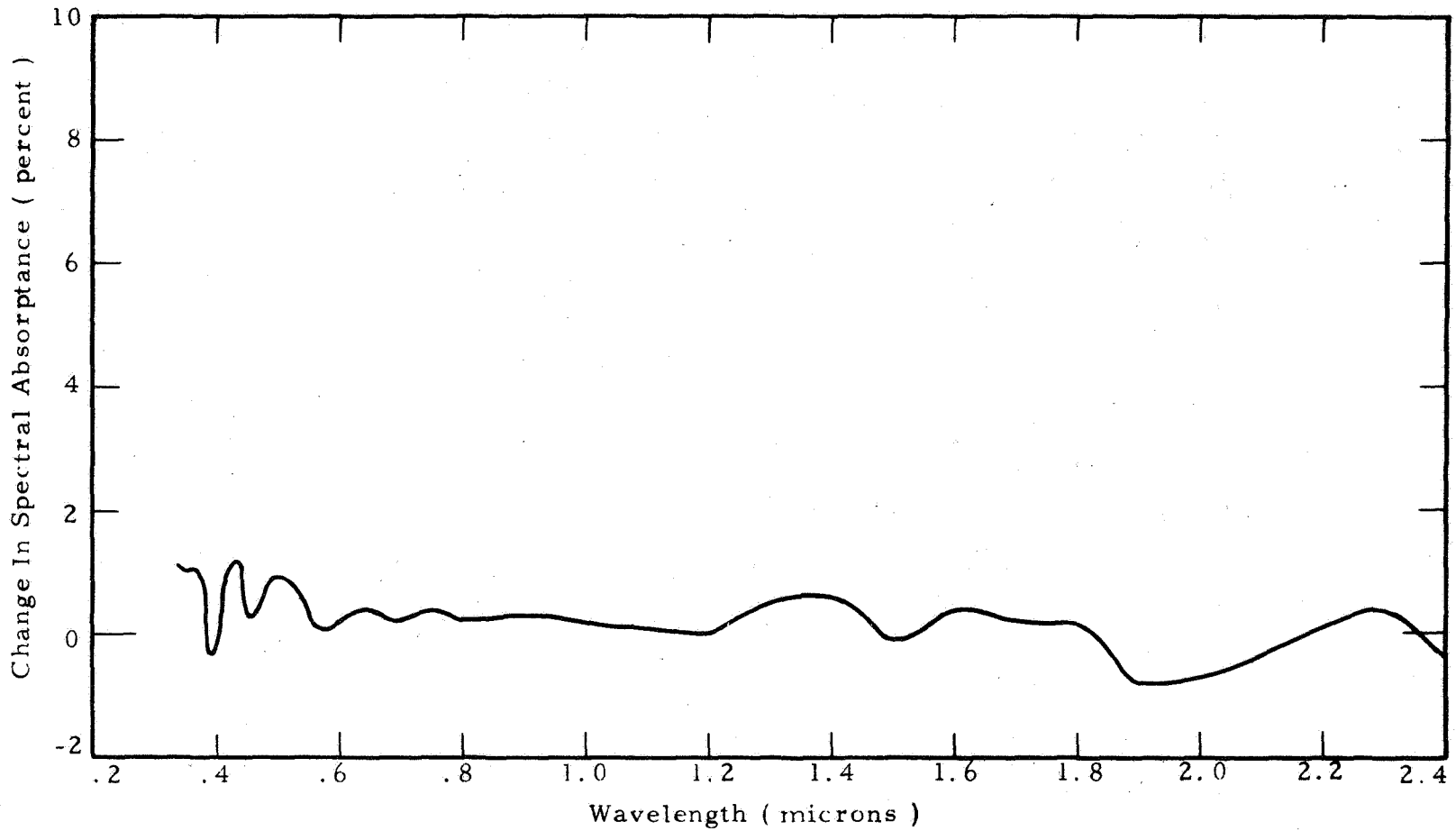


Figure 53-- Effect of ultraviolet exposure of SP 500 zinc oxide at 299°K. 750 sun hours of near and vacuum UV at 10 solar equivalents.

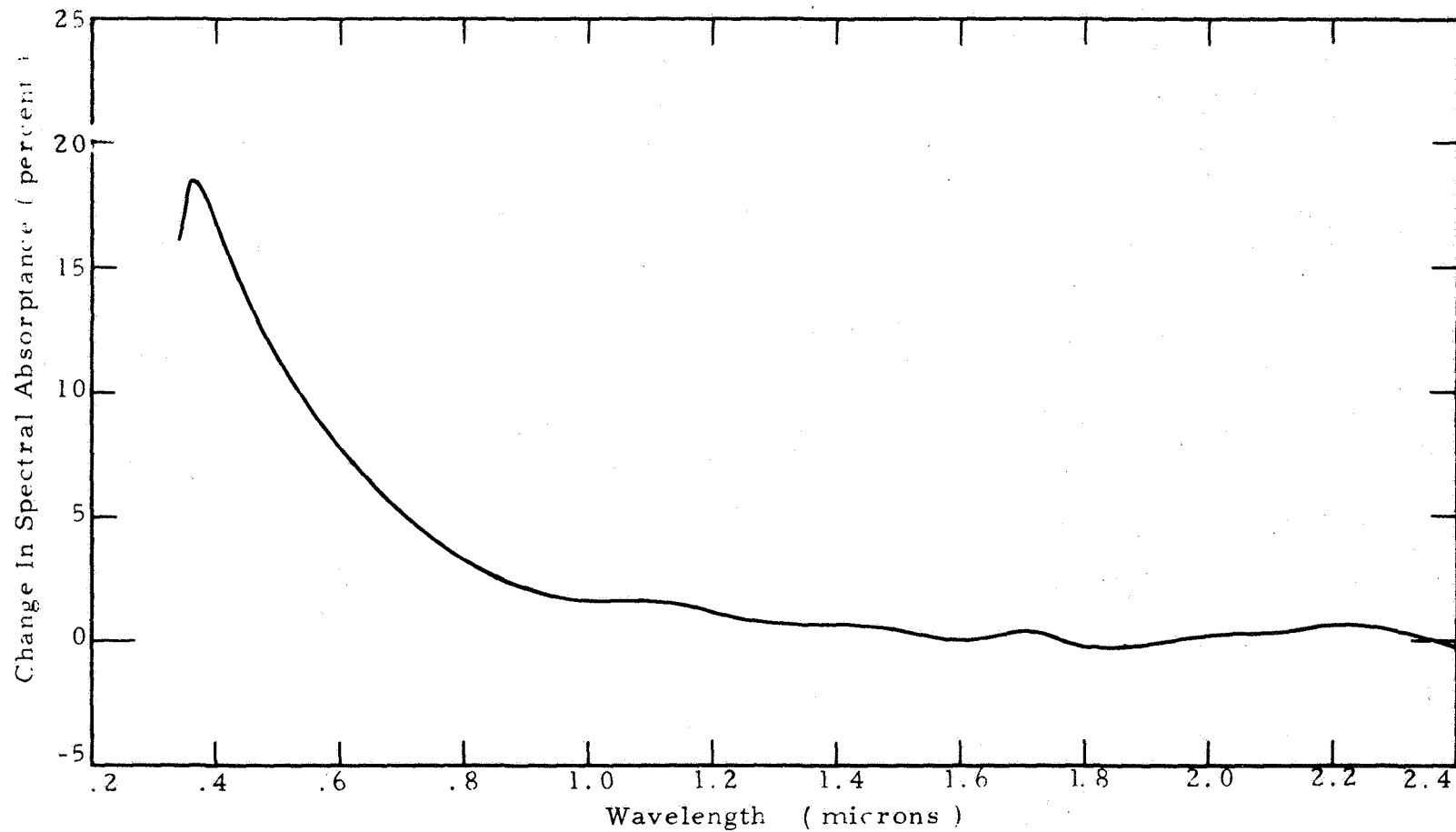


Figure 54-- Effect of combined environment exposure on vacuum deposited Ag on fused silica at 304°K. 10 Kev protons - 1.5×10^{17} p/cm² at 5.5×10^{11} p/cm²/sec. 750 sun hours of near and vacuum UV at 10 solar equivalents.

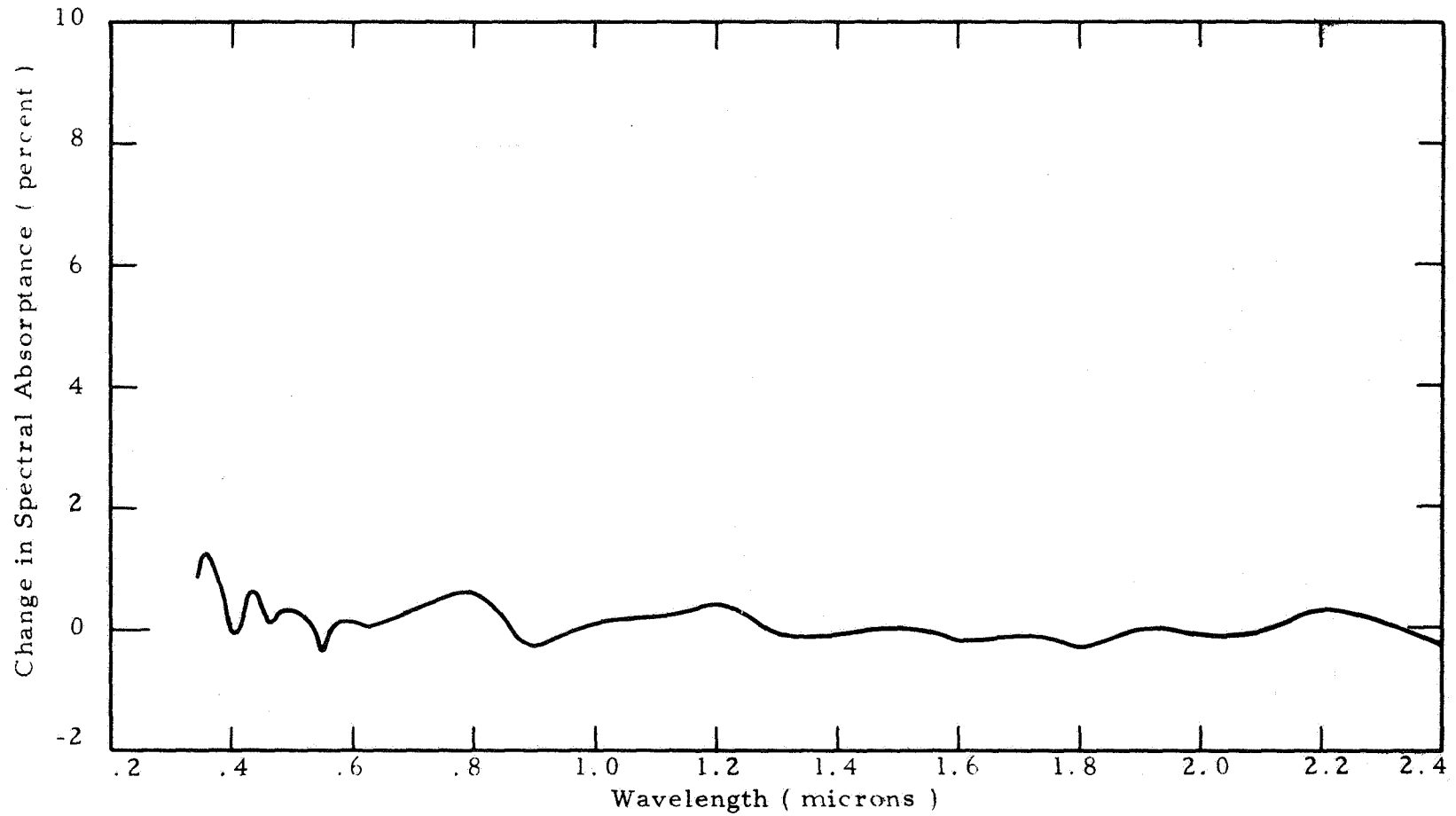


Figure 55--Effect of ultraviolet exposure on vacuum deposited Ag on fused silica at 304°K. 750 sun hours of near and vacuum UV at 10 solar equivalents.

VII.

CONCLUSIONS AND RECOMMENDATIONS

A. Conclusions

1. The ZnO/potassium silicate is more stable in an ultraviolet radiation environment than in a proton environment. It is apparently very susceptible to proton damage in the spectral range studied. A threshold of approximately 10^{15} p/cm² causes measurable damage with proportionate damages for doses in excess of this level.
2. There was not evidence to indicate that synergistic effects existed for the ZnO/K₂SiO₃ material. In all but one test, the combined environment tests including both protons and ultraviolet radiation produced less optical damage than the sum of the damages due to the individual environments.
3. There is definite evidence that the rate at which protons are applied to ZnO/K₂SiO₃ has a definite effect on the amount of damage to the material, especially in the infrared portion of the spectrum.
4. The 1-11-9-13 ZnO/K₂SiO₃ demonstrated comparable degradation effects to the F-1-47-D ZnO/K₂SiO₃. The 1-11-9-13 did exhibit less damage in the IR portion of the spectrum but had a larger change in absorptance near .4 micron.
5. The Lanthanum Oxide/Potassium Silicate is more susceptible to ultraviolet radiation damage and less susceptible to proton damage. Increasing the total protons by a factor of 5 did not increase the damage indicating a very good resistance to protons. In contrast to the ZnO/K₂SiO₃, the La₂O₃/K₂SiO₃ shows a definite damage effect, principally due to ultraviolet exposure. Of the two batches of La₂O₃/K₂SiO₃ tested, the F-1-38 was the least resistant to ultraviolet damage.

6. Combined environment tests including both protons and ultraviolet radiation produced comparable damage to the sum of the individual environments for the Lanthanum Oxide/Potassium Silicate.
7. The TiO_2 /Silicone is highly susceptible to proton damage and has very little susceptibility to ultraviolet radiation. This effect also showed up in the powdered samples since the TiO_2 was the only powder which showed significant damage due to proton radiation.

B. Recommendations

1. Further study should be conducted on the influence of the electromagnetic spectral distribution on the combined environment synergistic effects.
2. The reciprocity effects of accelerated testing for both electromagnetic and particulate radiation should be investigated.
3. Temperature effects should be investigated for materials studied in situ.
4. The effects of simulated space electron radiation should be studied.
5. The coatings should be subjected to proton and electron particle irradiation in order to establish the relation between particle energy and optical degradation.

VIII.

REFERENCES

1. Cooley, J. A., "Evaluation of Thermal Control Coatings in the Space Environment", NASA-CR 73028, December, 1966.
2. Pinson, J. D., and J. A. Wiebelt, "Synergistic and Accelerated Testing Effects on Space Thermal Control Materials", Proceedings of the AIAA/IES/ASTM Space Simulation Conference, Houston, Texas, September, 1966.
3. Pezdirtz, G. F., R. A. Jewell and P.M. Blair, Jr., "Ultraviolet Stability of Some White Thermal Control Coatings Characterized in Vacuum", AIAA Paper No. 67-345 (April, 1967).
4. Jorgenson, G. V., "Effects of Simulated Solar-Wind Bombardment on Spacecraft Thermal Control Surfaces," AIAA Thermophysics Specialist Conference, Monterey, Calif., Paper No. 65-647, September 13-15, 1965.
5. Breuch, R. A., "Exploratory Trapped-Particle and Trapped-Particle-plus-Ultraviolet Effects on the Optical Properties of Spacecraft Thermal Control Coatings," AIAA Thermophysics Specialist Conference, Monterey, Calif., Paper No. 65-646, Sept. 13-15, 1965.
6. Hass, G., et al., "Solar Absorptance and Thermal Emittance of Aluminum Coated With Surface Films of Evaporated Aluminum Oxide", AIAA Thermophysics Specialist Conference, Monterey, Calif., Paper No. 65-656, Sept. 13-15, 1965.
7. Crosby, J. R., and Perlow, M. A., "SNAP 10A Thermal Control Coatings", AIAA Thermophysics Specialist Conference, Monterey, Calif., Paper No. 65-652, September 13-15, 1965.

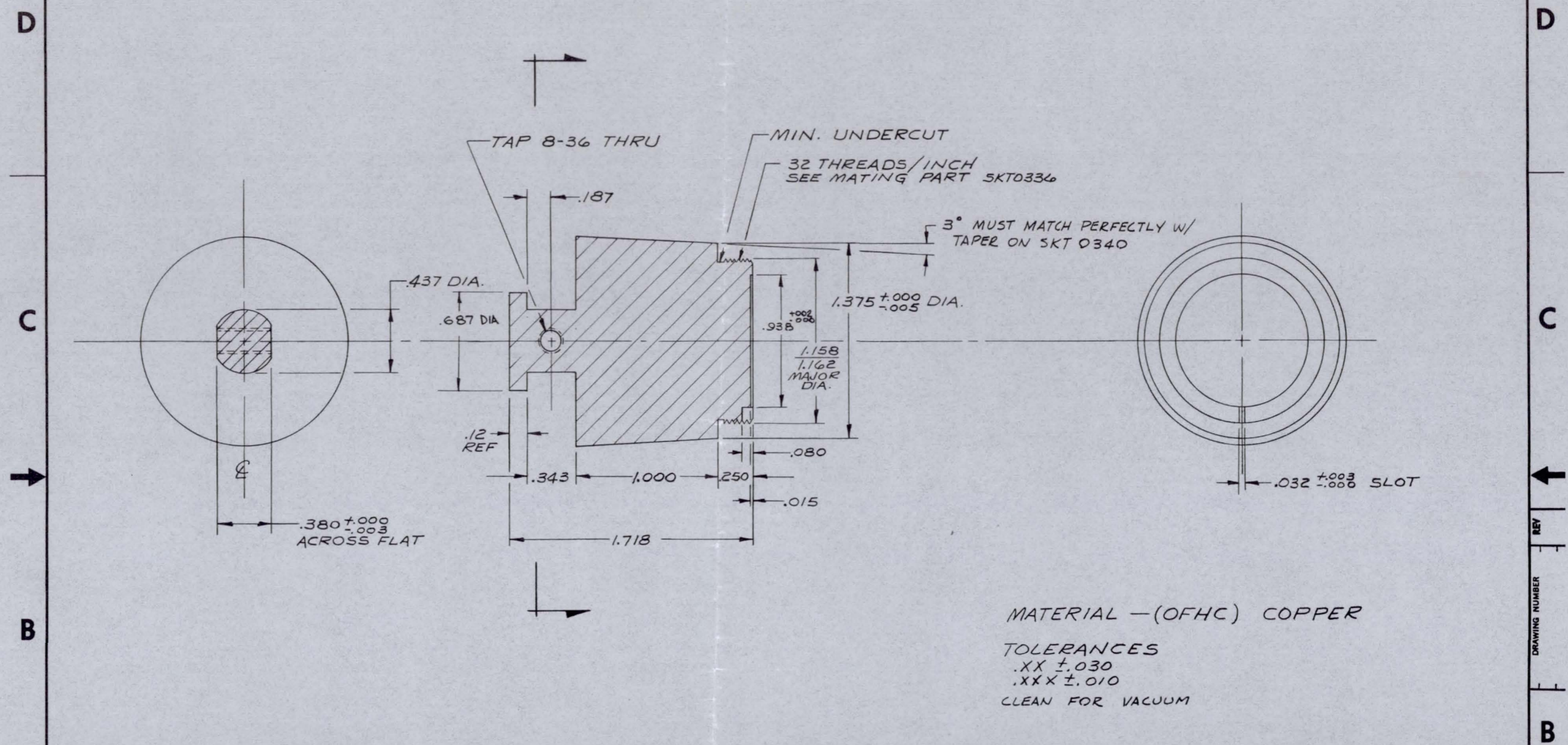
8. Johnson, F.S., "The Solar Constant", Journal of Meteorology, Vol. 11, pp 431-439, 1954.
9. Hinteregger, H. E. and K. Watanabe, "Photoelectric Cells for the Vacuum Ultraviolet", Jour. Opt. Soc. Am., Vol. 43, No. 7, pp 604-608, July, 1963.
10. Dunkleman, L., "Ultraviolet Photo Detectors", J. Quant. Spectrosc. Radiat. Transfer, Vol. 2, pp 533-544, 1962.

IX. APPENDIX

Following are prints of dimensional information for items fabricated under this contract.

4 3 2 1

REVISIONS				
ZONE	LTR	DESCRIPTION	DATE	APPROVED



MATERIAL — (OFHC) COPPER
 TOLERANCES
 .XX ±.030
 .XXX ±.010
 CLEAN FOR VACUUM

91

MACHINED
 DRILLED HOLES/AND-10387 THREADS/
 HANDBOOK H-28 AND MIL-STD-9
 BREAK SHARP EDGES AND COR. .005 TO
 .020 R
 -DIA ON COM CTR CONC WITHIN .010/
 TIR
 -SUR SQ TO RESP AXIS WITHIN .001/
 IN.
 -SUR SQ. FLATNESS, PAR., WITHIN
 .002/IN.
 -FILLETS .020 TO .040 R
 BEND AND BEND RELIEF RADII 2 x
 THK
 GEOMETRIC SYMBOLS/
 MIL-STD-8
 SURFACE ROUGHNESS/
 MIL-STD-10 ✓

MECHANICAL PROPERTIES			
YP			
TS			
EL2			
RA			
BH			
RH			
	NEXT ASSY	USED ON	
	APPLICATION		

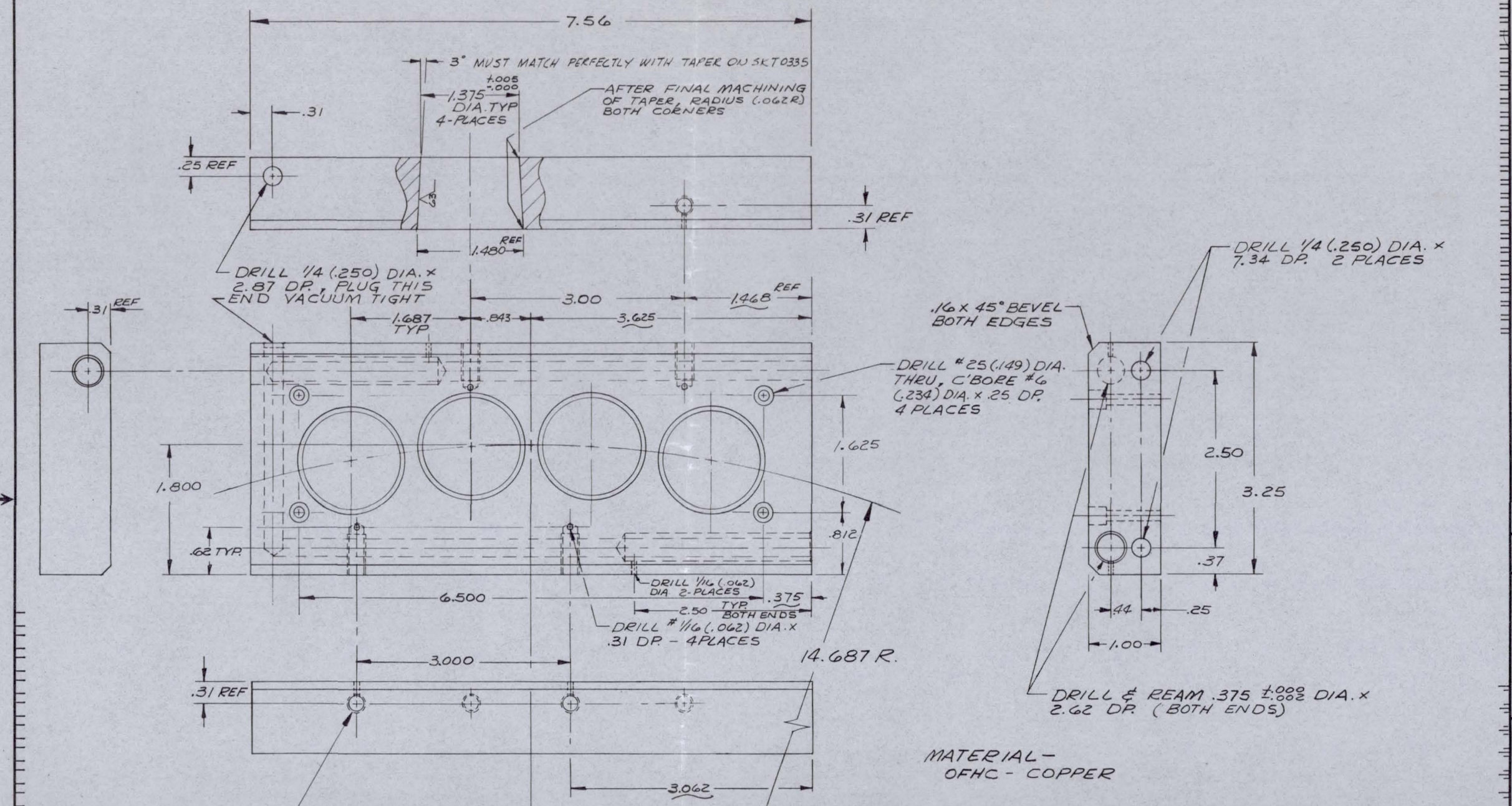
QTY REQD	PART OR IDENTIFYING NUMBER	NOMENCLATURE OR DESCRIPTION	MATERIAL OR NOTE	SPECIFICATION	ITEM NO.
← ASSY NO. LIST OF MATERIALS OR PARTS LIST					
UNLESS OTHERWISE SPECIFIED DIMENSIONS ARE IN INCHES TOLERANCES		CONTRACT NO.	AVCO CORPORATION TULSA, OKLAHOMA		
FRACT ±	DEC ±	ANGLES ±	TITLE		
MATERIAL:			SAMPLE PLUG G-235		
DWG. NO. Cooley		DATE 12/16/66			
APPROVED WILKERSON		DATE 12/16/66			
CKD	Boles	12/16/66	SIZE	CODE IDENT NO.	DWG. NO.
DRN	WILKERSON	12/16/66	C		SKT0335
DESIGN APPROVED		SCALE 2/1			
DESIGN APPROVED		WEIGHT SHEET			

DO NOT SCALE DRAWING

DRAWING NUMBER

A

REVISIONS				
EC	SYM	DESCRIPTION	DATE	APPROVED



QTY REQD	PART OR IDENTIFYING NO.	NOMENCLATURE OR DESCRIPTION	MATERIAL OR NOTE	SPECIFICATION	ITEM NO.
← ASSY NO. →					
LIST OF MATERIALS OR PARTS LIST					
-UNLESS OTHERWISE SPECIFIED- ALL DIM. ARE IN INCHES AND AFTER PLATING - TOLERANCES - .XX ± .06 .XX ± .03 .XXX ± .010 ANGLES 20°/30° DRILLED HOLES/AND-10387 THREADS/HANDBOOK H-28 AND MIL-STD-8 BREAK SHARP EDGES AND COR. .005 TO .020 R -DIA ON COM CTR CONC WITHIN .010 TIR -SUR SQ TO RESP AXIS WITHIN .001/IN. -SUR SQ, FLATNESS, PAR., WITHIN .002/IN. -FILLETS .020 TO .040 R BEND AND BEND RELIEF RADII 2 X THK GEOMETRIC SYMBOLS/MIL-STD-8 SURFACE ROUGHNESS/MIL-STD-10					
DWG APPD <i>Cooley</i> 12/16/66 CHECKED <i>BOLDS</i> 12/16/66 DRAWN <i>WILKERSON</i> 12/16/66 DESIGN APPROVAL			TITLE SAMPLE HOLDER G-235		
FINISH CLEAN FOR VAC			CODE IDENT. NO. SIZE DWG NO. C SKT0340		
SCALE			REL		SHEET

DO NOT SCALE DRAWING

92

8

7

6

5

4

3

2

1

REVISIONS				
ZONE	LTR	DESCRIPTION	DATE	APPROVED

D

C

B

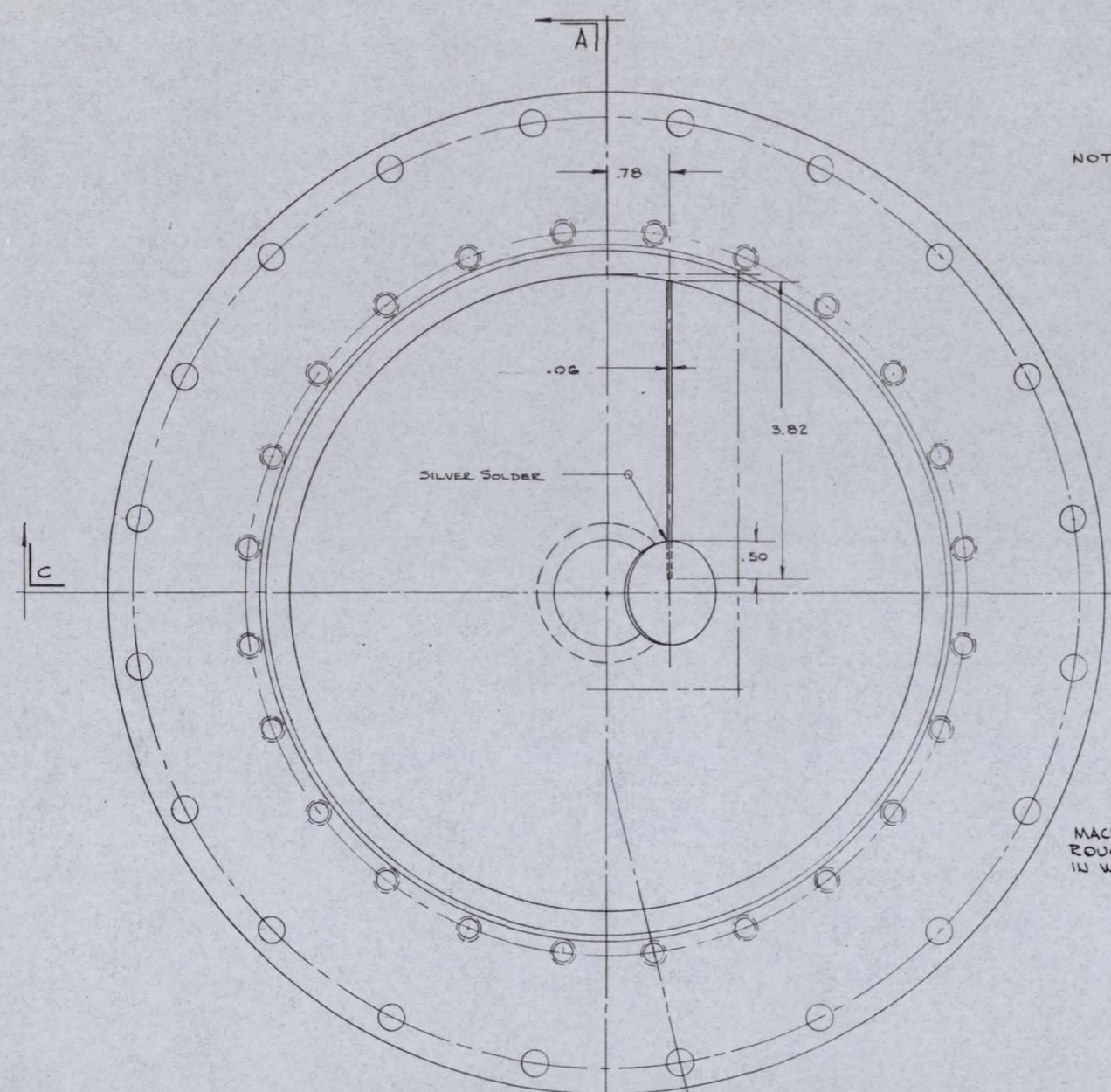
A

D

C

B

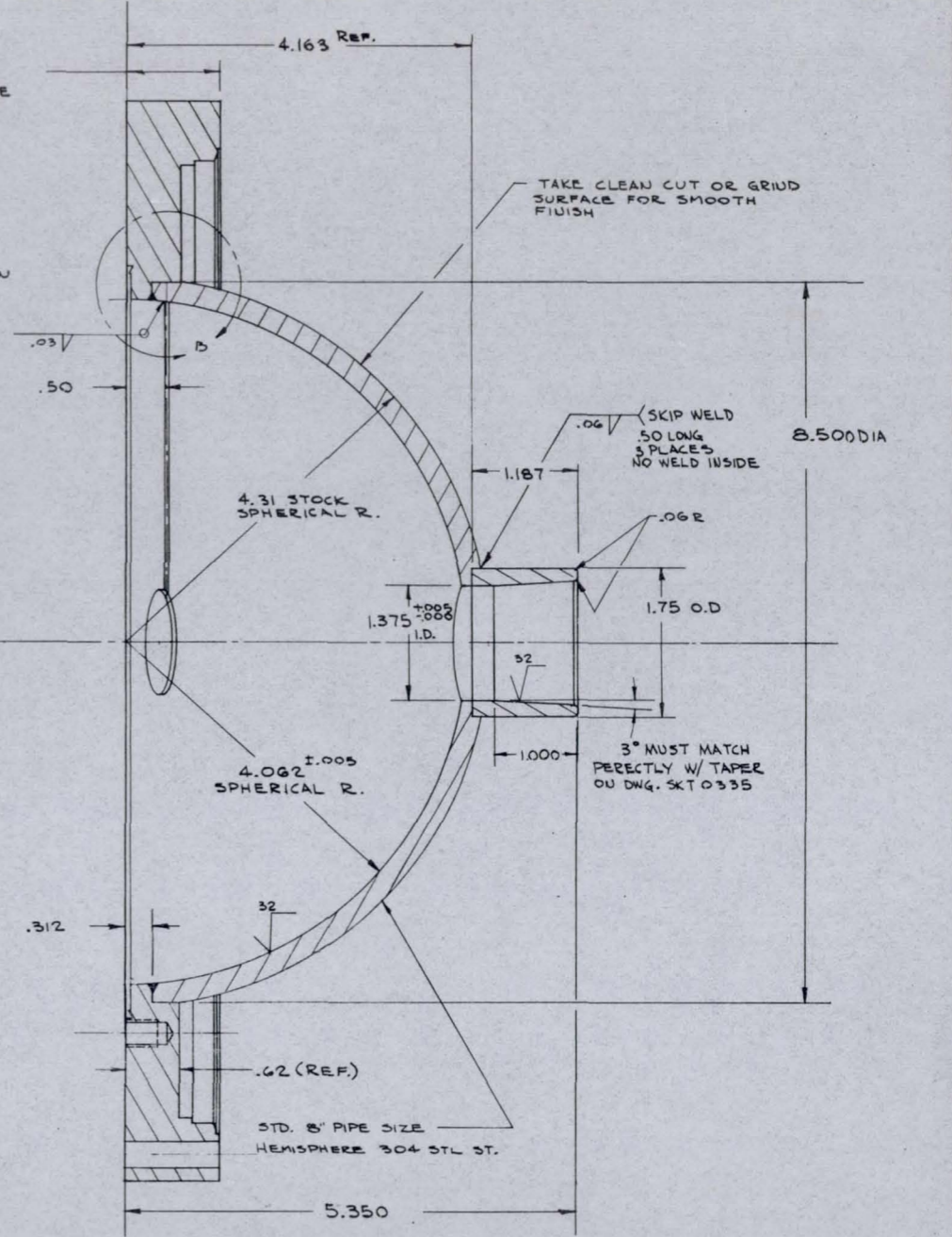
A



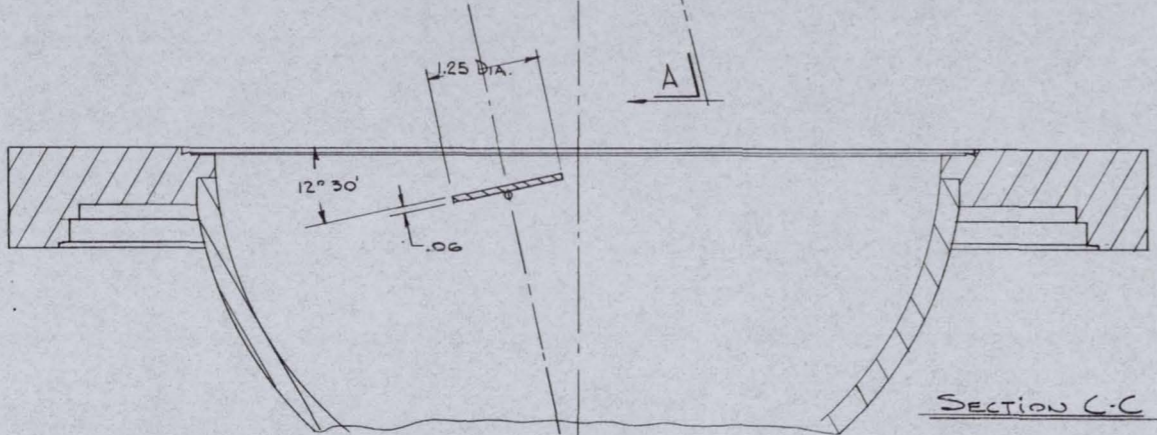
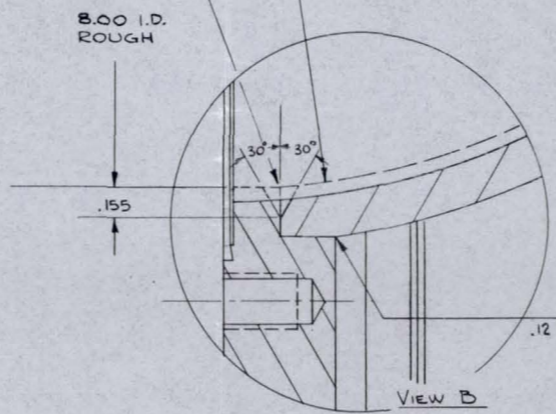
NOTES:

1. ALL MAT'L TO BE 304 STAINLESS
2. WELDING & MACHINING PROCEDURE
3. ROUGH OUT EXISTING WHEELER FLANGE TO I.D. SHOWN. TURN & FACE OFF & BORE 1.75 HOLE IN HEMISPHERE. MAKE ROUGH PIECE FOR 1.75 HOLE.
4. DO ALL WELDING.
5. NORMALIZE
6. FINAL MACHINE AS SHOWN.

1.12 STOCK WHEELER FLANGE 12.75 O.D.



MACHINE GROOVE IN ROUGH STOCK. FILL IN WITH WELD.



QTY REQD	PART OR IDENTIFYING NUMBER	NOMENCLATURE OR DESCRIPTION	MATERIAL OR NOTE	SPECIFICATION	ITEM NO.
← ASSY NO. LIST OF MATERIALS OR PARTS LIST					
UNLESS OTHERWISE SPECIFIED DIMENSIONS ARE IN INCHES TOLERANCES		CONTRACT NO.			
FRAC	DEC	ANGLES	DWG. NO. <i>Cosley</i> 1/6/67		
±	±.010	± 30'	APPROVED DATE		
MATERIAL:		NOTED ON F/D			
CLEAN FOR VACUUM		DRN Boles 1/6/67			
DESIGN APPROVED		DESIGN APPROVED			
DESIGN APPROVED		DESIGN APPROVED			
SIZE		CODE IDENT NO.		DWG. NO.	
D				SKT 0364	
SCALE		FULL		WEIGHT SHEET	

MECHANICAL PROPERTIES		APPLICATION	
YP		NEXT ASSY	USED ON
TS			
EL2			
RA			
BH			
RH			

DRILLED HOLES/AND-10387 THREADS/ HANDBOOK H-28 AND MIL-STD-9 BREAK SHARP EDGES AND COR. .005 TO .020 R -DIA ON COM CTR CONC WITHIN .010/ TIR -SUR SQ TO RESP AXIS WITHIN .001/ IN. -SUR SQ, FLATNESS, PAR., WITHIN .002/IN. -FILLETS .020 TO .040 R BEND AND BEND RELIEF RADII 2 x THK GEOMETRIC SYMBOLS/ MIL-STD-8 SURFACE ROUGHNESS/ MIL-STD-10

DO NOT SCALE DRAWING

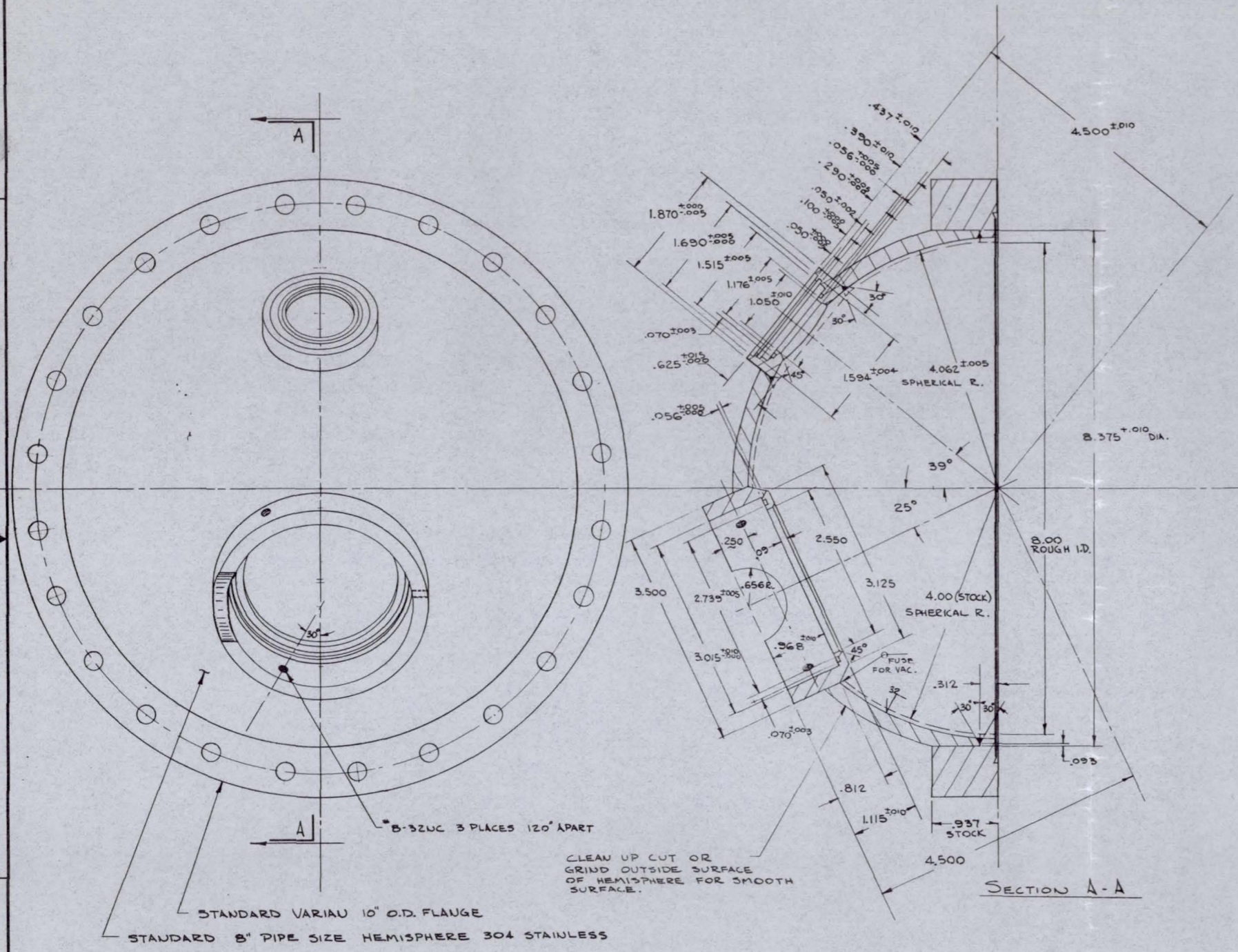
93

8 7 6 5 4 3 2 1

REVISIONS				
ZONE	LTR	DESCRIPTION	DATE	APPROVED

D
C
B
A

D
C
B
A



- NOTES:
1. ALL MATERIAL TO BE 304 STAINLESS STEEL.
 2. WELDING & MACHINING PROCEDURE
 3. ROUGH OUT EXISTING VARIAN FLANGE TO I.D. SHOWN. TURN O.D., FACE OFF & BORE HOLES IN HEMISPHERE.
 4. DO ALL WELDING EXCEPT 3.500 O.D. PIECE.
 5. NORMALIZE
 6. FINISH MACHINE INSIDE OF SPHERE, & OUTSIDE CLEANUP.
 7. WELD IN 3.500 O.D. PIECE.
 8. FINISH MACHINE 3.500 O.D. PIECE.

CLEAN UP CUT OR GRIND OUTSIDE SURFACE OF HEMISPHERE FOR SMOOTH SURFACE.

STANDARD VARIAN 10" O.D. FLANGE
STANDARD 8" PIPE SIZE HEMISPHERE 304 STAINLESS

SECTION A-A

QTY REQD	PART OR IDENTIFYING NUMBER	NOMENCLATURE OR DESCRIPTION	MATERIAL OR NOTE	SPECIFICATION	ITEM NO.
LIST OF MATERIALS OR PARTS LIST					
UNLESS OTHERWISE SPECIFIED DIMENSIONS ARE IN INCHES TOLERANCES					
FRACT		DEC	ANGLES		
±		±010	± 30'		
MATERIAL:					
NOTED ON F/D CLEAN FOR VACUUM					
CONTRACT NO.		AVCO CORPORATION TULSA, OKLAHOMA			
DWG. NO.		TITLE			
APPROVED		INTEGRATING SPHERE ENTRANCE HALF			
DATE		G-235			
DESIGN APPROVED		SIZE CODE IDENT NO. DWG. NO.			
DESIGN APPROVED		D SKT 0365			
SCALE FULL		WEIGHT		SHEET	

MECHANICAL PROPERTIES	APPLICATION	
	NEXT ASSY	USED ON
Y.P.		
T.S.		
ELZ		
RA		
BH		
RH		

DRILLED HOLES AND 10387 THREADS/HANDBOOK H-25 AND MIL-STD-9
BREAK SHARP EDGES AND COR. .065 TO .020 R
-DIA ON CON CTR CONC WITHIN .010/TIR
-SUR SQ TO RESP AXIS WITHIN .002/IN.
-SUR SQ FLATNESS, PAR., WITHIN .002/IN.
-FILLETS .020 TO .040 R
BEND AND BEND RELIEF RADII 2x THK
GEOMETRIC SYMBOLS/MIL-STD-4
SURFACE ROUGHNESS/MIL-STD-10 ✓

DO NOT SCALE DRAWING

94

8

7

6

5

↓

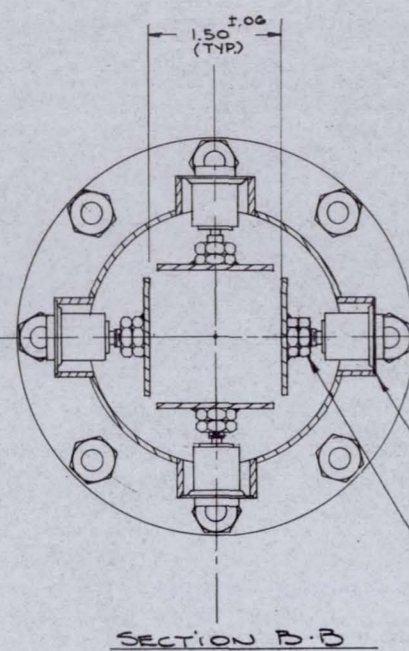
4

3

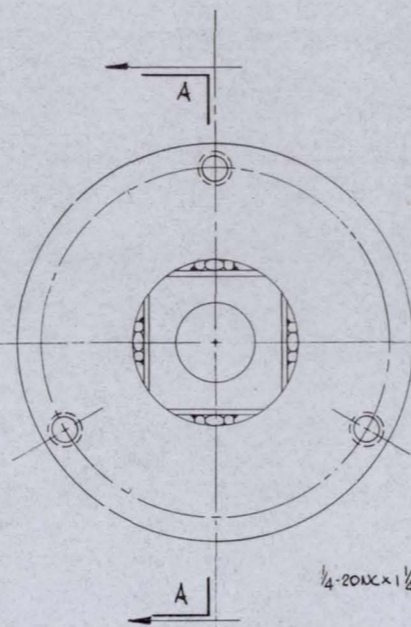
2

1

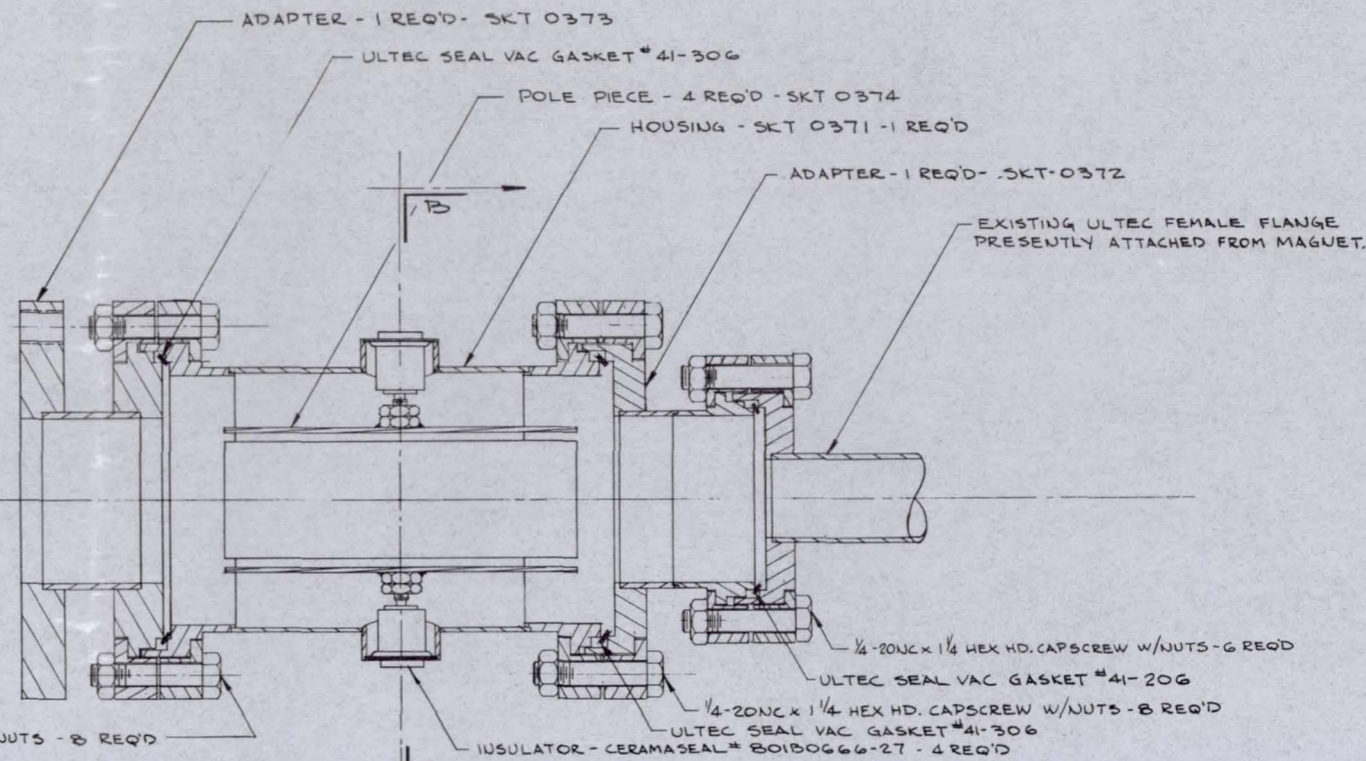
REVISIONS				
ZONE	LTR	DESCRIPTION	DATE	APPROVED



SECTION B-B



SECTION A-A



SEE ASSEMBLY NOTE 1.

#8-32NC HEX NUT 304 STLS. STEEL - 4 REQ'D

NOTES

1. ASSEMBLE THE LOCKING NUT (#8-32NC) ONTO THE INSULATOR. WITH THE POLE PIECE (SKT 0374) INSERTED INTO THE HOUSING (SKT 0371), SCREW THE INSULATOR INTO THE NUT WELDED ONTO THE POLE PIECE PLATE. DO NOT BOTTOM THE THREADS. LEAVE 2 THREADS OFF BOTTOM, OR WHATEVER IS NECESSARY TO MAKE THE 1.50" DIMENSION. SILVER SOLDER THE INSULATOR ONTO THE HOUSING. TIGHTEN #8-32 LOCKING NUT AFTER MAKING THE POLE PIECES SQUARE & TRUE WITH EACH OTHER.

2. ALL HARDWARE TO BE 304 STLS. STEEL.

MACHINING	MECHANICAL PROPERTIES	
	YP	TS
DRILLED HOLES/AND-1087 THREADS/ HANDBOOK H-28 AND MIL-STD-9 BREAK SHARP EDGES AND COR. .005 TO .020 R		
-DIA OR COM CTR CONC WITHIN .010/ TIR		
-SUR SQ TO RESP AXIS WITHIN .001/ IN.		
-SUR SQ FLATNESS, PAR., WITHIN .002/IN.		
-FILLETS .020 TO .040 R BEND AND BEND RELIEF RADII 2 x THK		
GEOMETRIC SYMBOLS/ MIL-STD-4		
SURFACE ROUGHNESS/ MIL-STD-10		

QTY REQ'D	PART OR IDENTIFYING NUMBER	NOMENCLATURE OR DESCRIPTION	MATERIAL OR NOTE	SPECIFICATION	ITEM NO.
← ASSY NO. LIST OF MATERIALS OR PARTS LIST					
UNLESS OTHERWISE SPECIFIED DIMENSIONS ARE IN INCHES TOLERANCES					
FRAC	DEC	ANGLES			
MATERIAL:					
CONTRACT NO.					
DWG. NO. <i>Cooley</i> 1/11/67 DATE					
APPROVED					
CHKD <i>BOLES</i> 1/17/67					
DESIGN APPROVED					
DESIGN APPROVED					
APPLICATION					

SIZE	CODE IDENT NO.	DWG. NO.
D		SKT 0370
SCALE	Full	WEIGHT SHEET

TULSA DIVISION		AVCO CORPORATION TULSA, OKLAHOMA	
TITLE QUADRAPOLE ASSEMBLY IN-SITU REFLECTOMETER SYSTEM G-235			
SIZE	CODE IDENT NO.	DWG. NO.	
D		SKT 0370	
SCALE	Full	WEIGHT	SHEET

DO NOT SCALE DRAWING

95

